RAPPORT *REPORT* 2006-8

The SIze REsolved Aerosol Model (SIREAM) and the Modal Aerosol Model (MAM). Technical documentation.

Bruno Sportisse, Karine Sartelet, Edouard Debry, Kathleen Fahey, Yelva Roustan and Maryline Tombette.

CEREA.
Joint Laboratory ENPC-EDF R&D.
Ecole Nationale des Ponts et Chaussées
6-8 Avenue Blaise Pascal, Cité Descartes 77455 Champs sur Marne.
or
EDF R&D, 6 quai Watier
78401 Chatou
Tel: (33) 1 64 15 36 25
Fax: (33) 1 64 15 21 70

Contents

Introduction

This report aims at presenting the aerosol models developed in the PAM project (Multiphase Air Pollution). This work has been partially funded by the french Research Program PRIMEQUAL during the period 2001-2005.

The kernel of the PAM project was:

- to develop numerical models that describe the atmospheric multiphase mixture of gaseous species, aqueous-phase species (inside cloud droplets) and aerosols;
- to couple the resulting models to host Chemistry-Transport Models;
- to perform model-to-data comparisons at regional and continental scales.

Two aerosol models have been developed:

- SIREAM (SIze REsolved Aerosol Model), based on a sectional description of the aerosol distribution;
- MAM (Modal Aerosol Model), based on a modal discretization.

Both models have common parameterizations, provided by the AtmoData library (figure 1). They have been hosted by a Chemistry-Transport Model, Polair3D, inside the modeling system Polyphemus. A preliminary coupling has also been performed with the atmospheric CFD model Mercure_Saturne.

This report is structured as follows.

The first chapter describes the background for aerosol modeling and the main parameterizations that are used. The second and third chapters present the numerical models SIREAM and MAM, respectively. The focus in on numerical algorithms. A 0D comparison between both models is also reported at the end of the third chapter. The fourth chapter details the coupling to a 3D Chemistry-Transport Model and the parameterizations that have to be added (emission, scavenging, deposition). This reports ends with a conclusion and a discussion for some future works. An appendix presents the main aerosol parameterizations used in the AtmoData library.

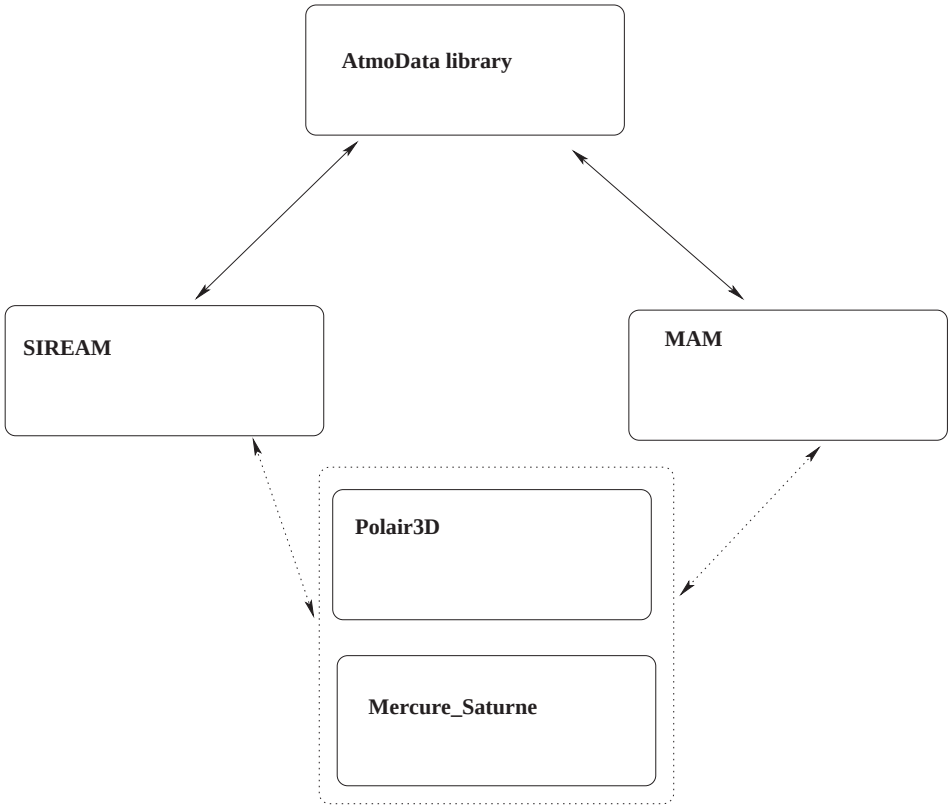

Figure 1: Architecture of models MAM and SIREAM

Chapter 1

Aerosol modeling: parameterizations used for the GDE

Summary:

This chapter describes the modeling of multiphase processes (General Dynamic Equation for aerosols and gas/cloud diphasic model). The parameterizations used for nucleation, condensation/evaporation, coagulation, mass transfer, aqueous-phase chemistry, heterogeneous chemistry and formation of Semi-Volatile Organic Compounds (SVOC) are also given.

1.1 Aerosol Dynamic

In this section, the General Dynamic Equation for aerosols (GDE) and the 0D processes are described. All processes related to a 3D Chemistry-Transport Model (transport, emission, scavenging) are described in chapter 4.

In the sequel, T stands for température (in Kelvin) and RH for the relative humidity (in %).

1.1.1 Notations

Description of aerosols distribution

We use an assumption of *internal mixing*: for a given size, there is a unique chemical composition.

$\{X_i\}_{i=1,n_e}$ is the set of n_e chemical species in the aerosol mixture. The aerosol population is then described by:

1. a size distribution, for instance $n(s,t)$ for the number distribution (number of aerosols per air volume), a function of the size parameter s (among volume v, diameter d or dry mass m) and of time;

2. a chemical composition for size s, $\{q_i(s,t)\}_{i=1,n_e}$, with $q_i(s,t)$ the mass distribution of species X_i ($1 \leq i \leq n_e$).

The mass distributions meet :

$$\sum_{i=1}^{i=n_e} q_i = m\, n \tag{1.1}$$

We also define the mass $m_i(m,t)$ of species X_i in aerosols of mass m with :

$$m_i(m,t) = \frac{q_i(m,t)}{n(m,t)} \tag{1.2}$$

Notice that :

$$\sum_{i=1}^{i=n_e} m_i(m,t) = m \tag{1.3}$$

Chemical composition

The following components are taken into account :

- liquid water;
- inert species : mineral dust (MD), elemental carbon (EC) and, in some applications, heavy trace metals (lead, cadmium);
- inorganic species : Na^+, SO_4^{2-}, NH_4^+, NO_3^- and Cl^-;
- organic species : one species for *Primary Organic Aerosols* (POA), 8 species for Secondary Organic Aerosols (ARO_1, ARO_2, LIM_1, LIM_2, API_1, API_2, ALK_1, OLE_1).

  We refer to section 1.2.5 for more details.

A typical version of the model (trace metals or radionuclides are not included) is given by 17 chemical species for a given size (1+2+5+1+8).

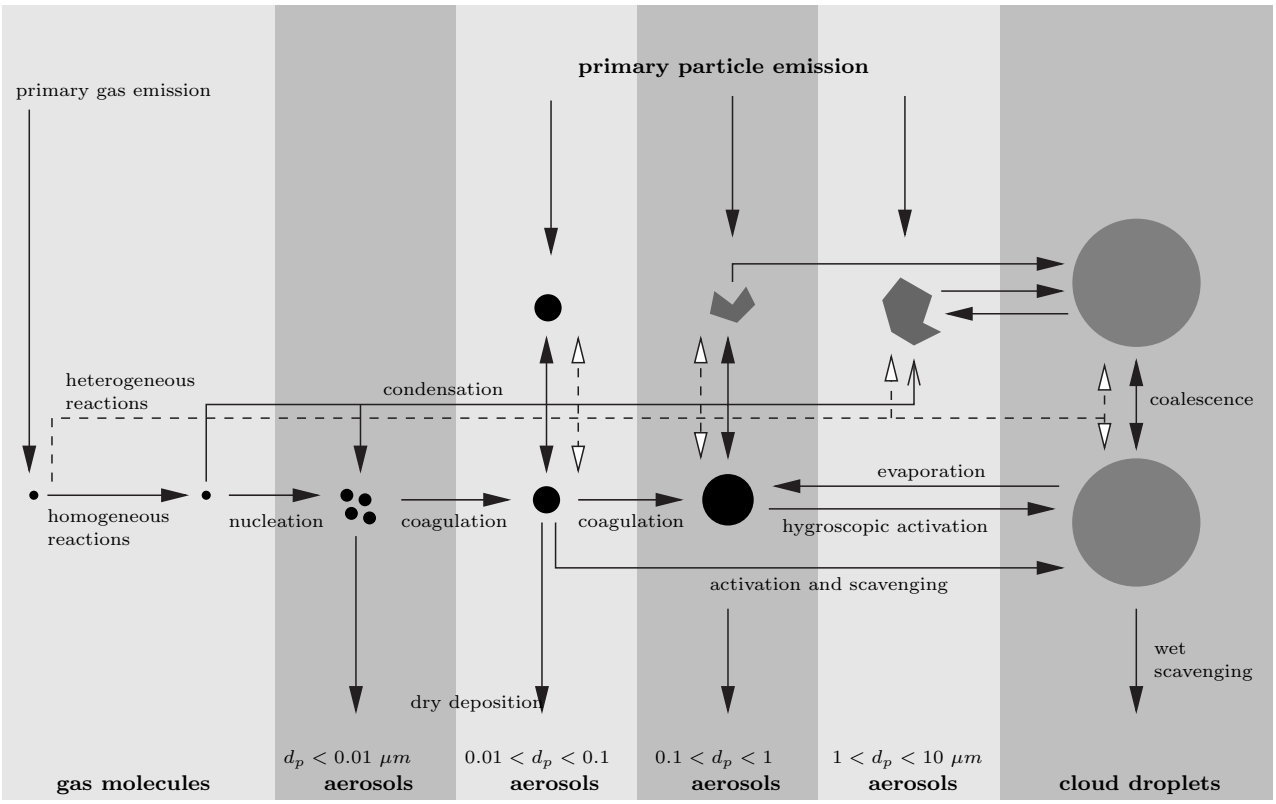

Figure 1.1: Aerosol Dynamic.

1.1.2 Some processes

The evolution of size distribution and chemical composition is governed by the following processes (see figure 1.1):

- **nucleation**:

  The formation of smallest nanometric aerosols is given by the aggregation of gaseous molecules leading to thermodynamically stable *clusters*. In practice, we use two kinds of parameterizations for this process: a first one for the binary mixture H_2O-H_2SO_4 ([Kulmala et al., 1998] or [Vehkamäki et al., 2002]), a second one for the ternary mixture H_2O-H_2SO_4-NH_3 ([Napari et al., 2002]).

  We refer to section 1.2.3.

- **coagulation**:

  The brownian coagulation of aerosols is related to brownian motion (thermal motion). We refer to section 1.2.1 for the description of coagulation kernels.

- **condensation/évaporation** or **gas-particle conversion**:

  Some gas-phase species with low saturation vapor pressure may condensate on existing aerosols. Some condensed species in the aerosol phase may also evaporate. These mass transfers are governed by the gradient between the gas-phase concentration and the concentration at the surface of aerosols. The surface concentration is supposed to be at equilibrium with the aerosol mixture ("local" equilibrium).

  The parameterizations for mass transfer and the computation of local equilibrium are given in section 1.2.2.

  A specific treatment is applied for organic species because gas-phase mechanisms are usually devoted to photochemistry and do not represent Semi-Volatile Organic Species (SVOC). We refer to section 1.2.5 for the description of the parameterizations for SVOC.

- **mass transfer for cloud droplets** :

  Part of the aerosol distribution is activated and leads to the formation of cloud droplets in saturated thermodynamic conditions. The model does not describe explicitely the activation of aerosols (there is no microphysical model for cloud formation) and a parameterization is used.

  Mass transfer between activated aerosols and cloud droplets is described in order to have a description of sulfate production (through aqueous-phase chemistry in cloud droplets).

  Following [Fahey, 2003, Fahey and Pandis, 2001], the parameterization assumes that activation/evaporation is performed in a single timestep for the activated part of the aerosol distribution. This allows to take into account the impact of aqueous-phase chemistry on the chemical composition of aerosols.

  We refer to section 1.2.4.

- **heterogeneous reactions**:

  The heterogeneous reactions at the surface of condensed matter (aerosols and cloud or fog droplets) may have a significant impact for gas-

phase photochemistry and aerosols . Following [Jacob, 2000], these processes are usually described by the first-order reactions :

$$HO_2 \xrightarrow{\text{condensed matter}} 0.5\,H_2O_2$$

$$NO_2 \xrightarrow{\text{condensed matter}} 0.5\,HONO + 0.5\,HNO_3$$

$$NO_3 \xrightarrow{\text{condensed matter}} HNO_3$$

$$N_2O_5 \xrightarrow{\text{condensed matter}} 2\,HNO_3$$

The kinetic rates are detailed in section 1.2.6.

The heterogeneous reactions for HO_2, NO_2 and NO_3 at surface of cloud droplets are supposed to be already taken into account by the diphasic aqueous-phase model (see below). They are therefore not taken into account for cloud droplets.

1.1.3 The General Dynamic Equation for aerosols (GDE)

The evolution of size distributions and chemical compositions is given by the so-called General Dynamic Equation for aerosols (GDE).

We use the following notations (the parameterizations are described in the appropriate sections).

m_0 is the dry mass for the smallest aerosol (given by nucleation).

$J_0(t)$ is the nucleation rate, in number of nucleated aerosols per second.

$I_i(m,t)$ is the condensation/evaporation (c/e) rate of condensable species X_i in an aerosol of dry mass m, in unit of mass per unit of time.

The total rate of c/e in an aerosol of dry mass m is I_0:

$$I_0(m,t) = \sum_{i=1}^{n_e} I_i(m,t) \tag{1.4}$$

The coagulation kernel $K(m_1, m_2)$ gives the coagulation between two aerosols of dry mass, respectively m_1 and m_2, in unit of volume per unit of time.

Number distribution

The equation for the number distribution is :

$$\frac{\partial n}{\partial t}(m,t) = \underbrace{\theta(m \geq 2m_0)\frac{1}{2}\int_{m_0}^{m-m_0} K(\tilde{m}, m-\tilde{m})n(\tilde{m},t)n(m-\tilde{m},t)\,d\tilde{m}}_{\text{coagulation gain}} - \underbrace{n(m,t)\int_{m_0}^{\infty} K(m,\tilde{m})n(\tilde{m},t)\,d\tilde{m}}_{\text{coagulation loss}} - \underbrace{\frac{\partial(I_0 n)}{\partial m}}_{\text{c/e advection}} + \underbrace{\delta_{(m,m_0)}J_0(t)}_{\text{nucleation}} \tag{1.5}$$

$\theta(\mathbf{A})$ is a dimensionless function equal to 1 if the condition $\mathbf{A}$ is met, 0 otherwise. δ is the Dirac function, given as the inverse of a mass unit.

Chemical composition

For the species labeled by $i = 1, \ldots, n_e$:

$$\frac{\partial q_i}{\partial t}(m,t) = \underbrace{\theta(m \geq 2m_0)\int_{m_0}^{m-m_0} K(\tilde{m}, m-\tilde{m})q_i(\tilde{m},t)n(m-\tilde{m},t)\,d\tilde{m}}_{\text{coagulation gain}} - \underbrace{q_i(m,t)\int_{m_0}^{\infty} K(m,\tilde{m})n(\tilde{m},t)\,d\tilde{m}}_{\text{coagulation loss}} - \underbrace{\frac{\partial(I_0 q_i)}{\partial m}}_{\text{c/e advection}} + \underbrace{(I_i n)(m,t)}_{\text{c/e mass transfer}} + \underbrace{\delta_{(m,m_0)}m_i(m_0,t)J_0(t)}_{\text{nucleation}} \tag{1.6}$$

For condensation/evaporation, we distinguish an advection term (which corresponds to a shift along the distribution) and a mass transfer term (which corresponds to a mass transfer among the gas phase and aerosols).

1.2 The main parameterizations

1.2.1 Coagulation

In order to simplify the analytical expressions for coagulation kernels, we use in this section the aerosol diameter d_p as the size variable. The relation

with the wet mass (the dry mass plus the mass of water in the aerosol) is of course :

$$m_{wet} = \pi \frac{d_p^2}{6} \rho_p \tag{1.7}$$

with ρ_p the aerosol density (computed as a function of the chemical composition or supposed to be fixed).

We write K_{12} the coagulation kernel between the aerosols of sizes d_{p_1} and d_{p_2}. For brownian coagulation, some regimes have to be distinguished.

Continuous regime

If d_{p_1} and $d_{p_2} \gg \lambda_{\text{air}}$:

$$K_{12} = 2\pi(D_1 + D_2)(d_{p_1} + d_{p_2}) \tag{1.8}$$

with D_1 and D_2 the diffusion coefficients in the air, respectively for aerosols of diameters d_{p_1} and d_{p_2} :

$$D_i = \frac{k_b T}{3\pi \mu_{air} d_{p_i}} \tag{1.9}$$

with k_b the Boltzmann constant and μ_{air} the air dynamic viscosity.

Free molecular regim

If d_{p_1} and $d_{p_2} \ll \lambda_{\text{air}}$, the coagulation kernel is given by:

$$K_{12} = \frac{\pi}{4}(d_{p_1} + d_{p_2})^2 (\bar{c}_1^2 + \bar{c}_2^2)^{\frac{1}{2}} \tag{1.10}$$

m_i and $\bar{c}_i$ stand respectively for the mass of aerosol i and the mean quadratic velocity, given by:

$$\bar{c}_i = \left(\frac{8 k_b T}{\pi m_i} \right)^{\frac{1}{2}} \tag{1.11}$$

Transition regime

If d_{p_1} and $d_{p_2} \sim \lambda_{\text{air}}$, the coagulation kernel of the continuous regim is modified with a coefficient β ([Fuchs, 1964]) :

$$\beta = \frac{d_{p_1} + d_{p_2}}{d_{p_1} + d_{p_2} + 2(g_1^2 + g_2^2)^{\frac{1}{2}}} + \frac{8(D_1 + D_2)}{(\bar{c}_1^2 + \bar{c}_2^2)^{\frac{1}{2}}(d_{p_1} + d_{p_2})} \tag{1.12}$$

where

$$g_i = \frac{1}{3d_{p_i}l_i}\left[(d_{p_i}+l_i)^3 - (d_{p_i}^2+l_i^2)^{\frac{3}{2}}\right] - d_{p_i} \ , \quad l_i = \frac{8D_i}{\pi \bar{c}_i} \tag{1.13}$$

The diffusion coefficient in the air is also modified with:

$$D_i \rightarrow D_i \frac{5+4K_{n_i}+6K_{n_i}^2+18K_{n_i}^3}{5-K_{n_i}+(8+\pi)K_{n_i}^2} \ , \quad K_{n_i} = \frac{2\lambda_{\text{air}}}{d_{p_i}} \tag{1.14}$$

1.2.2 Condensation/evaporation

Mass flux

The mass flux I_i is given by:

$$I_i = \underbrace{2\pi D_i^g d_p f(K_{n_i}, \alpha_i)}_{\text{condensation kernel}}\left(c_i^g - c_i^s(d_p,t)\right) \tag{1.15}$$

D_i^g and c_i^g are repsectively the diffusion coefficient in the air and the gas-phase concentration of species X_i.

The concentration c_i^s at the aerosol surface is supposed to be at *local* thermodynamic equilibrium with the aerosol composition:

$$c_i^s(d_p,t) = \eta(d_p)\ c_i^{eq}(m_1,\ldots,m_{n_e},RH,T) \tag{1.16}$$

$\eta(d_p)$ is related to the Kelvin effect (curvature effect) and is given by :

$$\eta(d_p) = \exp\left(\frac{4\sigma v_p}{R_g T d_p}\right) \tag{1.17}$$

with σ the surface tension.

The function f, the Fuchs-Sutugin function, describes the non-continuous effects ([Dahneke, 1983]). It depends on the Knudsen number of species X_i, K_{n_i}, and on the accomodation coefficient α_i :

$$f(K_{n_i},\alpha_i) = \frac{1+K_{n_i}}{1+2K_{n_i}(1+K_{n_i})/\alpha_i} \ , \quad K_{n_i} = \frac{2\lambda_i}{d_p} \tag{1.18}$$

where λ_i is the air mean free path for gas-phase species X_i in the air.

Fo high values of K_{n_i}, f is near $\frac{\alpha_i}{2K_{n_i}}$, which leads to the following expression for the mass transfer rate in the free molecular regim :

$$I_i = \alpha_i \frac{\bar{c}_i^g}{4}\pi d_p^2\left(c_i - c_i^s(d_p)\right) \tag{1.19}$$

with $\bar{c}_i^g$ the quadratic mean velocity for gas-phase species X_i, given by :

$$D_i^g = \frac{\lambda_i \bar{c}_i^g}{2} \tag{1.20}$$

Some typical values of these parameters are given in table 1.1, with temperature $T = 300\ K$ and pressure $P = 1\ atm$.

gas-phase species	$\bar{c}_i^g\ (m.s^{-1})$	$D_i^g\ (m^2.s^{-1})$
sulfate	254.58	1.07E-05
ammonium	611.24	2.17E-05
nitrate	317.51	1.47E-05
chloride	417.15	1.72E-05

Table 1.1: Some values of gas-phase diffusion coefficient and of quadratic mean velocity for $T = 300\ K$ and $P = 1\ atm$.

Local thermodynamic equilibrium

The key point is the computation of the local thermodynamic equilibrium, $c_i^{eq}(m_1, \ldots, m_{n_e}, RH, T)$.

The current model version does not describe the mixing between inorganics and organics. In practice, two independent equilibria are assumed.

The local equilibrium for inorganics is computed with the model ISORROPIA ([Nenes et al., 1998]). The local equilibrium for organics is given by an adsorption law, following [Schell, 2000, Schell et al., 2001] (see section 1.2.5).

The aerosol liquid water content is computed with the Zdanovskii-Stokes-Robinson relation (ZSR) as a function of the inorganic species.

This assumption is a limitation of the current model because some organic species may have an hydrophilic behaviour ([Griffin et al., 2002b, Griffin et al., 2002a, Pun et al., 2002]).

Moreover, some specific corrections may be applied to the case of liquid aerosols (limitation of the H^+ flux). In the case of solid aerosols, a specific computation is also performed ([Pilinis et al., 2000]).

1.2.3 Nucleation

For binary nucleation of sulfuric acid (H_2SO_4) and water, two parameterizations have been implemented: one from Kulmala [Kulmala et al., 1998]

and one from Vehkamaki [Vehkamäki et al., 2002]. For ternary nucleation of sulfuric acid, ammoniac (NH_3) and water, the parameterization of Napari ([Napari et al., 2002]) is used.

The nucleated aerosols are assigned to the first mode (the "nuclei" mode i) for MAM and to the first bin in SIREAM.

The nucleation diameter (of order $0.001\mu m$) is also computed but usually not used.

The different parameterizations differ from each other with the computation of J, whose magnitude is much larger for ternary nucleation than for binary nucleation.

In the following, $c_{\mathrm{H_2SO_4}}$ stands for the concentration in sulfuric acid (in molecules/cm^3).

Parameterization of Kulmala

In [Kulmala et al., 1998], J is given by :

$$J = \exp(\chi) \tag{1.21}$$

with

$$\begin{aligned}\chi = {} & 25.1289.N_{sulf} - 4890.8\frac{N_{sulf}}{T} - 2.2479.\delta.N_{sulf}.RH \\ & - \frac{1743.3}{T} + 7643.4\frac{x_{al}}{T} - 1.9712\frac{\delta.x_{al}}{RH}\end{aligned} \tag{1.22}$$

and

$$\begin{aligned}N_{sulf} &= \ln\frac{c_{\mathrm{H_2SO_4}}}{(c_{\mathrm{H_2SO_4}})_c} \\ N_{a,c} &= \exp(-14.5125 + 0.1335T - 10.5462RH + 1958.4\frac{RH}{T}) \\ x_{al} &= 1.2233 - 0.0154\frac{RA}{RA+RH} + 0.0102\ln(c_{\mathrm{H_2SO_4}}) \\ &- 0.0415\ln(N_{wv}) + 0.0016T \\ \delta &= 1 + \frac{T - 273.15}{273.15}\end{aligned} \tag{1.23}$$

N_{wv} is the concentration of water vapor and RA is the relative acidity. $(c_{\mathrm{H_2SO_4}})_c$ is a critical concentration.

Parameterization of Vehkamaki

The parameterization of Vehkamaki is a follow-up of the parameterization of Kulmala. The molar fraction in sulfuric acid x_* in the nucleated cluster is computed as a function of temperature T, of relative humidity RH and of gaseous concentration of sulfuric acid H_2SO_4 in cm^{-3} (equation (11) of [Vehkamäki et al., 2002]):

$$\begin{aligned} x^* &= 0.740997 - 0.00266379\ T \\ &\quad -0.00349998\ \ln(c_{H_2SO_4}) + 0.0000504022\ T\ \ln(c_{H_2SO_4}) \\ &\quad +0.00201048\ \ln\left(\frac{RH}{100}\right) - 0.000183289\ T\ \ln\left(\frac{RH}{100}\right) \\ &\quad +0.00157407\left[\ln\left(\frac{RH}{100}\right)\right]^2 - 0.0000179059\ T\ \left[\ln\left(\frac{RH}{100}\right)\right]^2 \\ &\quad +0.000184403\left[\ln\left(\frac{RH}{100}\right)\right]^3 - 1.50345\ 10^{-6}\ T\ \left[\ln\left(\frac{RH}{100}\right)\right]^3 \end{aligned} \quad (1.24)$$

The nucleation rate J in $cm^{-3}s^{-1}$ and the total number of molecules in the cluster N_{tot} are computed (equations (12) and (13) of [Vehkamäki et al., 2002]) with the following relations :

$$\begin{aligned} J &= \exp\left\{a(T,x^*) + b(T,x^*)\ln\left(\frac{RH}{100}\right)\right. \\ &\quad +c(T,x^*)\left[\ln\left(\frac{RH}{100}\right)\right]^2 + d(T,x^*)\left[\ln\left(\frac{RH}{100}\right)\right]^3 \\ &\quad +e(T,x^*)\ln(c_{H_2SO_4}) + f(T,x^*)\ln\left(\frac{RH}{100}\right)\ln(c_{H_2SO_4}) \\ &\quad +g(T,x^*)\left[\ln\left(\frac{RH}{100}\right)\right]^2\ln(c_{H_2SO_4}) + h(T,x^*)\left[\ln(c_{H_2SO_4})\right]^2 \\ &\quad \left.+i(T,x^*)\ln\left(\frac{RH}{100}\right)\left[\ln(c_{H_2SO_4})\right]^2 + j(T,x^*)\left[\ln(c_{H_2SO_4})\right]^3\right\} \end{aligned} \quad (1.25)$$

$$
\begin{aligned}
N_{tot} &= \exp\Bigg\{ A(T,x^*) + B(T,x^*)\ln\left(\frac{RH}{100}\right) \\
&+C(T,x^*)\left[\ln\left(\frac{RH}{100}\right)\right]^2 + D(T,x^*)\left[\ln\left(\frac{RH}{100}\right)\right]^3 \\
&+E(T,x^*)\ln(c_{\mathrm{H_2SO_4}}) + F(T,x^*)\ln\left(\frac{RH}{100}\right)\ln(c_{\mathrm{H_2SO_4}}) \\
&+G(T,x^*)\left[\ln\left(\frac{RH}{100}\right)\right]^2\ln(c_{\mathrm{H_2SO_4}}) + H(T,x^*)\left[\ln(c_{\mathrm{H_2SO_4}})\right]^2 \\
&+I(T,x^*)\ln\left(\frac{RH}{100}\right)\left[\ln(c_{\mathrm{H_2SO_4}})\right]^2 + J(T,x^*)\left[\ln(c_{\mathrm{H_2SO_4}})\right]^3\Bigg\} \qquad (1.26)
\end{aligned}
$$

where the coefficients $a(T,x^*)$ ... $i(T,x^*)$ and $A(T,x^*)$ ... $J(T,x^*)$ are given in [Vehkamäki et al., 2002]. Nucleation occurs only above a critical concentration of sulfuric acid $(c_{\mathrm{H_2SO_4}})_c$, that depends on relative humidity and temperature through:

$$
\begin{aligned}
&(c_{\mathrm{H_2SO_4}})_c = \exp\Bigg[-279.243 + 117.344\frac{RH}{100} \\
&+\frac{22700.9}{T} - \frac{1088.64}{T}\frac{RH}{100} + 1.14436T - 0.0302331\frac{RH}{100}T \\
&-0.00130254T^2 - 6.38697\log\left(\frac{RH}{100}\right) + 854.98\log\left(\frac{RH}{100}\right)T \\
&+0.00879662T\log\left(\frac{RH}{100}\right)\Bigg] \qquad (1.27)
\end{aligned}
$$

Parameterization of Napari

The parameterization of Napari describes the ternary nucleation for a mixture of water, sulfuric acid and ammoniac [Napari et al., 2002].

The nucleation rate J in $\mathrm{cm^{-3}s^{-1}}$ also depends on ζ (the mixing ratio

of NH_3 in ppt), as a complementary parameter to T, RH and $c_{H_2SO_4}$:

$$\begin{aligned}
\ln J &= -84.7551 + \frac{f_1(T)}{\ln c_{H_2SO_4}} + f_2(T)\ln c_{H_2SO_4} + f_3(T)\ln^2 c_{H_2SO_4} + f_4(T)\ln\zeta \\
&+ f_5(T)\ln^2\zeta + f_6(T)RH + f_7(T)\ln RH + f_8(T)\frac{\ln\zeta}{\ln c_{H_2SO_4}} \\
&+ f_9(T)\ln\zeta\ln c_{H_2SO_4} + f_{10}(T)RH\ln c_{H_2SO_4} + f_{11}(T)\frac{RH}{\ln c_{H_2SO_4}} \\
&+ f_{12}(T)RH\ln\zeta + f_{13}(T)\frac{\ln RH}{\ln c_{H_2SO_4}} + f_{14}(T)\ln RH\ln\zeta \\
&+ f_{15}(T)\frac{\ln^2\zeta}{\ln c_{H_2SO_4}} + f_{16}(T)\ln c_{H_2SO_4}\ln^2\zeta + f_{17}(T)\ln^2 c_{H_2SO_4}\ln\zeta \\
&+ f_{18}(T)RH\ln^2\zeta + f_{19}(T)\frac{RH\ln\zeta}{\ln c_{H_2SO_4}} + f_{20}(T)\ln^2 c_{H_2SO_4}\ln^2\zeta \qquad (1.28)
\end{aligned}$$

The functions $f_i(T)$ are third-order polynomial functions :

$$f_i(T) = a_{i0} + a_{i1}T + a_{i2}T^2 + a_{i3}T^3. \qquad (1.29)$$

The coefficients a_{ij} are given in Table 1 of [Napari et al., 2002].

The number of nucleated particles n_i^* for each species of the ternary mixture is given by:

$$\begin{aligned}
n^*_{H_2SO_4} &= 38.1645 + 0.774106\ln J + 0.00298879\ln^2 J \\
&\quad -0.357605T - 0.00366358T\ln J + 0.0008553T^2 \qquad (1.30) \\
n^*_{NH_3} &= 26.8982 + 0.682905\ln J + 0.00357521\ln^2 J \\
&\quad -0.265748T - 0.00341895T\ln J + 0.000673454T^2. \qquad (1.31)
\end{aligned}$$

The limits of validity for this parameterization are typically $T \in [240 - 300]$ K, $RH \in [0.05 - 0.95]$, $c_{H_2SO_4} \in [10^4 - 10^9]$ cm^{-3}, $\zeta \in [0.1 - 100]$ ppt and $J \in [10^{-5} - 10^6]$ cm^{-3}s^{-1}.

1.2.4 Aqueous-phase chemistry

Parameterization

The description of aqueous-phase chemistry is a key point, especially for sulfate production.

The model is basically related to the chemical mechanism developed at Carneggie Mellon University (CMU). Some parameterizations and some numerical strategies also refer to ([Djouad et al., 2002, Sportisse and Djouad, 2003, Djouad et al., 2003a, Djouad et al., 2003b]).

The microphysical processes that govern the evolution of cloud droplets are not described and only parameterized. We assume that a cloud droplet is formed and disappears instantaneously (during one numerical timestep). The objective is indeed to take into account the impact of aqueous-phase chemistry for the activated part of the aerosol distribution.

The following processes are modelized:

1. if the liquid water content is above a threshold (of magnitude 0.5 g/m^3), the grid cell is supposed to contain a cloud and a part of the aerosol distribution is activated.

   In order to lower the computational boarden, we have chosen to modelize the activated distribution as a monomodal distribution: the activated diameter is $d_{activ} = 0.7\mu m$ and the activated aerosols are mapped to a monomodal distribution of median diameter 0.4 μm and of variance 1.8 μm. The tests in [Fahey, 2003] illustrate the low impact of the choice made for this distribution.

   The cloud droplets have a fixed size with a default diameter $d_c = 20\mu m$.

   The chemical composition of the cloud droplet is then this of the activated aerosols.

2. aqueous-phase chemistry and mass transfer between the gaseous phase and the cloud droplet is then solved. Part of the mass transfer is solved dynamically, part is supposed to have reached the Henry's equilibrium.

3. the cloud droplet distribution is then mapped to the initial aerosol distribution.

Diphasic model

c_a and c_g stand for the concentrations in aqueous phase and in gas, respectively. The diphasic model is then given by the following evolution

system:

$$\begin{aligned} \frac{dc_g}{dt} &= \chi_g(c_g) + k_{mt}(\frac{c_a}{HRT} - c_g) \\ \frac{dc_a}{dt} &= \chi_a(c_a) - Lk_{mt}(\frac{c_a}{HRT} - c_g) \end{aligned} \tag{1.32}$$

where χ_g and χ_a are the reaction rates in gas phase and in aqueous phase, respectively. H is the Henry's constant, L is the liquid water content and k_{mt} is the parameterized coefficient for kinetic mass transfer.

The aqueous-phase model is described in [Strader et al., 1998]. It contains 18 gas-phase species and 28 aqueous-phase species. Aqueous-phase chemistry is modelized by a chemical mechanism of 99 chemical reactions and 17 equilibria (for ionic dissociation). We refer to table 1.2.

We distinguish the following status for the species:

- the species to be dynamically solved (the evolution equations are integrated along time);
- the species supposed to satisfy Henry's equilibrium for mass transfer (see below);
- the species for which the diphasic process are supposed not to modify the concentrations (the concentrations are kept constant);
- the species that are supposed to satisfy a Quasi Steady State Assumption (QSSA) and whose concentrations can be neglected;
- the gaseous species that are supposed to be dissolved.

Metal ions

4 metal ions are taken into account: Fe^{3+}, Mn^{2+}, Na^{+} and Ca^{2+}. The first three ions are computed as a fraction of "salt" in the activated aerosol (from Na), the last one is computed as a fraction of crustal content (MD).

Mass transfer

Mass transfer for the 17 species in gas phase is given by the following parameteization:

$$\frac{1}{k_{mt}} = \frac{r_c^2}{3D^g} + \frac{4r_c}{3\bar{c}^g\alpha} \tag{1.33}$$

Aqueous phase	Status	Gas phase	Status
S(IV)	dynamic	SO_2	dynamic
S[VI)	dynamic	H_2SO_4	dissoute
N(III)	equilibrium	HNO_2	equilibrium
N(V)	dynamic	HNO_3	dissolved
CO_2	equilibrium	CO_2	constant
H_2O_2	dynamic	H_2O_2	dynamic
HCHO	dynamic	HCHO	dynamic
HCOOH	dynamic	HCOOH	dynamic
NO	constant	NO	constant
NO_2	constant	NO_2	constant
O_3	constant	O_3	constant
PAN	constant	PAN	constant
HCl	dynamic	HCl	dissolved
OH	QSSA	OH	QSSA
HO_2	QSSA	HO_2	QSSA
NO_3	QSSA	NO_3	QSSA
NH_3	dynamic	NH_3	dynamic
CH_3O_2	constant	CH_3O_2	constant
$ClOH^-$	QSSA		
SO_4^-	QSSA		
SO_5^-	QSSA		
HSO_5^-	dynamic		
HMSA	dynamic		
CO_3^-	QSSA		
Na^+	constant		
Fe^{3+}	constant		
Mn^{2+}	constant		
Ca^{2+}	constant		

Table 1.2: Status for the species of the diphasic model

For each species, D^g is the diffusion coefficient in the gas phase, $\bar{c}^g$ is the thermal velocity and α is the accomodation coefficient. r_c is the radius of the cloud droplet. A part of mass transfer is very fast and an equilibrium is quickly reached (see for instance [Djouad et al., 2003b]):

$$c_a = HRT\, c_g \tag{1.34}$$

Computation of pH

The reversible reactions of ionic dissociation are supposed to be at equilibrium (they are very fast). The Henry's constants are then replaced by the so-called Henry's effective constants, as a function of H^+ concentration.

If the species XH (typically HNO_2) is at Henry's equilibrium and participates in the reaction of ionic dissociation

$$\mathrm{XH} \rightleftharpoons \mathrm{X^-} + \mathrm{H^+}$$

we have the following relations:

$$[\mathrm{XH}] = (\mathrm{HRT})[(\mathrm{XH})_\mathrm{g}]\ , \quad \frac{[\mathrm{X^-}][\mathrm{H^+}]}{[\mathrm{XH}]} = \mathrm{K} \tag{1.35}$$

where K is the equilibrium constant. With the constraint of mass conservation $[\mathrm{XH}] + [(\mathrm{XH})_\mathrm{g}] = [\Sigma]$ (initial mass), one gets:

$$[\mathrm{XH}] = \frac{[\mathrm{H^+}][\Sigma]}{[\mathrm{H^+}] + \mathrm{K}}\ , \quad [\mathrm{X^-}] = \frac{\mathrm{K}[\Sigma]}{[\mathrm{H^+}] + \mathrm{K}} \tag{1.36}$$

The computation of H^+ is made with the electroneutrality relation written as :

$$f_{\mathrm{electroneutrality}}(\mathrm{H^+}) = 0 \tag{1.37}$$

This nonlinear algebraic equation is solved with the bisection method. If no convergence occurs, we take a default value $pH = 4.16$.

Numerics for the diphasic equations

We use a *splitting* method, the gas-phase chemistry (given by χ_g) being solved elsewhere (in the gas-phase module of the Chemistry-Transport Model). The other terms are solved with an appropriate numerical scheme: DVODE or ROS2 (following [Djouad et al., 2002]).

1.2.5 Formation of the Semi Volatile Organic Compounds

Principle

The oxydation of COV lead to species that have more and more complicated chemical functions, high polarizations and lower saturation vapor pressure, the Semi Volatile Organic Compounds (SVOC).

The current version of the aerosol models MAM and SIREAM use a "two-products" formulation. The gas-phase chemical mechanism RACM has been extended by adding SVOC as products in some oxydation reactions on the basis of the SORGAM model ([Schell et al., 2001, Schell, 2000]).

Gas-phase reactions

Two products (among 8 classes of SVOC) have been added to some reactions of oxydation by OH, O_3 and NO_3 (table 1.3).

VOC	product P_1	product P_2
Aromatic	ARO_1	ARO_2
α-Apinen	API_1	API_2
Limonen	LIM_1	LIM_2
Alken	ALK_1	
Oléfin	OLE_1	

Table 1.3: Classes of SVOC added to RACM.

A reaction under the form

$$\mathrm{COV} + \mathrm{Ox} \longrightarrow \mathrm{P}$$

where Ox is OH, O_3 or NO_3 has been modified to

$$\mathrm{COV} + \mathrm{Ox} \longrightarrow \mathrm{P} + \alpha_1 \mathrm{P}_1 + \alpha_2 \mathrm{P}_2$$

with P_1 and P_2 stand for some SVOC.

The set of modified reactions is given in table 1.4.

Partition

Let n_{OM} be the number of organic species in the aerosol mixture (this includes primary and secondary species).

COV	Ox	"Double product"
HC_8	OH	0.048 ALK_1
OLT	OH	0.008 OLE_1
OLI	OH	0.008 OLE_1
API	OH	0.006384 API_1 + 0.054948 API_2
LIM	OH	0.037164 LIM_1 + 0.056316 LIM_2
TOL	OH	0.039 ARO_1 + 0.108 ARO_2
XYL	OH	0.039 ARO_1 + 0.108 ARO_2
CSL	OH	0.039 ARO_1 + 0.108 ARO_2
CSL	NO_3	0.039 ARO_1 + 0.108 ARO_2
OLT	NO_3	0.008 OLE_1
OLI	NO_3	0.008 OLE_1
OLT	O_3	0.008 OLE_1
OLI	O_3	0.008 OLE_1
API	O_3	0.021588 API_1 + 0.185811 API_2
LIM	O_3	0.125673 LIM_1 + 0.190437 LIM_2

Table 1.4: Modifications of RACM. The chemical species are detailed in [Stockwell et al., 1997].

We assume that the organic species constitute an *ideal mixture*. We have therefore for species i:

$$(q_i)_g = \gamma_i \, (x_i)_a \, q_i^{sat} \tag{1.38}$$

where q_i^{sat} is the saturation mass concentration of species i in a pure mixture, $(x_i)_a$ is the molar fraction of species i in the organic mixture and γ_i is the activity coefficient of species i in the organic mixture (supposed to be 1 by default).

$(x_i)_a$ is computed through:

$$(x_i)_a = \frac{\frac{(q_i)_a}{M_i}}{\frac{q_{OM}}{M_{OM}}} = \frac{\frac{(q_i)_a}{M_i}}{\sum_{j=1}^{j=n_{OM}} \frac{(q_j)_a}{M_j} + \frac{(q_{POA})_a}{M_{POA}}} \tag{1.39}$$

with q_{OM} the total concentration of organic matter (primary and secondary) in aerosols. The molar mass M_i of component i is expressed in μg/mol (in the same unit as the mass concentrations q_i); M_{OM} is the aver-

age molar mass for organic matter in μg/mol. POA stands for the primary organic matter, supposed not to evaporate.

q_i^{sat} is computed from the saturation vapor pressure as:

$$q_i^{sat} = \frac{M_i}{RT} p_i^{sat} \tag{1.40}$$

A similar way to proceed is to define the partitioning coefficient K_i (in $\mathrm{m}^3/\mu g$) as:

$$K_i = \frac{(q_i)_a}{q_{OM}(q_i)_g} \tag{1.41}$$

K_i can be computed from the thermodynamical conditions and the saturation vapor pressure through:

$$K_i = \frac{RT}{p_i^{sat}\gamma_i(M_{OM})} \tag{1.42}$$

The saturation vapor pressure $p_i^{sat}(T)$ is given by the Clausius-Clapeyron law:

$$p_i^{sat}(T) = p_i^{sat}(298\,K) \exp\left(-\frac{\Delta H_{vap}}{R}(\frac{1}{T} - \frac{1}{298})\right) \tag{1.43}$$

with ΔH_{vap} the vaporization enthalpy. Some data are reported in Table 1.5.

Species	$p_i^{sat}(298\,K)$ [Pa]	ΔH_{vap} [J/mol]	Molar mass [g/mol]
ARO_1	5.710^{-5}	1560.	150.
ARO_2	1.610^{-3}	1560.	150.
ALK_1	5.010^{-6}	1560.	140.
OLE_1	5.010^{-6}	1560.	140.
API_1	4.010^{-6}	1560.	184.
API_2	1.710^{-4}	1560.	184.
LIM_1	2.510^{-5}	1560.	200.
LIM_2	1.210^{-4}	1560.	200.

Table 1.5: Data used for the SVOC.

Computing the themodynamical equilibria

Local equilibrium The mass concentration of a gas at local equilibrium with the aerosol mixture is given by equation (1.38).

Global equilibrium The global equilibrium between a gas and the aerosol mixture is given by equation (1.38) and mass conservation:

$$\sum_{j=1}^{j=n_{OM}} (q_j)_a + (q_j)_a = (q_j)_{tot} \tag{1.44}$$

with $(q_j)_{tot}$ the total mass concentration (for both phases) to be partitioned.

This leads, through equation (1.39), to a system of n_{OM} algrebraic equations of second degree under the form:

$$-a_i \left((q_i)_a\right)^2 + b_i (q_i)_a + c_i = 0 \tag{1.45}$$

The coefficients depend on concentrations $\{(q_j)_a\}_{j \neq i}$ through:

$$a_i = \frac{1}{M_i} \ , \quad b_i = \frac{q_i^{sat}}{M_i} - \Sigma_i \ , \quad c_i = q_i^{sat} \Sigma_i \tag{1.46}$$

with $\Sigma_i = \sum_{j=1, j \neq i}^{j=n_{OM}} \frac{(q_j)_a}{M_j} + \frac{(q_{POA})_a}{M_{POA}}$.

The resulting system is solved by an iterative approach with a fixed point algorithm. Each equation of second degree is solved in an exact way: the only positive root is computed for each equation (1.45).

1.2.6 Heterogeneous reactions

The reactions at the surface of condensed matter (aerosols or fog and cloud droplets) may have a significant impact for tropospheric chemistry, especially for ozone. Following Jacob ([Jacob, 2000]), these processes are usually parameterized as first-order reactions:

$$\mathrm{HO_2} \xrightarrow{\text{condensed matter}} 0.5\mathrm{H_2O_2} \tag{R 1}$$

$$\mathrm{NO_2} \xrightarrow{\text{condensed matter}} 0.5\,\mathrm{HONO} + 0.5\,\mathrm{HNO_3} \tag{R 2}$$

$$\mathrm{NO_3} \xrightarrow{\text{condensed matter}} \mathrm{HNO_3} \tag{R 3}$$

$$\mathrm{N_2O_5} \xrightarrow{\text{condensed matter}} 2\,\mathrm{HNO_3} \tag{R 4}$$

As explained above, for cloud droplets, only the heterogeneous reaction for N_2O_5 is taken into account.

Kinetic rates for heterogeneous reactions

The first-order kinetic rate is computed for gas-phase species X_i with:

$$k_i = \left(\frac{a}{D_i^g} + \frac{4}{\bar{c}_i^g \gamma} \right)^{-1} S_a \tag{1.47}$$

a is the particle radius, D_i^g the molecular diffusion coefficient in the air, $\bar{c}_i^g$ the thermal velocity in the air, γ the reaction probability and S_a the available surface for condensed matter per air volume.

γ strongly depends on the chemical composition and on the aerosol size. The parameterizations advocated in [Jacob, 2000] have a focus on ozone. We have therefore decided to keep the variation ranges for these parameters in order to evaluate the resulting uncertainties (tableau 1.6).

	Default value	variation range
γ_{HO_2}	0.2	[0.1-1]
γ_{NO_2}	10^{-4}	[10^{-6}-10^{-3}]
γ_{NO_3}	10^{-3}	[2.10^{-4}-10^{-2}]
$\gamma_{N_2O_5}$	0.03	[0.1-1]

Table 1.6: Default values and variation ranges for γ (heterogeneous reactions).

The initial recommended value of γ_{NO_3} (0.1, in [Jacob, 2000]), lead to too high values of nitrate inside aerosols. After discussion with D.Jacob and members of his team, we have decided to take the value $\gamma_{NO_3} = 0.03$.

Coupling to the gas-phase mechanism

In the host Chemistry-Transport Model POLAIR3D, we have chosen to couple these reactions to the gas-phase chemical mechanism. One motivation is the numerical stability (tests not reported here). The kinetic rates are then computed with a function of the ATMODATA library on the basis on the computed size distribution for aerosols. The cloud droplets are supposed to have a constant diameter $d_c = 20\,\mu m$. Tests in [Fahey, 2003] indicate that the results are not sensitive to this value.

Chapter 2

The SIze REsolved Aerosol Model (SIREAM)

Summary:
In this chapter we describe the size resolved aerosol model SIREAM. *We particularly focus on the condensation/evaporation process.*

2.1 Some remarks for the size-resolved model

In the sequel we only deal with aerosol dynamics, i.e. with nucleation, condensation/evaporation and coagulation processes. Other processes are modelized and computed in the host 3D model.

Let us first focus on some model characteristics before entering into the numerical resolution :

- distinction between external and internal composition;
- dry mass logarithmic scale description;
- aerosol specific mass computation with respect to its composition;
- ion hydronium H^+ flux limitation for condensation/evaporation;
- dry aerosol thermodynamics.

2.1.1 Model Formulation

External composition, internal composition

One may distinguish between

- the *external composition* composed of chemical components $\{\mathrm{X_i}\}_{i=1,n_e}$, each of these refer to one *family* of chemical species, gathering all physical and chemical states the component may take in the condensed phase (liquid, solid or ionic).

- the *internal composition* composed of chemical components $\{\mathrm{X_{ij}^{int}}\}_j$ which gives the distribution of each $\mathrm{X_i}$ between its various chemical and physical states.

  We note n_c the total number of chemical species in one aerosol (dissolved, ionic or solid).

GDE equations for external composition

Let us recall the GDE equations applied to external composition:

- Aerosol number distribution :

$$\begin{aligned}\frac{\partial n}{\partial t}(m,t) =& \frac{1}{2}\int_{m_0}^{m-m_0} K(u,m-u)n(u,t)n(m-u,t)\,du \\ &- n(m,t)\int_{m_0}^{\infty} K(m,u)n(u,t)\,du - \frac{\partial(I_0 n)}{\partial m}\end{aligned} \tag{2.1}$$

- Aerosol mass distribution of each external component $\mathrm{X_i}$:

$$\begin{aligned}\frac{\partial q_i}{\partial t}(m,t) =& \int_{m_0}^{m-m_0} K(u,m-u)q_i(u,t)n(m-u,t)\,du \\ &- q_i(m,t)\int_{m_0}^{\infty} K(m,u)n(u,t)\,du \\ &- \frac{\partial(I_0 q_i)}{\partial m} + I_i(m_1,\ldots,m_{n_c},t)n(m,t)\end{aligned} \tag{2.2}$$

- Gaseous concentration in semi-volatile component $\mathrm{X_i}$:

$$\frac{\partial c_i^g}{\partial t} = -m_i(m_0,t)J_0(t) - \int_{m_0}^{\infty}(I_i n)(m,t)\,dm \tag{2.3}$$

- Mass conservation in $\mathrm{X_i}$:

$$\int_{m_0}^{\infty} q_i(m,t)\,dm + c_i^g \triangleq K_i \tag{2.4}$$

- Limit conditions at m_0 :

$$(I_0 n)(m_0, t) = J_0(t) \ , \quad (I_0 q_i)(m_0, t) = m_i(m_0, t) J_0(t) \tag{2.5}$$

where K_i is the total mass of $\mathrm{X_i}$ in the whole gas/aerosol system.

As the internal chemistry conserves total mass in $\mathrm{X_i}$, it does not appear in GDE equations.

Internal composition

The internal composition is determined by thermodynamic equilibrium, solved by ISORROPIA ([Nenes et al., 1998]) model for inorganic phase and SORGAM ([Schell et al., 2001]) for organic phase.

Water processing

Due to its relative abundance in the atmosphere, water reaches equilibrium between gas and aerosol phases faster than any other component, $I_{\mathrm{H_2O}} \simeq 0$.

Then water is not solved by one equation (2.4) but through thermodynamic resolution (ZSR relation).

Consequently the aerosol mass m now refers to its *dry* mass. In the same way the c/e growth rate I_0 no longer takes into account the water mass transfer.

2.1.2 Logarithmic scale

In order to reduce the wide range of magnitudes for the size distribution and to better represent small aerosols, the logarithm $x = \ln m$ of dry aerosol mass m is used instead of m ([Wexler et al., 1994, Meng et al., 1998, Gaydos et al., 2003]).

The number and mass densities with respect to x are respectively defined by (we keep the same notations for new densities for the sake of clarity):

$$n(x,t)\,dx \triangleq n(m,t)\,dm \ , \quad q_i(x,t)\,dx \triangleq q_i(m,t)\,dm \tag{2.6}$$

They are linked to the previous densities through:

$$n(x,t) = m n(m,t) \ , \quad q_i(x,t) = m q_i(m,t) \tag{2.7}$$

The number density $n(x,t)$ is usually expressed in $\#\mathrm{aerosols}.m^{-3}$ and mass densities $q_i(x,t)$ in $\mu g.m^{-3}$.

The GDE equations become :

- Aerosol number distribution :

$$\frac{\partial n}{\partial t}(x,t) = \int_{x_0}^{\tilde{x}} K(y,z)n(y,t)n(z,t)\,dy \\ - n(x,t)\int_{x_0}^{\infty} K(x,y)n(y,t)\,dy - \frac{\partial(H_0 n)}{\partial x} \tag{2.8}$$

- Aerosol mass distribution of each external component $\mathrm{X_i}$:

$$\frac{\partial q_i}{\partial t}(x,t) = \int_{x_0}^{\tilde{x}} K(y,z)[q_i(y,t)n(z,t) + n(y,t)q_i(z,t)]\,dy \\ - q_i(x,t)\int_{x_0}^{\infty} K(x,y)n(y,t)\,dy - \frac{\partial(H_0 q_i)}{\partial x} + (I_i n)(x,t) \tag{2.9}$$

- Gaseous concentration in semi-volatile component $\mathrm{X_i}$:

$$\frac{dc_i^g}{dt}(t) = -m_i(x_0,t)J_0(t) - \int_{x_0}^{\infty}(I_i n)(x,t)\,dx \tag{2.10}$$

- Mass conservation in $\mathrm{X_i}$:

$$c_i^g(t) + \int_{x_0}^{\infty} q_i(x,t)\,dx = K_i \tag{2.11}$$

- Limit conditions at $x_0 = \ln m_0$:

$$(H_0 n)(x_0,t) = J_0(t)\ , \quad (H_0 q_i)(x_0,t) = m_i(x_0,t)J_0(t) \tag{2.12}$$

where H_0, expressed in s^{-1}, refers to the logarithmic growth rate :

$$H_0 = \frac{I_0}{m} \tag{2.13}$$

In the sequel we will use the logarithmic formulation.

2.1.3 Aerosol specific mass

Parameterizations of coagulation and condensation/evaporation process explicitely depend on the aerosol "real" diameter d_p. But only its internal mass composition $(m_1, \ldots, m_{n_c})$ is known. It is then necessary to provide a closure scheme for the aerosol diameter.

Most of 3D models use a constant specific aerosol mass ρ_p ([Wexler et al., 1994, Pilinis and Seinfeld, 1988]) supposed to satisfy:

$$\rho_p \frac{\pi d_p^3}{6} = \sum_{i=1}^{n_c} m_i \tag{2.14}$$

Moreover, pure species specific masses may sensitively differ between organic, inorganic or inert species. That is why the organic and inorganic phases are sometimes distinguished ([Pilinis et al., 2000]) :

$$\frac{\pi d_p^3}{6} = V_{\text{inorg}} + V_{\text{org}} \ , \quad V_{\text{inorg}} = \frac{1}{\rho_p^{\text{inorg}}} \sum_{i_{\text{inorg}}} m_i \ , \quad V_{\text{org}} = \frac{1}{\rho_p^{\text{org}}} \sum_{i_{\text{org}}} m_i \tag{2.15}$$

We use here a more rigorous way to compute the aerosol volume, also used in [Jacobson, 2002], based on the internal composition.

The aerosol volume may be splitted between its solid and liquid part :

$$\frac{\pi d_p^3}{6} = V_{\text{liq}} + V_{\text{sol}} \tag{2.16}$$

As each solid represents one single phase (from a chemical point of view) the total solid aerosol volume is the sum of each solid volume :

$$V_{\text{sol}} = \sum_{i_s} \frac{m_{i_s}}{\rho_{i_s}^*} \tag{2.17}$$

where $\rho_{i_s}^*$ represents the specific mass of pure component X_{i_s}.

The liquid aerosol phase is a concentrated mixing of inorganic species, whose volume is a non linear function of its inorganic internal composition:

$$V_{\text{liq}} = \sum_{i_l} V_{i_l} n_{i_l} \tag{2.18}$$

where V_{i_l} is the partial molar volume of ionic or dissolved species X_{i_l} and n_{i_l} is the molar quantity in X_{i_l}. Due to some molecular processes wihthin the mixture (e.g. volume exclusion), the partial molar volume is a complicated function of internal composition itself.

Nevertheless this latter does not widely change with respect to internal composition so that it can be approximated by :

$$V_{i_l} \simeq \frac{M_i}{\rho_{i_l}^*} \tag{2.19}$$

where M_i and $\rho_{i_l}^*$ respectively denote the molar mass of X_i and specific mass of a pure liquid solution of X_i.

The table 2.1 gathers specific masses for pure components.

X_i	ρ_i	X_i	ρ_i^*
EC	2.25	NH_4Cl	1.53
MD(Si)	2.33	$NaNO_3$	2.26
Na	0.97	$NaHSO_4$	2.74
H_2SO_4	1.84	Na_2SO_4	2.7
HNO_3	1.5	NH_4NO_3	1.725
HCl	1.15	NH_4HSO_4	1.78
NH_3	0.91	$(NH_4)_2SO_4$	1.77
H_2O	1.0	$(NH_4)_3H(SO_4)_2$	1.77
NaCl	2.165	SOA	1.3

Table 2.1: Specific mass for some pure component (in g.cm^{-3}).

2.1.4 Hydronium ion flux limitation during condensation/evaporation

When aerosols are in liquid state, the condensation of one acid component may free hydronium ions and that of a basic component may catch hydronium ions. Thus the condensation/evaporation process may have an effect on the aerosol pH. The hydronium ion flux induced by c/e is the following one :

$$J_{H^+} = 2J_{H_2SO_4} + J_{HCl} + J_{HNO_3} - J_{NH_3} \tag{2.20}$$

with J_i the molar flux in species X_i. The pH evolution due to c/e can be very stiff and cause instabilities, due to the very small quantity n_{H^+} of hydronium ions inside the aerosol. The hydronium ion flux is then limited to a given fraction A of the hydronium ions quantity ([Pilinis et al., 2000]) :

$$|J_{H^+}| \leq An_{H^+} \tag{2.21}$$

where A is usually taken arbitrarily between 0.01 and 0.1. A is a numerical parameter which has no physical meaning and does not influence the final state of c/e. It just modifies the numerical path to reach this state. This can be illustrated in figure 2.1: the flux limitation comes to project the initial state to the line of slope $+A$.

We now detail how this limitation is achieved. The mass transfer rate for inorganic species X_i (H_2SO_4, HNO_3, HCl and NH_3) is:

$$I_i = a_i(c_i - \eta c_i^{eq}) \ , \quad a_i = \frac{2\pi D_i d_p f(K_{n_i}, \alpha_i)}{M_i} \tag{2.22}$$

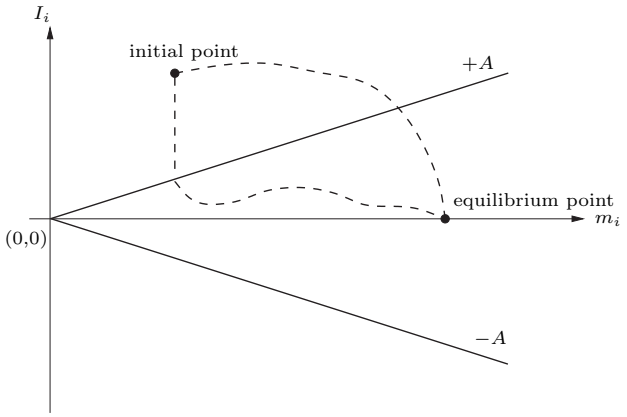

Figure 2.1: Limitation of flux

The gas equilibrium concentration of sulfate is usually neglected: $c^{eq}_{H_2SO_4} = 0$.

The flux limitation (2.21) comes to inequality :

$$\begin{aligned} &|2a_{H_2SO_4}c^g_{H_2SO_4} + a_{HNO_3}(c^g_{HNO_3} - \eta c^{eq}_{HNO_3}) \\ &+ a_{HCl}(c^g_{HCl} - \eta c^{eq}_{HCl}) - a_{NH_3}(c^g_{NH_3} - \eta c^{eq}_{NH_3})| \leq An_{H^+} \end{aligned} \tag{2.23}$$

When this condition is not met, we introduce a correcting factor Q such that:

$$\begin{aligned} &2a_{H_2SO_4}c^g_{H_2SO_4} + a_{HNO_3}(c^g_{HNO_3} - \eta c^{eq}_{HNO_3}Q) + a_{HCl}(c^g_{HCl} - \eta c^{eq}_{HCl}Q) \\ &- a_{NH_3}(c^g_{NH_3} - \eta c^{eq}_{NH_3}/Q) = (-1)^p An_{H^+} \end{aligned} \tag{2.24}$$

where p equals 1 if the hydronium flux is positive, 0 otherwise.

Equality (2.24) leads to a second order equation in Q :

$$\alpha Q^2 + \beta Q - \gamma = 0 \tag{2.25}$$

with

$$\begin{aligned} \alpha &= \eta(a_{HNO_3}c^{eq}_{HNO_3} + a_{HCl}c^{eq}_{HCl}) \\ \beta &= (-1)^p An_{H^+} - 2a_{H_2SO_4}c^g_{H_2SO_4} - a_{HNO_3}c^g_{HNO_3} - a_{HCl}c^g_{HCl} + a_{NH_3}c^g_{NH_3} \\ \gamma &= \eta a_{NH_3}c^{eq}_{NH_3} \end{aligned} \tag{2.26}$$

Several cases may appear:

- if $c^{eq}_{\mathrm{HNO_3}} > 0$ and $c^{eq}_{\mathrm{HCl}} > 0$, then $\alpha > 0$:
  - if $c^{eq}_{\mathrm{NH_3}} > 0$:
$$Q = \frac{-\beta + \sqrt{\beta^2 + 4\alpha\gamma}}{2\alpha} \tag{2.27}$$
  - if $c^{eq}_{\mathrm{NH_3}} = 0$ equation (2.25) is reduced to $\alpha Q + \beta = 0$:
    - if $\beta \geq 0$:
$$Q = 1 \tag{2.28}$$
    - if $\beta < 0$:
$$Q = \frac{-\beta}{\alpha} \tag{2.29}$$
- if $c^{eq}_{\mathrm{HNO_3}} = 0$ and $c^{eq}_{\mathrm{HCl}} = 0$, equation (2.25) reduces to $\beta Q - \gamma = 0$:
  - if $c^{eq}_{\mathrm{NH_3}} = 0$ then $\gamma = 0$:
$$Q = 1 \tag{2.30}$$
  - if $c^{eq}_{\mathrm{NH_3}} > 0$ then $x = 0$:
    - if $\beta > 0$:
$$Q = \frac{\gamma}{\beta} \tag{2.31}$$
    - if $\beta \leq 0$:
$$Q = 1 \tag{2.32}$$

It can be shown that cases for which $Q = 1$ are naturally limited by condensation process.

2.1.5 Equilibrium concentrations for solid aerosols

When the aerosols become solid, fluxes of inorganic species are governed by gas/solid reactions at the aerosol surface :

$$(\mathrm{NH_4NO_3})_\mathrm{s} \rightleftharpoons (\mathrm{NH_3})_\mathrm{g} + (\mathrm{HNO_3})_\mathrm{g} \tag{R 5}$$

$$(\mathrm{NH_4Cl})_\mathrm{s} \rightleftharpoons (\mathrm{NH_3})_\mathrm{g} + (\mathrm{HCl})_\mathrm{g} \tag{R 6}$$

$$(\mathrm{NaCl})_\mathrm{s} + (\mathrm{HNO_3})_\mathrm{g} \rightleftharpoons (\mathrm{NaNO_3})_\mathrm{s} + (\mathrm{HCl})_\mathrm{g} \tag{R 7}$$

The equilibrium constants are :

$$K_1 = c^{eq}_{\mathrm{NH_3}} c^{eq}_{\mathrm{HNO_3}} \ , \quad K_2 = c^{eq}_{\mathrm{NH_3}} c^{eq}_{\mathrm{HCl}} \ , \quad K_3 = \frac{c^{eq}_{\mathrm{HCl}}}{c^{eq}_{\mathrm{HNO_3}}} \tag{2.33}$$

In this case, thermodynamic models are not efficient to find gas equilibrium concentrations c_i^{eq} for inorganic species X_i. Consider for example a pure NH_4NO_3 solid aerosol, the only thermodynamic equation is then :

$$K_1 = c^{eq}_{\mathrm{NH_3}} c^{eq}_{\mathrm{HNO_3}} \tag{2.34}$$

for which there exists an infinity of solutions $(c^{eq}_{\mathrm{NH_3}}, c^{eq}_{\mathrm{HNO_3}})$.

Various approaches have been developed to remedy this indecisiveness ([Jacobson et al., 1996],[Wexler and Seinfeld, 1990, Meng and Seinfeld, 1996]). We present in the sequel the one we use ([Pilinis et al., 2000]).

The ISORROPIA model is used to determine which solid species are present in the aerosol. If one solid species is present then its gas/solid surface reaction may be active :

- (R 5) if NH_4NO_3 exists or if $K_1 < c^g_{\mathrm{NH_3}} c^g_{\mathrm{HNO_3}}$;
- (R 6) if NH_4Cl exists or if $K_2 < c^g_{\mathrm{NH_3}} c^g_{\mathrm{HCl}}$;
- (R 7) if NaCl and $NaNO_3$ are presents, or if $NaNO_3$ is present and $K_3 < c^g_{\mathrm{HCl}}/c^g_{\mathrm{HNO_3}}$, or if NaCl is present and $K_3 > c^g_{\mathrm{HCl}}/c^g_{\mathrm{HNO_3}}$.

Furthermore, when the aerosol is solid, the inorganic fluxes are constrained by electroneutrality, which brings another equation :

$$2J_{\mathrm{H_2SO_4}} + J_{\mathrm{HCl}} + J_{\mathrm{HNO_3}} = J_{\mathrm{NH_3}} \tag{2.35}$$

that enables to close the system.

When the gaseous sulfate condenses onto aerosols, one has first to take into account the following reactions:

$$(\mathrm{NaCl})_\mathrm{s} + (\mathrm{H_2SO_4})_\mathrm{g} \longrightarrow (\mathrm{Na_2SO_4})_\mathrm{s} + 2\,(\mathrm{HCl})_\mathrm{g} \tag{R 8}$$

$$(\mathrm{NaNO_3})_\mathrm{s} + (\mathrm{H_2SO_4})_\mathrm{g} \longrightarrow (\mathrm{Na_2SO_4})_\mathrm{s} + 2\,(\mathrm{HNO_3})_\mathrm{g} \tag{R 9}$$

$$2\,(\mathrm{NH_4NO_3})_\mathrm{s} + (\mathrm{H_2SO_4})_\mathrm{g} \longrightarrow ((\mathrm{NH_4})_2\mathrm{SO_4})_\mathrm{s} + 2\,(\mathrm{HNO_3})_\mathrm{g} \tag{R 10}$$

$$2\,(NH_4Cl)_s + (H_2SO_4)_g \longrightarrow ((NH_4)_2SO_4)_s + (HCl)_g \qquad (R\,11)$$

which are not equilibrium reactions due to the high sulfate reactivity. Three cases have to be distinguished :

1. if NaCl or NH_4Cl are presents, then $J_{HNO_3} = J_{NH_3} = 0$ and $J_{HCl} = -2J_{H_2SO_4}$ from electroneutrality (2.35);

2. if $NaNO_3$ or NH_4NO_3 exist, then $J_{HCL} = J_{NH_3} = 0$ and $J_{HNO_3} = -2J_{H_2SO_4}$ from (2.35);

3. if none of solids NaCl, NH_4Cl, $NaNO_3$ and NH_4NO_3 are present then $J_{HCl} = J_{HNO_3} = 0$ and only the gaseous sulfate and ammonia may condense. The gas equilibrium concentration for ammonia $c^{eq}_{NH_3}$ satisfies the electroneutrality condition $2J_{H_2SO_4} = J_{NH_3}$. Nevertheless in this last case, the electroneutrality condition may not be met as sulfate can only condense, and there may have not enough gas ammonia to equilibrate the sulfate flux. This happens if

$$2J_{H_2SO_4} \leq 2\pi D_{NH_3} d_p f(K_n, \alpha) \frac{c^g_{NH_3}}{M_{NH_3}} \qquad (2.36)$$

The electroneutrality is no longer met and $c^{eq}_{NH_3}$ is set to zero.

2.2 Numerical simulation

2.2.1 Numerical approach

Several numerical algorithms have been tested ([Debry, 2004]). Our final choice has been oriented toward methods that ensure stability and low CPU cost.

Here are the main characteristics of our numerical strategy based on :

- a splitting approach for coagulation and condensation/evaporation;
- size-binning methods which remains stable even with a few discretization points, on the contrary to spectral methods;
- a lagrangian treatment of condensation/evaporation in order to avoid numerical diffusion with eulerian schemes due to the small number of discretization points in 3D models.

Treatment of each physical process

The nucleation process is not a numerical issue and is solved simultaneously with condensation/evaporation. The splitting sequence goes from the slowest process to the fastest one (first coagulation and then condensation/evaporation-nucleation).

Discretization of the aerosol distribution

The aerosol mass distribution is discretized in n_s bins $[x^j, x^{j+1}]$, for which integrated quantities are defined :

$$N^j(t) = \int_{x^j}^{x^{j+1}} n(x,t)\,dx \ , \quad i = 1, \ldots, n_e \ , \ Q_i^j = \int_{x^j}^{x^{j+1}} q_i(x,t)\,dx \quad (2.37)$$

2.2.2 Coagulation

Coagulation is solved by the so-called *size binning* method. Equations (2.8) and (2.9) are integrated over each bin, giving:

$$\begin{aligned} \frac{dN^k}{dt}(t) =& \frac{1}{2}\sum_{j_1=1}^{k}\sum_{j_2=1}^{k} f_{j_1 j_2}^k K_{j_1 j_2} N^{j_1} N^{j_2} - N^k \sum_{j=1}^{n_s} K_{kj} N^j \\ i = 1, \ldots, n_e \ , \quad \frac{dQ_i^k}{dt}(t) =& \sum_{j_1=1}^{k}\sum_{j_2=1}^{k} f_{j_1 j_2}^k K_{j_1 j_2} Q_i^{j_1} N^{j_2} - Q_i^k \sum_{j=1}^{n_s} K_{kj} N^j \end{aligned} \quad (2.38)$$

$K_{j_1 j_2}$ is an approximation of the coagulation kernel between bins j_1 and j_2.

Closure scheme for partition coefficients

These latest equations make appear partition coefficients $f_{j_1 j_2}^k$ that takes into account the fact that coagulation between 2 bins may recover one or more sections. Then $f_{j_1 j_2}^k$ represents the fraction of aerosol coagulations between bins j_1 and j_2 which fall into bin k. As these coefficients only depend on the choosen size discretization they can be computed once for all.

There are several ways to compute these coefficients depending on the assumed shape of continuous densities inside each bin (closure scheme). According to numerical tests ([Debry, 2004]) we choose a closure scheme similar to [Fernàndez-Dìaz et al., 2000].

Time integration

The system (2.38) can be rewritten as an evolution equation :

$$\frac{dy}{dt} = f(y,t) \ , \quad y^T = (N^1, \ldots, N^{n_s}, Q_1^1, \ldots, Q_1^{n_s}, \ldots, Q_{n_e}^1, \ldots, Q_{n_e}^{n_s}) \quad (2.39)$$

As coagulation is not a stiff process, we solve it by a second order explicit scheme ETR (with a timestep Δt):

$$\tilde{y}^{t+1} = y^t + \Delta t f(y^t, t) \ , \quad y^{t+1} = y^t + \frac{\Delta t}{2}\Big(f(y^t,t) + f(\tilde{y}^{t+1}, t+\Delta t) \Big) \quad (2.40)$$

The time step Δt is adjusted as follows :

$$\Delta t_{\text{new}} = \Delta t_{\text{old}} \sqrt{\frac{\varepsilon_r |y^{t+1}|_2}{|\tilde{y}^{t+1} - y^{t+1}|_2}} \quad (2.41)$$

where ε_r is a user parameter, usually included between 0.5 and 0.01. The higher ε_r is , the faster Δt increases.

2.2.3 Condensation/evaporation-nucleation

A lagrangian approach is used for condensation/evaporation-nucleation. Equations obtained through this approach are solved by an implicit time solver.

Let us first introduce the characteristic curves that motivate the lagrangian approach.

Characteristic curves

The characteristic curves are the trajectories of aerosols within the size spectrum due to condensation/evaporation. We note $\bar{x}^j(t)$ the logarithmic size of one aerosol at time t whose initial value corresponds to point x^j of the fixed size discretization. The time evolution of $\bar{x}^j(t)$ is given by the characteristic curve equation :

$$\frac{d\bar{x}^j}{dt}(t) = H_0(\bar{x}^j, t) \ , \ \bar{x}^j(0) = x^j \quad (2.42)$$

One crucial issue is to ensure that the characteristic curves do not cross themselves. When this occurs, one has (figure 2.2):

$$\exists\, j_1,\ j_2 \ , \ t_c > 0 \ \text{ such that } \ \bar{m}^{j_1}(0) \neq \bar{m}^{j_2}(0) \text{ and } \bar{m}^{j_1}(t_c) = \bar{m}^{j_2}(t_c) \quad (2.43)$$

If this happens the following lagrangian bins formulation is no more valid. In real cases we have no proof that this does not happen ([Debry, 2004]), even we have not met such situation up to now.

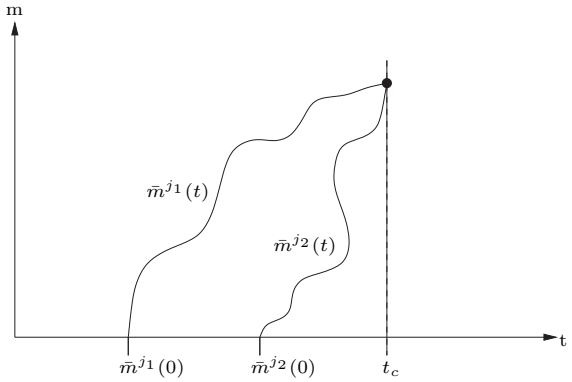

Figure 2.2: Crossing of characteristic curves

Lagrangian bins formulation

Provided that the characteristic curves do not cross, we can define integrated quantities N^j and Q_i^j for each lagrangian bin $[\bar{x}^j, \bar{x}^{j+1}]$:

$$N^j(t) = \int_{\bar{x}^j}^{\bar{x}^{j+1}} n(x,t)\,dx \ , \quad Q_i^j = \int_{\bar{x}^j}^{\bar{x}^{j+1}} q_i(x,t)\,dx \tag{2.44}$$

If at time t the characteristic curves j and $j+1$ cross, these quantities are not more defined.

Mass conservation (2.11) can be easily written under the form :

$$i = 1, \ldots, n_e \ , \quad c_i^g(t) + \sum_{j=1}^{n_s} Q_i^j(t) = K_i \tag{2.45}$$

The time derivation of integrated quantities (2.44) leads to equations

$$\frac{dN^j}{dt} = 0 \ , \quad \frac{dQ_i^j}{dt} = N^j \tilde{I}_i^j \tag{2.46}$$

with

$$\tilde{m}_i^j = \frac{Q_i^j}{N^j} \tag{2.47}$$

and $\tilde{I}_i^j$ is an approximation of the mass transfer rate I_i for species X_i in bin j. This formulation has the advantage of conserving the aerosol number concentration N^j.

For the nucleation process, the first bound x^1 is assumed to be the nucleation size, so that the lagrangian bound $\bar{x}^1$ no longer checks (2.42) but rather

$$\frac{d\bar{x}^1}{dt} = j(t) \ , \quad \bar{x}^1(0) = x^1 \tag{2.48}$$

where $j(t)$ is the growth law of the first bound due to nucleation.

The equations for the first lagangian bin have to be written under the form :

$$\frac{dN^1}{dt} = J_0(t) \ , \quad \frac{dQ_i^1}{dt} = N^1 \tilde{I}_i^1 + m_i(x^1, t) J_0(t) \tag{2.49}$$

where $[m_1(x^1, t), \ldots, m_{n_e}(x^1, t)]$ is the chemical composition of newly nucleated aerosols, also given by the nucleation process.

The lagrangian bin formulation then consists in solving equations (2.42), (2.46) and (2.49). The next section is devoted to the numerical treatment.

Interpolation of lagrangian boundaries

One also needs to solve the characteristic curves equations in order to know the boundary of each bin :

$$j = 1, \ldots, n_s + 1 \ , \quad \frac{d\bar{x}^j}{dt} = H_0(\bar{x}^j, t) \ , \quad \bar{x}^j = \ln(\bar{m}^j) \tag{2.50}$$

Notice that the c/e equations for boundaries are similar to those for integrated quantities. For $j = 1, \ldots, n_s$ and $\tilde{x}^j = \ln(\tilde{m}^j)$:

$$\frac{d\tilde{x}^j}{dt} = \tilde{H}_0^j \ , \quad \tilde{H}_0^j = \frac{\tilde{I}_0^j}{\tilde{m}^j} \ , \tag{2.51}$$

In practice we avoid solving boundary equations and interpolate boundaries from integrated quantities.

One first idea ([Koo and Pandis, 2003]) consists in performing the geometric mean of two adjacent bins. For $k = 2, \ldots, n_s$:

$$\bar{m}^k(t) = \sqrt{\tilde{m}^{k-1}(t) \tilde{m}^k(t)} \tag{2.52}$$

The outer boundaries $\bar{m}^1(t)$ and $\bar{m}^{n_s+1}(t)$ may be extrapolated as follows :

$$\bar{m}^1(t) = \frac{(\tilde{m}^1)^2}{\bar{m}^1} \ , \quad \bar{m}^{n_s+1}(t) = \frac{(\tilde{m}^{n_s})^2}{\bar{m}^{n_s}} \tag{2.53}$$

This alogrithm would have a physical meaning if equations (2.50) and (2.51) were conserving formula (2.52), which is not the case. We have therefore developed another algorithm.

The key point is to note that equations (2.50) and (2.51) are similar, and therefore that $\tilde{x}^j$ and $\bar{x}^j$ evolve in the same proportions (figure 2.3). This proportion can be assessed by $\alpha^j(t)$:

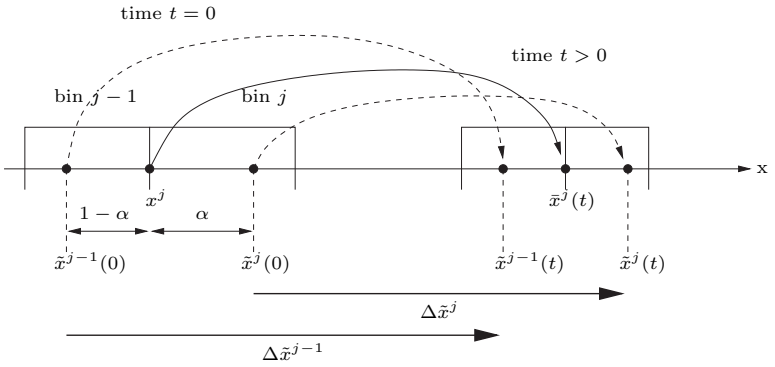

Figure 2.3: Boundary interpolation

$$j \geq 2 \ , \quad \alpha^j(t) = \frac{\bar{x}^j(t) - \tilde{x}^{j-1}(t)}{\tilde{x}^j(t) - \tilde{x}^{j-1}(t)} \tag{2.54}$$

which is only known at initial time :

$$j \geq 2 \ , \quad \alpha^j(0) = \frac{x^j - \tilde{x}^{j-1}(0)}{\tilde{x}^j(0) - \tilde{x}^{j-1}(0)} \tag{2.55}$$

The time integration over $[0, t]$ of equations (2.50) and (2.51) gives :

$$\begin{aligned} &j \geq 1 \ , \quad \bar{x}^j(t) = x^j + \Delta\bar{x}^j \ , \quad \Delta\bar{x}^j = \int_0^t H_0^j(t')\, dt' \\ &j \geq 1 \ , \quad \tilde{x}^j(t) = \tilde{x}^j(0) + \Delta\tilde{x}^j \ , \quad \Delta\tilde{x}^j = \int_0^t \tilde{H}_0^j(t')\, dt' \end{aligned} \tag{2.56}$$

The variation of each boundary $\bar{x}^j$ is then interpolated by these of its two adjacent bins $\tilde{x}^{j-1}$ and $\tilde{x}^j$:

$$j \geq 1 \ , \quad \Delta\bar{x}^j \simeq (1 - \alpha^j(0))\Delta\tilde{x}^{j-1} + \alpha^j(0)\Delta\tilde{x}^j \tag{2.57}$$

At last we assume that α^j remains constant, equal to its initial value. In the same way outer boundaries can be extrapolated.

In the sequel we will use this algorithm.

Redistribution on a fixed size grid

Using a lagrangian approach for condensation/evaporation implies to redistribute (or project) numerical and mass concentrations onto the fixed size grid of 3D model.

Les us note N and $(Q_i)_{i=1}^{n_e}$ the integrated quantities of one lagrangian bin after condensation/evaporation. We assume that this lagrangian bin is covered by two adjacent fixed sections labeled by 1 and 2.

The redistribution algorithm must be conservative for the mass distribution of species $i = 1, \ldots, n_e$:

$$Q_i = Q_i^1 + Q_i^2 \tag{2.58}$$

Two algorithms have been developed: the first algorithm ensures that the number is conserved ($N = N^1 + N^2$) while the second one ensures that the average mass is conserved (Q/N).

1. If $\bar{x}_{lo}$ and $\bar{x}_{hi}$ are the lagrangian bin boundaries after condensation/evaporation, the redistribution is performed as follows :

$$\begin{aligned} N^1 &= \frac{\bar{x}_{hi}^1 - \bar{x}_{lo}}{\bar{x}_{hi} - \bar{x}_{lo}} N \ , \ \ i = 1, \ldots, n_e \ , \ Q_i^1 = \frac{\bar{x}_{hi}^1 - \bar{x}_{lo}}{\bar{x}_{hi} - \bar{x}_{lo}} Q \\ N^2 &= \frac{\bar{x}_{hi} - \bar{x}_{lo}^2}{\bar{x}_{hi} - \bar{x}_{lo}} N \ , \ \ i = 1, \ldots, n_e \ , \ Q_i^2 = \frac{\bar{x}_{hi} - \bar{x}_{lo}^2}{\bar{x}_{hi} - \bar{x}_{lo}} Q \end{aligned} \tag{2.59}$$

   Nevertheless the average mass of aerosols in each section (Q/N) may not be conserved by this algorithm.

2. Another way to proceed consists in making the average mass conserved :

$$Q = \tilde{m} N \ , \quad Q^1 = \tilde{m}^1 N^1 \ , \quad Q^2 = \tilde{m}^2 N^2 \tag{2.60}$$

   which leads to

$$\begin{aligned} N^1 &= \frac{1 - \frac{\tilde{m}}{\tilde{m}^2}}{1 - \frac{\tilde{m}^1}{\tilde{m}^2}} N \ , \ \ i = 1, \ldots, n_e \ , \ Q_i^1 = \frac{\frac{\tilde{m}^2}{\tilde{m}} - 1}{\frac{\tilde{m}^2}{\tilde{m}^1} - 1} Q_i \\ N^2 &= \frac{1 - \frac{\tilde{m}}{\tilde{m}^1}}{1 - \frac{\tilde{m}^2}{\tilde{m}^1}} N \ , \ \ i = 1, \ldots, n_e \ , \ Q_i^1 = \frac{1 - \frac{\tilde{m}^1}{\tilde{m}}}{1 - \frac{\tilde{m}^1}{\tilde{m}^2}} Q_i \end{aligned} \tag{2.61}$$

Both schemes are available in SIREAM.

In the next section we detail the various numerical strategies to solve condensation/evaporation, which is by far the most challenging point in aerosol simulation.

2.3 Condensation/evaporation processing

Mass conservation (2.45) leads to a closed system from lagrangian equations (2.46) :

$$\frac{dQ_i^j}{dt} = a_i^j \left(K_i - \sum_{k=1}^{n_s} Q_i^j - \eta^j \ (c_i^{eq})^j \right) \tag{2.62}$$

with

$$a_i^j = 2\pi D_i d_p^j N^j f(K_{n_i}^j, \alpha_i) \ , \quad \eta^j = e^{\frac{4\sigma v_p}{R_g T d_p^j}} \tag{2.63}$$

We re-write this system in a general form :

$$\frac{dx}{dt} = f(x,t) \ , \quad x = (\underbrace{Q_1^1, \ldots, Q_{n_e}^1}_{\text{size } 1}, \ldots, \underbrace{Q_1^{n_s}, \ldots, Q_{n_e}^{n_s}}_{\text{size } n_s})^T \tag{2.64}$$

with $n_x = n_e \times n_s$ the dimension of vector x.

2.3.1 Dynamic resolution

Let $t_0, \ldots, t_n, t_{n+1} \ldots$ be the discretization times. The n^{th} time step is defined by :

$$\Delta t_n = t_{n+1} - t_n \tag{2.65}$$

We note x_n the numerical approximation of vector x at time t_n.

Aerosol thermodynamics needs to be computed for each bin at every calls of function f, so that we choose implicit algorithms in order to minimize the number of calls to function f ([Debry, 2004]).

Rosenbrock **implicit scheme**

The second order Rosenbrock scheme ([Rosenbrock, 1963]) (ROS2) is applied to the system (2.64) :

$$x_{n+1} = x_n + \frac{\Delta t_n}{2}(3k_1 + k_2) \tag{2.66}$$

where k_1 and k_2 are respectively given by :

$$\begin{aligned} [I - \gamma \Delta t_n J(f)]k_1 &= f(x_n, t_n) \\ [I - \gamma \Delta t_n J(f)]k_2 &= f(\tilde{x}_{n+1}, t_{n+1}) - 2k_1 \end{aligned} \tag{2.67}$$

with

$$\tilde{x}_{n+1} = x_n + \Delta t_n k_1 \ , \quad \gamma = 1 + \frac{1}{\sqrt{2}} \tag{2.68}$$

This scheme needs the Jacobian computation.

The time step is adjusted according to the difference between $\tilde{x}_{n+1}$ and x_{n+1} an approximation of $x(t_{n+1})$:

$$\Delta t_{n+1} \simeq \Delta t_n \sqrt{\frac{\varepsilon_r |x_{n+1}|_2}{|x_{n+1} - \tilde{x}_{n+1}|_2}} \tag{2.69}$$

The ε_r parameter represents the maximum error accepted by the user.

Jacobian computation

The ROS2 scheme needs the Jacobian of function f which is one matrix of size $n_x \times n_x$ defined by :

$$k = 1, \ldots, n_x \ , \quad l = 1, \ldots, n_x \ , \quad J(f)_{kl} = \frac{\partial f^k}{\partial x^l} \tag{2.70}$$

where f^k is the k^{th} element of function f and x^l the l^{th} element of x.

Let us note $k = (i-1)n_s + j$ and $l = (i'-1)n_s + j'$ where labels i and i' denote the semi-volatile species, and labels j et j' refer to aerosol size bins.

The Jacobian $(kl)^{\text{th}}$ element may then be written as

$$\frac{\partial f^k}{\partial x^l} = \frac{\partial I_i^j}{\partial Q_{i'}^{j'}} \tag{2.71}$$

The derivation of f^k may be split into one linear part, due to mass conservation, and one non-linear part due to coefficient a_i^j, to Kelvin effect η^j, and above all to gas equilibrium concentration $(c_i^{eq})^j$.

The linear part is analytically derived :

$$\left(\frac{\partial f^k}{\partial x^l}\right)_{\text{lin}} = -a_i^j N^{j'} \triangleq (d^{jj'})_i \tag{2.72}$$

The non-linear part has to be differentiated by numerical methods, like finite difference method :

$$\left(\frac{\partial f^k}{\partial x^l}\right)_{\text{non-lin}} = \frac{f^k(\ldots, x^l(1+\varepsilon_{\text{jac}}), \ldots) - f^k(\ldots, x^l, \ldots)}{x^l \varepsilon_{\text{jac}}} \tag{2.73}$$

where ε_{jac} is generaly close to 10^{-8}. During the numerical computation, the linear part is arbitrarily kept constant to avoid derive it twice.

A default option is to approximate the Jacobian matrix by its diagonal. The motivation is of course to reduce the CPU time.

2.3.2 Hybrid resolution

Solving the system (2.64), even with an implicit scheme, can be expensive in CPU time. In order to lower the stiffness, hybrid methods for condensation/evaporation have been developed ([Capaldo et al., 2000]). The method consists in partitioning the concentration vector x between its fast evolving part, x^r, and its slow evolving part x^l. The system (2.64) now becomes :

$$\frac{dx^l}{dt} = f^l(x^l, x^r, t) \ , \quad f^r(x^l, x^r, t) = 0 \tag{2.74}$$

The second equation directly gives an expression of the fast part as a function of the slow part :

$$f^r(x^l, x^r, t) = 0 \Longrightarrow x^r(t) = g(x^l(t), t) \tag{2.75}$$

The time evolution of the slow part is now governed by the following equation :

$$\frac{dx^l}{dt} = f^l\Big(x^l, g(x^l(t), t), t\Big) \tag{2.76}$$

As x^l gathers aerosol species and sizes which have a slow c/e characteristic time, siffness is substantially reduced.

The issue is now to determine whether aerosol sizes and species are "slow" or "fast".

Cutting diameter

The spectral study ([Debry and Sportisse, 2005]) of system (2.64) indicates how to compute a cutting diameter d_c between "slow" and "fast" species/-sizes, such that the partitioning consists in cutting into two parts the aerosol distribution: the smallest bins are at equilibrium while the coarsest ones are governed by kinetic mass transfer.

The cutting diameter can be computed by QSSA criteria, defined by :

$$QSSA_i^j = \frac{c_i^g - \eta_i^j (c_i^{eq})^j}{c_i^g + \eta_i^j (c_i^{eq})^j} \tag{2.77}$$

for a given chemical species $\mathrm{X_i}$ and one aerosol size j. The more this ratio close to unity, the more the species and the size are at equilibrium.

In practice all bins j for which $(QSSA_i^j)_{i=1}^{n_e}$ are greater than one user parameter ε_{QSSA} (close to unity) will be considered as fast and solved by an equilibrium equation. In the sequel we write j_c the cutting bin corresponding to the cutting diameter. Bin j_c is the largest fast bin and bin $j_c + 1$ is the smallest slow bin.

Thermodynamic equilibrium

The fast species and sizes satisfy (2.75) written under the form:

$$1 \leq i \leq n_e \ , \ 1 \leq k \leq j_c \ , \ \tilde{K}_i - \sum_{j=1}^{j_c} Q_i^j - \eta_i^k \ c_i^{eq}(Q_1^k, \ldots, Q_{n_e}^k) = 0 \quad (2.78)$$

$\tilde{K}_i$ is the total mass of species X_i for fast bins:

$$1 \leq i \leq n_e \ , \ \tilde{K}_i = K_i - \sum_{j=j_c+1}^{n_s} Q_i^j \quad (2.79)$$

This system represents the thermodynamic equilibrium between gas and fast aerosols bins.

In the sequel we present several numerical methods to solve this so-called size-resolved equilibrium which cannot be solved directly by current thermodynamic models such as ISORROPIA.

Bulk equilibrium

The bulk equilibrium approach, developed in [Pandis et al., 1993], consists in merging all fast bins $j \leq j_c$ into one bin, referred as the "bulk" aerosol phase :

$$1 \leq i \leq n_e \ , \quad B_i = \sum_{j=1}^{j_c} Q_i^j \quad (2.80)$$

The thermodynamic model ISORROPIA is then applied to the "bulk" aerosol phase $(B_i)_{i=1}^{n_e}$ and one gets equilibrium "bulk" concentrations $(B_i^{eq})_{i=1}^{n_e}$.

The variation from initial to final "bulk" concentrations has then to be redistributed among fast bins $1 \leq k \leq j_c$ for species $1 \leq i \leq n_e$:

$$(Q_i^k)^{eq} = Q_i^k + f_i^k (B_i^{eq} - B_i) \ , \quad f_i^k = \frac{a_i^k N^k}{\sum_{j=1}^{j_c} a_i^j N^j} \quad (2.81)$$

This redistribution scheme is taken from [Pandis et al., 1993] and is exact provided that the aerosol composition is uniform over fast bins and that the variation of the aerosol diameter can be neglected for fast bins.

Size resolved equilibrium

The former method does not solve size-resolved equilibrium. We propose here two size-resolved algorithms :

1. The fixed point algorithm ([Jacobson et al., 1996]).

   The thermodynamic model is applied sequentially for all fast aerosol bins until concentrations reach a stable value.

   Let us detail one iteration of the process. The thermodynamic model is applied to fast bins from the slowest one ($j = j_c$) to the fastest one ($j = 1$). Equilibrium of bin $j = j_c$ reads :

   $$1 \leq i \leq n_e \ , \quad K_i^{j_c} = Q_i^{j_c} + c_i^g \tag{2.82}$$

   Equilibrium concentrations $(Q_i^{j_c})^{eq}$ and $(c_i^{eq})^{j_c}$ are obtained for respectively bin $j = j_c$ and gas phase. Gas equilibrium concentrations are then used for next bin :

   $$1 \leq i \leq n_e \ , \quad K_i^{j_c-1} = Q_i^{j_c-1} + (c_i^{eq})^{j_c} \tag{2.83}$$

   The k^{th} step consists in solving

   $$1 \leq i \leq n_e \ , \quad K_i^k = Q_i^k + (c_i^{eq})^{k+1} \tag{2.84}$$

   Final gas concentrations $(c_i^{eq})^1$ are re-used in next iteration.

2. The minimization algorithm.

   The resolution of (2.75) is equivalent to finding the minimum of functional F defined by :

   $$F(x^r) = \frac{1}{2} \sum_{j=1}^{n_x^r} [(f^r)_j]^2 \tag{2.85}$$

   where n_x^r is the size of fast species vector x^r. The minimum of F can be computed with well-known minimization algorithms, such as BFGS ([H. Byrd and Zhu, 1995]).

2.3.3 Some results

A detailed study of various aproaches may be found in [Debry and Sportisse, 2005].

Figure 2.4 illustates the dependence of the c/e characteristic timescales with respect to aerosol sizes. A linearized analysis and the computation of Jacobian eigenvalues confirm the wide range covered by the timescales (figure 2.5).

Figure 2.6 compares various hybrid methods tested in [Debry and Sportisse, 2005].

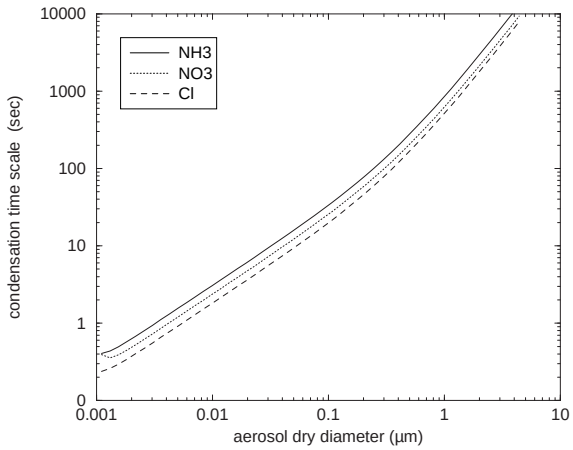

Figure 2.4: Distribution of the c/e characteristic timescales as a function of aerosol sizes.

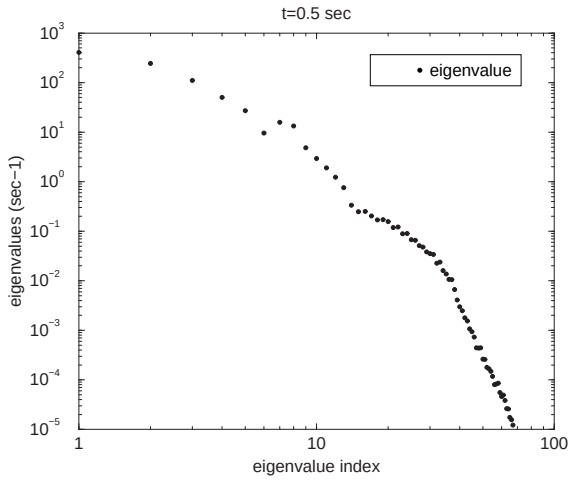

Figure 2.5: Distribution of the eigenvalues for the c/e Jacobian matrix.

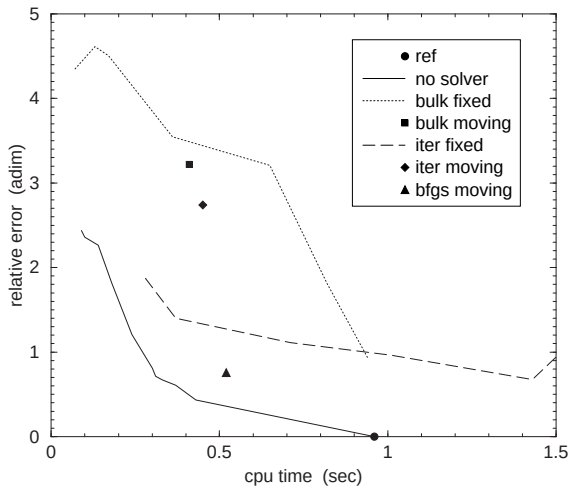

Figure 2.6: CPU/RMS diagram of several hybrid strategies (from [Debry and Sportisse, 2005]).

Chapter 3

The Modal Aerosol Model (MAM)

Summary:

This chapter aims at presenting the modal model MAM. *We also investigate the main difficulty related to modal models, that is to say mode merging and mode splitting.*

3.1 Description of the modal model

MAM is described in more details in [Sartelet et al., 2005] and [Sartelet, 2004].

3.1.1 The modal distribution

The particulate matter (PM) distribution is represented by three modes in the fine range (nucleation i, Aitken j, and accumulation k), and one mode in the coarse range (c). Each of these modes correspond to a distinct range of particle diameters d:

- $d < 0.01\mu m$ for the nucleation mode,
- $0.01\mu m < d < 0.1\mu m$ for the Aitken mode,
- $0.1\mu m < d < 2.5\mu m$ for the accumulation mode,
- $d > 2.5\mu m$ for the coarse mode.

Each of the four modes is made of sulfate, nitrate, ammonium, chloride, sodium, mineral dust, carbon, and water. A recent version also includes SOA in a way similar to SIREAM.

The aerosol distribution is described for example by the number distribution

$$n(d_p,t) = n_i(d_p,t) + n_j(d_p,t) + n_k(d_p,t) + n_c(d_p,t) \tag{3.1}$$

where n_i is the log-normal distribution for mode i, n_j for mode j, n_k for mode k, n_c for mode c, and d_p is the "dry" particle diameter. For $l = i, j, k, c$

$$n_l(d_p) \;=\; \frac{N_l}{\sqrt{2\pi}\ln(\sigma_l)\ d_l}\exp[-\frac{1}{2}(\frac{\ln^2(d_p/d_l)}{\ln^2(\sigma_l)})] \tag{3.2}$$

where N_l is the total number of particles within mode l, d_l is the "dry" median diameter and σ_l is the standard deviation. The moment of order h of the distribution is defined as

$$M_h^l \;=\; \int_{-\infty}^{\infty} d_p^h\ n_l(d_p)\ d(d_p) \;=\; N_l\ d_l^h\ \exp(\frac{h^2}{2}\ln^2\sigma_l). \tag{3.3}$$

The modal distribution is known once the three parameters N, d_g and σ_g are.

For each mode, PM dynamic equations are solved for three moments, i.e. moments of order 0 (M_0), of order 3 (M_3), and of order 6 (M_6), from which the three parameters may be computed as follows:

$$N = M_0 \tag{3.4}$$

$$d_g = (\frac{M_3^4}{M_6 M_0^3})^{\frac{1}{6}} \tag{3.5}$$

$$\sigma_g = \exp(\sqrt{\frac{1}{9}\ln(\frac{M_0 M_6}{M_3^2})}). \tag{3.6}$$

M_3 relates to the total volume of particles per volume of air V as follows $M_0 = N$ and $M_3 = \frac{6}{\pi}V$. Third moments are computed for each chemical species in order to follow the chemical composition of particles in each mode with time.

Note that in the formulation (3.2), particles are modeled as "dry" particles, i.e. the particle liquid water content is not taken into account.

However, because coagulation and condensation processes do act on wet particles rather than on dry particles, wet particles need to be considered when computing coagulation and condensation kernels. Wet particles are assumed to follow a log normal distribution of mean wet diameters d_l^w. For each mode, the particle liquid content l_{wc} is deduced from particle concentrations using the thermodynamic model ISORROPIA.

The wet mean diameter is computed from the dry mean diameter d_l by assuming that number concentrations and standard deviations are unchanged by considering wet or dry particles. Finally,

$$d_l^w = d_l \left(\frac{M_3^w}{M_3} \right)^{2/3}, \tag{3.7}$$

where M_3 and M_3^w are respectively the dry and wet moments.

3.1.2 The different processes

Coagulation

The evolution equation of a moment of order h due to coagulation processes may be expressed as

$$\begin{aligned} &\left(\frac{\partial M_h}{\partial t} \right)_{coag} = \\ &\frac{1}{2} \int_0^\infty \int_0^\infty \left(d_{p_1}^3 + d_{p_2}^3 \right)^{h/3} \beta(d_{p_1}^w, d_{p_2}^w) n(d_{p_1}) n(d_{p_2}) d(d_{p_1}) d(d_{p_2}) \\ &- \frac{1}{2} \int_0^\infty \int_0^\infty \left(d_{p_1}^h + d_{p_2}^h \right) \beta(d_{p_1}^w, d_{p_2}^w) n(d_{p_1}) n(d_{p_2}) d(d_{p_1}) d(d_{p_2}) \end{aligned} \tag{3.8}$$

The expression of the coagulation kernel β may be found in [Fuchs, 1964].

The evolution equations of the moments of each mode i, j, k and c are obtained by substituting $n(d_p, t) = n_i(d_p, t) + n_j(d_p, t) + n_k(d_p, t) + n_c(d_p, t)$ into equation (3.8), and by assuming that:

- when particles from the same mode collide (intra-modal coagulation) the agglomerated particle stays in that mode ([Whitby and McMurry, 1997]),

- when particles from two different modes collide (inter-modal coagulation) the agglomerated particle is assigned to the mode with the larger mean size.

This leads to the following set of equations:

$$
\begin{aligned}
&\left(\frac{\partial M_{h_i}}{\partial t}\right)_{coag} = \\
&\frac{1}{2}\int_0^\infty\int_0^\infty \left(d_{p_1}^3 + d_{p_2}^3\right)^{h/3} \beta(d_{p_1}, d_{p_2})\; n_i(d_{p_1}) n_i(d_{p_2})\; d(d_{p_1}) d(d_{p_2}) \\
&-\int_0^\infty\int_0^\infty d_{p_1}^h \beta(d_{p_1}, d_{p_2})\; n_i(d_{p_1}) n_i(d_{p_2})\; d(d_{p_1}) d(d_{p_2}) \\
&-\int_0^\infty\int_0^\infty d_{p_1}^h \beta(d_{p_1}, d_{p_2})\; n_i(d_{p_1}) n_j(d_{p_2})\; d(d_{p_1}) d(d_{p_2}) \\
&-\int_0^\infty\int_0^\infty d_{p_1}^h \beta(d_{p_1}, d_{p_2})\; n_i(d_{p_1}) n_k(d_{p_2})\; d(d_{p_1}) d(d_{p_2}) \\
&-\int_0^\infty\int_0^\infty d_{p_1}^h \beta(d_{p_1}, d_{p_2})\; n_i(d_{p_1}) n_c(d_{p_2})\; d(d_{p_1}) d(d_{p_2})
\end{aligned}
\tag{3.9}
$$

$$
\begin{aligned}
&\left(\frac{\partial M_{h_j}}{\partial t}\right)_{coag} = \\
&\frac{1}{2}\int_0^\infty\int_0^\infty \left(d_{p_1}^3 + d_{p_2}^3\right)^{h/3} \beta(d_{p_1}, d_{p_2})\; n_j(d_{p_1}) n_j(d_{p_2})\; d(d_{p_1}) d(d_{p_2}) \\
&+\int_0^\infty\int_0^\infty \left(d_{p_1}^3 + d_{p_2}^3\right)^{h/3} \beta(d_{p_1}, d_{p_2})\; n_i(d_{p_1}) n_j(d_{p_2})\; d(d_{p_1}) d(d_{p_2}) \\
&-\int_0^\infty\int_0^\infty d_{p_1}^h \beta(d_{p_1}, d_{p_2})\; n_i(d_{p_1}) n_j(d_{p_2})\; d(d_{p_1}) d(d_{p_2}) \\
&-\int_0^\infty\int_0^\infty d_{p_1}^h \beta(d_{p_1}, d_{p_2})\; n_j(d_{p_1}) n_j(d_{p_2})\; d(d_{p_1}) d(d_{p_2}) \\
&-\int_0^\infty\int_0^\infty d_{p_1}^h \beta(d_{p_1}, d_{p_2})\; n_j(d_{p_1}) n_k(d_{p_2})\; d(d_{p_1}) d(d_{p_2}) \\
&-\int_0^\infty\int_0^\infty d_{p_1}^h \beta(d_{p_1}, d_{p_2})\; n_j(d_{p_1}) n_c(d_{p_2})\; d(d_{p_1}) d(d_{p_2})
\end{aligned}
\tag{3.10}
$$

$$
\begin{aligned}
&\left(\frac{\partial M_{h_k}}{\partial t}\right)_{coag} = \\
&\frac{1}{2}\int_0^\infty\int_0^\infty \left(d_{p_1}^3 + d_{p_2}^3\right)^{h/3} \beta(d_{p_1}, d_{p_2})\; n_k(d_{p_1}) n_k(d_{p_2})\; d(d_{p_1}) d(d_{p_2}) \\
&+\int_0^\infty\int_0^\infty \left(d_{p_1}^3 + d_{p_2}^3\right)^{h/3} \beta(d_{p_1}, d_{p_2})\; n_i(d_{p_1}) n_k(d_{p_2})\; d(d_{p_1}) d(d_{p_2}) \\
&+\int_0^\infty\int_0^\infty \left(d_{p_1}^3 + d_{p_2}^3\right)^{h/3} \beta(d_{p_1}, d_{p_2})\; n_j(d_{p_1}) n_k(d_{p_2})\; d(d_{p_1}) d(d_{p_2}) \\
&-\int_0^\infty\int_0^\infty d_{p_1}^h \beta(d_{p_1}, d_{p_2})\; n_i(d_{p_1}) n_k(d_{p_2})\; d(d_{p_1}) d(d_{p_2}) \\
&-\int_0^\infty\int_0^\infty d_{p_1}^h \beta(d_{p_1}, d_{p_2})\; n_j(d_{p_1}) n_k(d_{p_2})\; d(d_{p_1}) d(d_{p_2}) \\
&-\int_0^\infty\int_0^\infty d_{p_1}^h \beta(d_{p_1}, d_{p_2})\; n_k(d_{p_1}) n_k(d_{p_2})\; d(d_{p_1}) d(d_{p_2}) \\
&-\int_0^\infty\int_0^\infty d_{p_1}^h \beta(d_{p_1}, d_{p_2})\; n_k(d_{p_1}) n_c(d_{p_2})\; d(d_{p_1}) d(d_{p_2})
\end{aligned} \tag{3.11}
$$

$$
\begin{aligned}
&\left(\frac{\partial M_{h_c}}{\partial t}\right)_{coag} = \\
&\frac{1}{2}\int_0^\infty\int_0^\infty \left(d_{p_1}^3 + d_{p_2}^3\right)^{h/3} \beta(d_{p_1}, d_{p_2})\; n_c(d_{p_1}) n_c(d_{p_2})\; d(d_{p_1}) d(d_{p_2}) \\
&+\int_0^\infty\int_0^\infty \left(d_{p_1}^3 + d_{p_2}^3\right)^{h/3} \beta(d_{p_1}, d_{p_2})\; n_i(d_{p_1}) n_c(d_{p_2})\; d(d_{p_1}) d(d_{p_2}) \\
&+\int_0^\infty\int_0^\infty \left(d_{p_1}^3 + d_{p_2}^3\right)^{h/3} \beta(d_{p_1}, d_{p_2})\; n_j(d_{p_1}) n_c(d_{p_2})\; d(d_{p_1}) d(d_{p_2}) \\
&+\int_0^\infty\int_0^\infty \left(d_{p_1}^3 + d_{p_2}^3\right)^{h/3} \beta(d_{p_1}, d_{p_2})\; n_k(d_{p_1}) n_c(d_{p_2})\; d(d_{p_1}) d(d_{p_2}) \\
&-\int_0^\infty\int_0^\infty d_{p_1}^h \beta(d_{p_1}, d_{p_2})\; n_i(d_{p_1}) n_c(d_{p_2})\; d(d_{p_1}) d(d_{p_2}) \\
&-\int_0^\infty\int_0^\infty d_{p_1}^h \beta(d_{p_1}, d_{p_2})\; n_j(d_{p_1}) n_c(d_{p_2})\; d(d_{p_1}) d(d_{p_2}) \\
&-\int_0^\infty\int_0^\infty d_{p_1}^h \beta(d_{p_1}, d_{p_2})\; n_k(d_{p_1}) n_c(d_{p_2})\; d(d_{p_1}) d(d_{p_2}) \\
&-\int_0^\infty\int_0^\infty d_{p_1}^h \beta(d_{p_1}, d_{p_2})\; n_c(d_{p_1}) n_c(d_{p_2})\; d(d_{p_1}) d(d_{p_2})
\end{aligned} \tag{3.12}
$$

Coagulation does not differentiate chemical species. However, because modes i, j, k and c have different chemical compositions, chemical compo-

sitions of modes j, k and c are modified by coagulation. These changes are identified by assuming that volume is conserved during coagulation, and by considering the provenance of volume which is added to mode j, k or c by coagulation.

For numerical optimization and in order to identify changes in chemical compositions in modes j, k and c by coagulation, the equations (3.9), (3.10), (3.11) and (3.12)) are rewritten as

$$\begin{aligned}
(\frac{\partial M_{0_i}}{\partial t})_{coag} &= 0.5\ I_{i,i}^{0,0} - I_{i,j}^{0,0} - I_{i,k}^{0,0} - I_{i,c}^{0,0} \\
(\frac{\partial M_{0_j}}{\partial t})_{coag} &= 0.5\ I_{j,j}^{0,0} - I_{j,k}^{0,0} - I_{j,c}^{0,0} \\
(\frac{\partial M_{0_k}}{\partial t})_{coag} &= 0.5\ I_{k,k}^{0,0} - I_{k,c}^{0,0} \\
(\frac{\partial M_{0_c}}{\partial t})_{coag} &= 0.5\ I_{c,c}^{0,0} \\
(\frac{\partial M_{3_i}^{cs}}{\partial t})_{coag} &= -F_i^{cs}\ I_{i,j}^{3,0} - F_i^{cs}\ I_{i,k}^{3,0} - F_i^{cs}\ I_{i,c}^{3,0} \\
(\frac{\partial M_{3_j}^{cs}}{\partial t})_{coag} &= F_i^{cs}\ I_{i,j}^{3,0} - F_j^{cs}\ I_{j,k}^{3,0} - F_j^{cs}\ I_{j,c}^{3,0} \\
(\frac{\partial M_{3_k}^{cs}}{\partial t})_{coag} &= F_i^{cs}\ I_{i,k}^{3,0} + F_j^{cs}\ I_{j,k}^{3,0} - F_k^{cs}\ I_{k,c}^{3,0} \\
(\frac{\partial M_{3_c}^{cs}}{\partial t})_{coag} &= F_i^{cs}\ I_{i,c}^{3,0} + F_j^{cs}\ I_{j,c}^{3,0} + F_k^{cs}\ I_{k,c}^{3,0} \\
(\frac{\partial M_{6_i}}{\partial t})_{coag} &= I_{i,i}^{3,3} - I_{i,j}^{6,0} - I_{i,k}^{6,0} - I_{i,c}^{6,0} \\
(\frac{\partial M_{6_j}}{\partial t})_{coag} &= I_{i,j}^{6,0} + I_{j,j}^{3,3} + 2\ I_{i,j}^{3,3} - I_{j,k}^{6,0} - I_{j,c}^{6,0} \\
(\frac{\partial M_{6_k}}{\partial t})_{coag} &= I_{i,k}^{6,0} + I_{j,k}^{6,0} + 2\ I_{i,k}^{3,3} + 2\ I_{j,k}^{3,3} + I_{k,k}^{3,3} - I_{k,c}^{6,0} \\
(\frac{\partial M_{6_c}}{\partial t})_{coag} &= I_{i,c}^{6,0} + I_{j,c}^{6,0} + I_{k,c}^{6,0} + 2I_{i,c}^{3,3} + 2I_{j,c}^{3,3} + 2I_{k,c}^{3,3} + I_{c,c}^{3,3} \qquad (3.13)
\end{aligned}$$

where cs denotes chemical species, F_l^{cs} denotes the volume proportion of chemical species in mode l ($l = i, j, k$)

$$F_l^{cs} = \frac{M_{3,l}^{cs}}{\sum_{cs} M_{3,l}^{cs}} \qquad (3.14)$$

and

$$I_{i,j}^{a,b} = \int_0^\infty \int_0^\infty d_{p_1}^a\ d_{p_2}^b\ \beta(d_{p_1}^w, d_{p_2}^w)\ n_i(d_{p_1}) n_j(d_{p_2})\ d(d_{p_1}) d(d_{p_2}). \qquad (3.15)$$

Integrals (3.15) are computed by Gauss-Hermite quadrature as follows

$$I_{i,j}^{a,b} = K_{i,j}^{a,b} \sum_{q=1}^{N_g} w_q \; f_j(x_q) \sum_{p=1}^{N_g} w_p \; f_i(x_p, x_q) \tag{3.16}$$

where N_g is the number of quadrature points, x_p and w_p $(p = 1, N_g)$ are the abscissas and weights of the Gauss-Hermite quadrature,

$$\begin{aligned} K_{i,j}^{a,b} &= \frac{N_i N_j}{\pi} d_i^a d_j^b \\ f_j(x_q) &= \exp\left(b\sqrt{2}\ln(\sigma_j)\; x_q\right) \\ f_i(x_p, x_q) &= \exp\left(a\sqrt{2}\ln(\sigma_i)\; x_p\right)\; \beta(d_p^w, d_q^w) \end{aligned} \tag{3.17}$$

with N_i and N_j the number of aerosols in modes i and j, and d_i and d_j the mean diameters of modes i and j respectively. The "quadrature" diameters are

$$d_p = d_i \; \exp\left(\sqrt{2}\ln(\sigma_i)\; x_p\right) \quad \text{and} \quad d_q = d_j \; \exp\left(\sqrt{2}\ln(\sigma_j)\; x_q\right), \tag{3.18}$$

and the corresponding wet diameters d_p^w and d_q^w are

$$d_p^w = d_p \left(M_{3,i}^w / M_{3,i}\right)^{2/3} \quad \text{and} \quad d_q^w = d_q \left(M_{3,j}^w / M_{3,j}\right)^{2/3} \tag{3.19}$$

Integrals of the evolution equations are computed by Gauss-Hermite quadrature of order four. The simulation results have been shown to be insensitive to the use of higher order quadratures.

Condensation/evaporation

For condensation/evaporation processes, mass transfer between the PM and gas phases relaxes the system toward thermodynamic equilibrium. The time rate of change of a moment of order h due to condensation/evaporation of species s may be expressed as

$$\frac{\partial M_{h_s}}{\partial t} = \frac{2h}{\pi} \int_0^\infty d_p^{h-3} I_v^s(d_p^w, t) \; n(d_p, t) d(d_p). \tag{3.20}$$

where d_p is the dry diameter of a particle, $I_v^s(d_p^w, t)$ is the rate of change of total volume of a particle of wet diameter d_p^w as a result of condensation/evaporation of a species s. It is written, as Dahneke (1983):

$$I_v^s(d_p^w, t) = 2\pi D_s \; d_p^w \; f(Kn, \alpha_s) \left(c_s - c_s^{eq} \eta\left(d_l^w, cs\right)\right), \tag{3.21}$$

with c_s the concentration of species s in the bulk gas phase, c_s^{eq} the concentration at the surface of particles, D_s the diffusivity of species s in air, $Kn = 2\,\lambda/d_p^w$ the Knudsen number, λ the mean free path in air, $f(Kn, \alpha_s)$ a correction factor for non-continuum effects and imperfect accommodation (Dahneke 1983), α_s the accommodation coefficient, and η the Kelvin effect correction coefficient

$$\eta\left(d_l^w, cs\right) = exp\left(\frac{4\sigma m_{cs}}{RTd_p^w\rho_p}\right) \tag{3.22}$$

where σ is the particle surface tension, ρ_p is the particle density, T is the temperature, R is the universal gas constant, m_{cs} is the molar weight of species cs and d_l^w is the mean wet diameter of mode l for which the condensation rate is computed.

The thermodynamic model ISORROPIA with the metastable option is used to determine the liquid water content of the PM and the surface concentrations for each mode of the distribution when the particles are liquid.

If the liquid water content is zero, i.e. if particles are solid, then surface concentrations are computed according to [Pilinis et al., 2000]. Although the accommodation coefficient should depend on particle composition and diameter, it is commonly assumed to be constant.

As for coagulation, the condensation rate equations are integrated by fourth order Gauss-Hermite quadrature. For numerical stability, surface concentrations are corrected by limiting the flux of hydrogen ion, as for the size-resolved model.

If thermodynamic equilibrium is assumed then thermodynamic equilibrium is computed by the method of CMAQ v4.3. The partitioning between the PM and gas phases is first computed using ISORROPIA. Then a weighting scheme is used to redistribute total PM equilibrium concentrations between the fine and coarse modes, depending on the initial concentrations in each mode. Equation (3.20) is only used to compute the condensation rate of species of low volatility such as sulfate.

Nucleation

New particles created by homogeneous nucleation are assigned to the nucleation mode i, and are assumed to mix instantaneously with existing particles in that mode. For sulfuric acid–water binary nucleation, two parameterizations are implemented in MAM: that of Kulmala ([Kulmala et al., 1998]) and the recently revised parameterization of Vehkamaki ([Vehkamäki et al., 2002]).

Sulfuric acid-ammonia-water ternary nucleation is also modeled in MAM, with the parameterization of Napari ([Napari et al., 2002]). The rate of change of moments due to nucleation may be written as

$$\left(\frac{\partial M_h}{\partial t}\right)_{nuc} = J d_{g0}^h . \exp\left(\frac{h^2}{2} \ln^2 \sigma_{g0}\right) \tag{3.23}$$

where J is the nucleation rate, d_{g0} is the mean diameter and σ_{g0} the standard deviation of aerosols that nucleate The different parameterisations differ mostly in the computation of J.

Because the Kulmala parameterization only predicts the nucleation rate, d_{g0} and σ_{g0} must be specified ($d_i = 0.001\mu m$ and σ_i= 1.05 by default).

In the Vehkamaki and the Napari parameterizations, σ_{g0} must also be specified. If the mean diameter of the cluster is chosen to be computed by the Vehkamaki parameterisation rather than being fixed as in other parameterisations, the time derivative of the third order moment is obtained from the volume of the critical cluster

$$\begin{aligned}
\left(\frac{\partial M_3^{NH_3}}{\partial t}\right)_{nuc} &= \frac{6}{\pi} J \; N_{tot,NH_3} \frac{m_{NH_3}}{N_{avog} \; \rho_{NH_3}} \\
\left(\frac{\partial M_3^{H_2SO_4}}{\partial t}\right)_{nuc} &= \frac{6}{\pi} J \; N_{tot,H_2SO_4} \frac{x_* m_{H_2SO_4}}{N_{avog} \; \rho_{H_2SO_4}} \\
\left(\frac{\partial M_3}{\partial t}\right)_{nuc} &= \left(\frac{\partial M_3^{NH_3}}{\partial t}\right)_{nuc} + \left(\frac{\partial M_3^{H_2SO_4}}{\partial t}\right)_{nuc}
\end{aligned} \tag{3.24}$$

where x_* is the mole fraction of sulfuric acid in the critical cluster formed by nucleation (exists only in the Vehkamaki parameterization), N_{tot,NH_3} and N_{tot,H_2SO_4} are the total numbers of molecules of NH_3 and H_2SO_4 in the critical cluster, m_{NH_3} and $m_{H_2SO_4}$ are the molar weights of NH_3 and H_2SO_4 and N_{avog} is the Avogadro number.

The mean diameter d_{g0} is computed from the nucleation rate, the time derivative of the third order moment, and the standard deviation

$$d_{g0} = \left(\frac{\left(\frac{\partial M_3}{\partial t}\right)_{nuc}}{J} \exp\left(-\frac{9}{2} \ln^2 \sigma_{g0}\right) \right)^{1/3} \tag{3.25}$$

The derivative of the sixth order moment is then computed by equation (3.23).

3.1.3 Numerical schemes

Two numerical schemes may be used in MAM: a simple explicit trapezoidal rule of order 2 (ETR), or EBI (Euler Backward Iterative).

Note that operator splitting between processes is not applied but all processes are solved simultaneously.

ETR

By noting M_h^n the moment of order h at time t_n, the time-stepping discretization may be written as

$$M_h^{n+1} = M_h^n + \frac{\Delta t}{2}\left[F\left(M_h^n\right) + F\left(M_h^*\right)\right] \quad \text{with} \quad M_h^* = M_h^n + \Delta t\, F\left(M_h^n\right) \tag{3.26}$$

where $F(M_h)$ represents the time derivative of M_h due to coagulation, condensation and nucleation processes. After each iteration, the time step is adjusted as follows

$$\Delta t = \Delta t \frac{\Delta_0}{\Delta_1} \quad \text{with} \quad \Delta_1 = \left|\left| \frac{M_h^{n+1} - M_h^*}{M_h^*} \right|\right|_2 \tag{3.27}$$

and Δ_0 is the desired accuracy (0.01 by default).

EBI

By noting M_h^n the moment of order h at time t_n, the time-stepping discretization may be written as

$$\tilde{M}_0 = M_h^n \text{ and } \tilde{M}_* = M_h^n \tag{3.28}$$

$$\tilde{M}_* = \frac{F^+\left(\tilde{M}_*\right)\Delta t + \tilde{M}_0}{1 + \frac{F^-\left(\tilde{M}_*\right)\Delta t}{\tilde{M}_*}} \tag{3.29}$$

$$M_h^{n+1} = \tilde{M}_* \tag{3.30}$$

where $F^+(M_h)$ represents the positive part of the time derivative of M_h due to coagulation, condensation and nucleation processes, and $F^-(M_h)$ the negative part. The step described in (3.29) is repeated a number Nit of times, where Nit is the number of iterations of the EBI scheme, usually chosen equal to 3.

After the last iteration, the time step is adjusted as follows

$$\Delta t = \Delta t \frac{\Delta_0}{\Delta_1} \quad \text{with} \quad \Delta_1 = \left|\left| \frac{\tilde{M}_* - \tilde{M}_{*,0}}{\tilde{M}_{*,0}} \right|\right|_2 \tag{3.31}$$

where $\tilde{M}_{*,0}$ is the value of $\tilde{M}_*$ at the previous iteration and Δ_0 is the desired accuracy (0.01 by default).

3.2 Mode merging and mode splitting

3.2.1 Mode merging

Mode merging schemes are often used with modal models in 3-D simulations. Merging between two modes is required to force modes to be of distinct size ranges throughout the simulations.

In the merging scheme of [Binkowski and Roselle, 2003], if two modes l and $l+1$ overlap, then mode l is partially merged into mode $l+1$. The fraction of mode l to be merged into mode $l+1$ is computed for each moment by integrating the moment distribution for diameters larger than a threshold diameter. This threshold diameter is chosen as the diameter where the number distributions of the two modes overlap.

In the dynamic mode merger of [Whitby et al., 2002], two modes that are in proximity to each other are completely merged, and modes are continually remapped into mode indices (e.g. i, j, k, c) that correspond to their "home position" in size space.

If two modes satisfy given proximity criteria, the fraction to be merged is computed from the flux of one of the moment distribution across a boundary, which corresponds to the geometric average of the mean diameter of the two modes. This fraction is modified depending on how far each mode is from its home position.

In MAM, mode merging can be applied in a way similar to the one of [Pirjola et al., 2003], which is based on the merging of [Binkowski and Roselle, 2003], i.e. by defining lower and upper boundary diameters for each mode.

Let us write b_l the lower boundary diameter for mode $l+1$ and the upper boundary diameter for mode l, with $l = i, j, k$ and $l+1 = j, k, c$. Typical values for the boundary diameters of the mass distribution are $b_{m_i} = 0.01\mu m$, $b_{m_j} = 0.1\mu m$ and $b_{m_k} = 2.5\mu m$. The diameter of the lognormal number distribution b_l is related to the diameter of the lognormal mass distribution b_{m_l} ($l = i, j, k$) as follows

$$b_l = b_{m_l} \exp\left(-3\sigma^2\right) \tag{3.32}$$

Mode merging between two modes is applied when $b_l < 2\sigma_l d_l$, i.e. when the boundary diameter is in the 95% confidence interval of the mean diameter of the mode d_l. To quantify the transfer of particles of diameters greater than b_l, fractions to be transferred are computed from the complementary error function

$$F_h = 0.5 erfc(x_h) \tag{3.33}$$

with

$$x_h = x_0 - \frac{h \ln \sigma_l}{\sqrt{2}} \text{ and } x_0 = \frac{\ln (b_l/d_l)}{\sqrt{2} \ln \sigma_l} \tag{3.34}$$

The moments of order h after transfer ($\tilde{M}_{h_{l+1}}$ and $\tilde{M}_{h_l}$) are computed from the moments of order h before transfer ($M_{h_{l+1}}$ and M_{h_l}) as follow

$$\begin{aligned} \tilde{M}_{h_{l+1}} &= M_{h_{l+1}} + F_h \, M_{h_l} \\ \tilde{M}_{h_l} &= (1 - F_h) \, M_{h_l}. \end{aligned} \tag{3.35}$$

In MAM, mode merging can be chosen to be applied or not depending on the user's choice. Mode splitting, which is now detailed, can also be applied, instead of mode merging in the present version.

3.2.2 Mode splitting

When the combined effect of nucleation and condensation and the effect of coagulation are of same order of magnitude but act in opposite direction, a mode may split into two modes.

This is particularly likely to happen for the nucleation mode i during high nucleation episodes. Although this splitting is usually not reproduced by modal models ([Pirjola et al., 1999], [Landgrebe and Pratsinis, 1990]), good results are obtained by applying a "splitting scheme".

The splitting scheme used in MAM represents the splitting of mode i by partially splitting modes i into mode j with a merging scheme, as now detailed.

After each iteration in time, splitting of mode i is applied when the two following criteria are satisfied:

- when the characteristic time scale of coagulation is smaller than the characteristic time of coagulation, condensation, and nucleation com-

bined, i.e.

$$\text{Min}\left(\frac{M_{0,i}}{\left|\frac{\partial M_{0,i}}{\partial t}\Big|_{coag}\right|}, \quad \frac{M_{3,i}}{\left|\frac{\partial M_{3,i}}{\partial t}\Big|_{coag}\right|}, \quad \frac{M_{6,i}}{\left|\frac{\partial M_{6,i}}{\partial t}\Big|_{coag}\right|}\right) < \text{Min}\left(\frac{M_{0,i}}{\left|\frac{\partial M_{0,i}}{\partial t}\right|}, \quad \frac{M_{3,i}}{\left|\frac{\partial M_{3,i}}{\partial t}\right|}, \quad \frac{M_{6,i}}{\left|\frac{\partial M_{6,i}}{\partial t}\right|}\right) \tag{3.36}$$

where $\frac{\partial M_{h,i}}{\partial t}\Big|_{coag}$ represents the time derivative of the moment of order h due to coagulation, and $\frac{\partial M_{h,i}}{\partial t}$ the time derivative due to coagulation, condensation, and nucleation;

- when the characteristic time scale of condensation/nucleation is smaller than the characteristic time of coagulation, condensation, and nucleation combined, i.e.

$$\text{Min}\left(\frac{M_{0,i}}{\left|\frac{\partial M_{0,i}}{\partial t}\Big|_{cd+nl}\right|}, \quad \frac{M_{3,i}}{\left|\frac{\partial M_{3,i}}{\partial t}\Big|_{cd+nl}\right|}, \quad \frac{M_{6,i}}{\left|\frac{\partial M_{6,i}}{\partial t}\Big|_{cd+nl}\right|}\right) < \text{Min}\left(\frac{M_{0,i}}{\left|\frac{\partial M_{0,i}}{\partial t}\right|}, \quad \frac{M_{3,i}}{\left|\frac{\partial M_{3,i}}{\partial t}\right|}, \quad \frac{M_{6,i}}{\left|\frac{\partial M_{6,i}}{\partial t}\right|}\right) \tag{3.37}$$

where $\frac{\partial M_{h,i}}{\partial t}\Big|_{cd+nl}$ represents the time derivative of the moment of order h due to condensation and nucleation.

The splitting scheme is applied when the characteristic time of all processes combined is larger than either the characteristic time of coagulation alone or that of condensation/nucleation. This happens when coagulation and the effects of condensation/nucleation are of same order of magnitude but of opposite strength.

The merging scheme used to do the splitting by merging modes i and j is based on that of [Binkowski and Roselle, 2003], which correspond to equations (3.33), (3.34) and (3.35), except for the calculation of the boundary diameter b_i.

Because the splitting scheme aims at reproducing the splitting of mode i when it occurs due to the simultaneous occurrence of strong nucleation/-condensation and coagulation, the threshold diameter for mode merging is

chosen independently of mode j. The threshold diameter is chosen depending on the mean evolution of the mode i, as follows.

When the evolution of mode i due to coagulation opposes the evolution due to condensation/nucleation, modal models have difficulties in representing the mean evolution of the mode. These two opposite evolutions are measured respectively by a_{coag} and a_{cl+nl} where

$$a_{coag} = \frac{\left.\frac{\partial M_{3,i}}{\partial t}\right|_{coag}}{\frac{\partial M_{3,i}}{\partial t}}, \quad a_{cd+nl} = \frac{\left.\frac{\partial M_{3,i}}{\partial t}\right|_{cd+nl}}{\frac{\partial M_{3,i}}{\partial t}}. \tag{3.38}$$

Note that a_{coag} and a_{cd+nl} have opposite signs but similar amplitudes when mode splitting occurs.

The threshold diameter b_i for mode splitting is chosen as the harmonic mean of $|a_{coag}|$ times d_{coag} and of $|a_{cd+nl}|$ times d_{cd+nl}, where d_{coag} is the mean diameter that mode i would have if it was subject to coagulation only and d_{cd+nl} is the mean diameter that mode i would have if it was subject to condensation/nucleation only.

These diameters are determined after taking a tentative time step with forward Euler scheme, taking into account only coagulation for d_{coag} and only condensation/nucleation for d_{cd+nl}.

Chapter 4

Coupling to a Chemistry-Transport Model and 3D parameterisations

Abstract:

The aim of this chapter is to present the coupling to a "host" Chemistry-Transport Model, Polair3D. *It is however possible to use another one. Additional parameterizations are necessary in the tridimensional framework. These parameterizations concern processes like emissions (anthropogenic and natural) or scavenging and dry deposition (figure 4.1). These parameterization have been developed in the framework of the parameterizations library* AtmoData *of the modeling system* Polyphemus.

4.1 Coupling to a 3D model

4.1.1 Interface

The interface is very easy and consists in labelling or pointing the gaseous chemical species (for condensation/evaporation processes).

4.1.2 Parameterization for aerosol liquid water content

The aerosol wet diameter is used in every 0D aerosol process, particularly coagulation, condensation/evaporation and dry deposition. In principle, this wet diameter should be computed through aerosol thermodynamic equilibrium, that determines among other species its liquid water content.

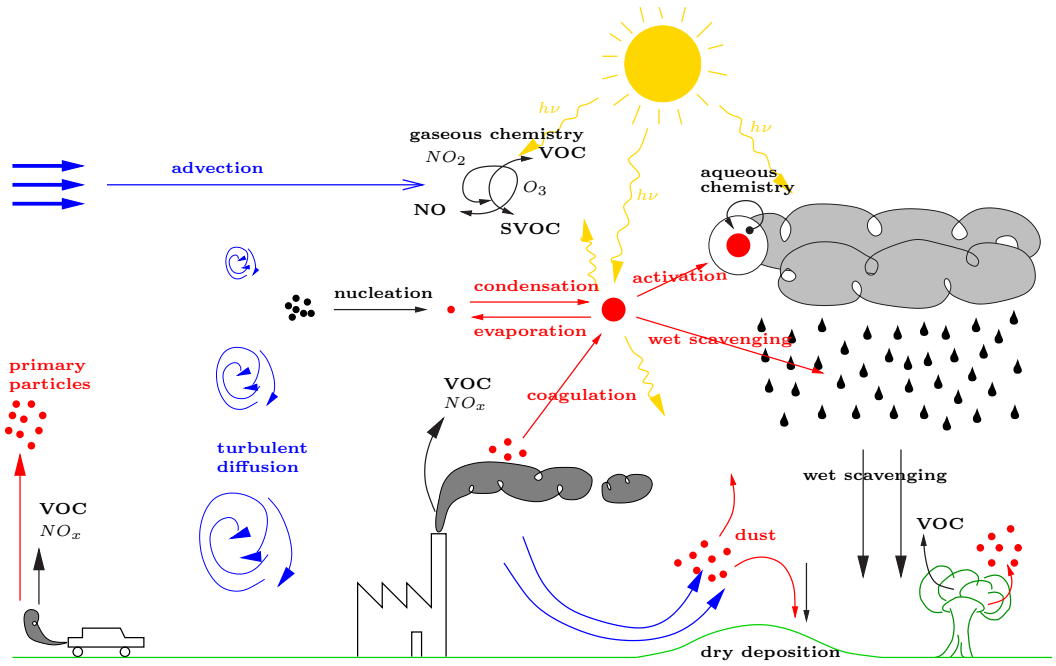

Figure 4.1: Atmospheric dispersion of aerosols.

Computing the wet diameter is essentially computing thermodynamic, solved with the model ISORROPIA ([Nenes et al., 1998]) for the inorganic phase. In the case of condensation/evaporation, computing thermodynamic is justified because this process governs the evaporation through Henry's laws. Whereas for processes like coagulation or wet deposition, it is more convenient to use a more approximative formula, with a lower computational burden.

We now present a parameterization for computing the wet diameter from the dry one. It is optimized by comparisons to results obtained with ISORROPIA.

Gerber's Formula

The Gerber's formula ([Gerber, 1985a]) is a parameterization of the wet diameter, function of the dry diameter for different aerosol types:

$$r_w = \left[\frac{C_1 (r_d)^{C_2}}{C_3 (r_d)^{C_4} - \log RH} + (r_d)^3 \right]^{\frac{1}{3}} \tag{4.1}$$

where r_w and r_d are respectively the wet and dry aerosol diameters (in centimeter). RH is the atmospheric relative humidity (between 0 and 1). The coefficients C_1, C_2, C_3 and C_4 depend on the aerosol type and the original values proposed by Gerber are given in table 4.1.2.

aerosol type	C_1	C_2	C_3	C_4
sea salt	0.7674	3.079	2.573×10^{-11}	-1.424
urban	0.3926	3.101	4.190×10^{-11}	-1.404
rural	0.2789	3.115	5.415×10^{-11}	-1.399
$(NH_4)_2SO_4$	0.4809	3.082	3.110×10^{-11}	-1.428

Table 4.1: Original coefficients for Gerber's formula

C_3 depends on temperature through the Kelvin effect:

$$C_3(T) = C_3[1 + 0.004(298 - T)] \tag{4.2}$$

Comparison with ISORROPIA

In this section, the Gerber's formula is evaluated with respect to the model ISORROPIA for different types of coefficients.

The test protocol is described below. N aerosols are generated with a random diameter and chemical composition, as well as a temperature value T and a relative humidity RH for each aerosol. Bounds for each parameter are given in table 4.1.2.

Parameter	minimum	maximum
Wet diameter ($[\mu m]$)	0.01	10.0
RH ([])	0.2	0.95
T ([K])	260.0	310.0

Table 4.2: Bounds for random parameters.

Once the databasis is built, the dry diameter D_{dry} is computed for each aerosol with the formula:

$$\frac{\pi (D_{\text{dry}})^3}{6} = \sum_{i=1}^{n_c} n_i v_i^* \ , \quad v_i^* \simeq \frac{M_i}{\rho_i^*} \tag{4.3}$$

where n_c is the number of inorganic compounds, $(n_1, \ldots, n_{n_c})$ is the aerosol molar chemical composition, and v_i^* is the partial molar volume of component X_i, approximated by the rate between its molar mass and its volumic mass at pure state.

The wet diameter D_{ger} is computed with Gerber's fomula from the dry diameter. The wet diameter from ISORROPIA, D_{iso}, is computed directly by adding the liquid water content to the dry diameter.

Statistical indicators (given in annexe) like $RMSE$, $MNBE$ and $MNGE$ are then evaluated on these database, with N equal to 10^6. As the random generation of the databasis could result to a bias, the evaluation is reiterated on different databases. Table 4.1.2 presents the obtained mean values and standard deviation.

	sea salt	urban
RMSE	$0.24739 \pm 5.077\ 10^{-4}$	$0.47163 \pm 4.593\ 10^{-4}$
MNBE	$-0.02842 \pm 3.829\ 10^{-5}$	$-0.11753 \pm 3.961\ 10^{-5}$
MNGE	$0.06318 \pm 2.483\ 10^{-5}$	$0.12079 \pm 3.814\ 10^{-5}$
	rural	$(NH_4)_2SO_4$
RMSE	$0.60729 \pm 5.890\ 10^{-4}$	$0.34787 \pm 3.408\ 10^{-4}$
MNBE	$-0.14557 \pm 4.319\ 10^{-5}$	$-0.08477 \pm 3.724\ 10^{-5}$
MNGE	$0.14656 \pm 4.256\ 10^{-5}$	$0.09396 \pm 3.236\ 10^{-5}$

Table 4.3: Differences between Gerber's formula and ISORROPIA for the different coefficient types.

Negative values for MNBE indicate that Gerber's formula often drift to under-evaluation of the wet diameter in comparison to the wet diameter obtained with ISORROPIA. The values for MNGE show that the difference between Gerber's and ISORROPIA diameter is located at the second non-zero decimale. The lowest RMSE is obtained for coefficient corresponding to sea salt.

Optimisation of coefficients

The previous comparison indicates that some coefficients give results very closed to the model ISORROPIA. We now try to determine the coefficients that minimize this model error.

In addition to the four coefficients of the formula (4.1), we also choose

to change the coefficient 0.004 of (4.2), written as C_5.

$$C_3(T) = C_3[1 + C_5(298 - T)] \tag{4.4}$$

Minimizing the MNBE would not make sense because of error compensations. Minimizing the RMSE would result to neglect small diameters. Minimizing the MNGE is not possible because it is not differentiable everywhere.

Then we choose to minimize the following function:

$$F[(C_j)_1^5] = \sum_{i=1}^{N} \left(\frac{D_{\text{ger}}[D^i_{\text{dry}}, (C_j)_1^5] - D^i_{\text{iso}}}{D^i_{\text{iso}}} \right)^2 \tag{4.5}$$

The process of minimisation is done with the BFGS solver ([H. Byrd and Zhu, 1995]). It uses the gradient of F:

$$j = 1, \ldots, 5 \ , \quad G_j = \frac{\partial F}{\partial C_j} \tag{4.6}$$

that we calculate by finite differences:

$$j = 1, \ldots, 5 \ , \quad G_j = \frac{F(.., C_j(1+\varepsilon), ..) - F(.., C_j(1-\varepsilon), ..)}{2C_j\varepsilon} + o(\varepsilon^2) \tag{4.7}$$

where ε is of magnitude 10^{-9}.

The minimisation process needs an initial value for each coefficient and eventually a range of variation. Minimisation results could be sensitive to the initial value, leading to local or global minima. Then we choose for initial value the harmonic mean of the different cases from table 4.1.2.

	initial value	minimum	maximum
C_1	0.4483	0.01	2.0
C_2	3.094	1.0	5.0
C_3	$3.671\ 10^{-11}$	10^{-13}	10^{-10}
C_4	-1.414	-3.0	-0.1
C_5	0.004	0.001	0.1

Table 4.4: Initial values for Gerber's coefficients.

We arbitrarily fix a variation range for each coefficient. In practice, if the optimisation does not reach the bounds of each range, the optimisation process is supposed to have reached convergence.

C_1	$0.49893 \pm 6.277\ 10^{-4}$
C_2	$3.02618 \pm 1.966\ 10^{-4}$
C_3	$5.37221\ 10^{-13} \pm 9.495\ 10^{-13}$
C_4	$-1.37105 \pm 8.291\ 10^{-4}$
C_5	$3.94246\ 10^{-4} \pm 5.052\ 10^{-5}$

Table 4.5: Optimized Gerber's coefficient.

The minimisation is done on several databases. Table 4.1.2 presents the average of the obtained coefficients.

The variability of coefficients is admissible except for C_3, that remains difficult to optimize, due certainly to its difference of magnitude with the other coefficients.

We compare Gerber's formula with the model ISORROPIA in the same way as previously, on several databases, with the optimized coefficients. Table 4.1.2 collects for these coefficients the errors RMSE, MNBE and MNGE with respect to ISORROPIA.

RMSE	$0.24602 \pm 4.894\ 10^{-4}$
MNBE	$-6.67689\ 10^{-3} \pm 4.041\ 10^{-5}$
MNGE	$5.56975\ 10^{-2} \pm 2.155\ 10^{-5}$

Table 4.6: Differences between Gerber's formula and ISORROPIA for the optimized coefficients.

By comparison between this table and the table 4.1.2, we confirm that optimised coefficient minimize the different errors. In the next section, we wish to confirm this result on a real 3D simulation case.

3D tests

If optimized coefficients agree more with the model ISORROPIA, we expect that they minimize the distance between a 3D simulation with ISORROPIA and a 3D simulation with Gerber's formula.

We run a reference simulation with ISORROPIA and then 2 simulations with Gerber's formula: one with the initial values of the optimization for coefficients (see table 4.1.2) and the other one with the optimized coefficients (see table 4.1.2). These two simulations are respectively called "initial Gerber" and "optimized Gerber".

The common features of the 3 simulations are the following ones:

- 3D dispersion model POLAIR3D : all 3D processes are taken into account.
- Aerosol model SIREAM : 10 sections, all $0D$ aerosol processes are taken into account, condensation/evaporation solved by bulk equilibrium. Uniform initial conditions are taken from [Putaud et al., 2003], and boundary conditions are taken from Gocart simulations.
- Aqueous model VSRM.
- Period: 14 days in April 2001.
- European domain (mesh of $65 \times 33 \times 5$ cells).

Tables 4.1.2 and 4.1.2 collect the errors for different gaseous and aerosol species for simulations "initial Gerber" and "optimized Gerber".

We note that the error decreases between "initial Gerber" and "optimized Gerber" for particulate species PNO_3, PNH_4, PHCL and PNA and also for PM10 and PM2.5. The maximum RMSE is reached for ozone in both cases, but decreases also. In the same way the maximum MNGE is reached for HONO in both case, and is slightly lower for the simulation "optimized Gerber".

The use of Gerber's formula has also lowered the CPU time by 32% with respect to the reference simulation without bringing important differences, the MNGE always remaining below 1.

On that basis, the default computation of wet diameters is performed with the optimized Gerber's formula. Computation though resolution of internal equilibrium remains possible.

4.2 Parametrizations

4.2.1 Gravitational sedimentation

Gravitational sedimentation is taken into account as an additional term for vertical advection of particles. The vertical velocity for an advected particle is then $w - v_g$, with v_g the velocity of gravitational sedimentation that depends on particle size.

An approximation is given by the Stokes velocity, given in equation (4.23). Rigorously, we should take into account the deviation from Stokes

Species	RMSE	MNGE	MNBE
CVALK1	0.0001128	0.0111500	0.0041904
CVAPI1	0.0000065	0.0047525	−0.0024908
CVAPI2	0.0005171	0.0067592	−0.0049581
CVAR01	0.0002440	0.0085380	0.0051602
CVAR02	0.0021814	0.0067359	0.0033807
CVLIM1	0.0001294	0.0073089	−0.0053657
CVLIM2	0.0005582	0.0072172	−0.0055425
CVOLE1	0.0000245	0.0037832	0.0014609
H2O2	0.0695234	0.0537246	−0.0496363
HCL	0.0446078	0.0105519	−0.0037380
HNO3	0.0813974	0.0490655	−0.0169447
HONO	0.1813701	0.1729995	−0.1395780
NH3	0.0629281	0.0239098	0.0193505
NO	0.0342040	0.0196585	0.0143971
NO2	0.4581412	0.0482401	0.0456124
O3	1.0713284	0.0104498	0.0097836
PALK1	0.0012316	0.0120245	0.0048411
PAPI1	0.0001862	0.0039705	−0.0028347
PAPI2	0.0011430	0.0087640	−0.0072792
PARO1	0.0009937	0.0099366	0.0043780
PARO2	0.0013510	0.0091574	0.0013531
PBC	0.0005904	0.0005632	0.0000109
PHCL	0.0364257	0.0083213	0.0031255
PLIM1	0.0012921	0.0086615	−0.0076212
PLIM2	0.0017170	0.0094920	−0.0082921
PM10	0.3924960	0.0072821	−0.0063617
PM2.5	0.3924960	0.0072821	−0.0063617
PMD	0.0214279	0.0007612	−0.0001252
PNA	0.0161749	0.0031767	−0.0012851
PNH4	0.0777295	0.0118042	−0.0094591
PNO3	0.3098293	0.0223167	−0.0198306
POLE1	0.0001750	0.0038701	0.0021444
PPOA	0.0007257	0.0005738	0.0000499
PSO4	0.0222568	0.0062173	0.0014639
SO2	0.0118966	0.0015191	−0.0006176

Table 4.7: Errors between reference simulation and "initial Gerber". $CVALK_1$ indicates the species ALK_1 in gaseous phase, $PALK_1$ the same species in aerosols.

Species	RMSE	MNGE	MNBE
CVALK1	0.0000691	0.0135077	−0.0124369
CVAPI1	0.0000074	0.0050740	0.0046254
CVAPI2	0.0002936	0.0063263	0.0060503
CVAR01	0.0000711	0.0040808	−0.0006418
CVAR02	0.0009306	0.0038374	−0.0022457
CVLIM1	0.0000849	0.0069516	0.0066459
CVLIM2	0.0003095	0.0066153	0.0063517
CVOLE1	0.0000064	0.0034172	0.0022576
H2O2	0.0717403	0.0392091	0.0384572
HCL	0.0535698	0.0102179	0.0051862
HNO3	0.0466438	0.0660728	0.0526271
HONO	0.0679391	0.1289918	0.1129869
NH3	0.0232839	0.0110572	−0.0042806
NO	0.0138132	0.0168023	0.0051062
NO2	0.1877896	0.0256472	−0.0159620
O3	0.8502031	0.0088896	−0.0088575
PALK1	0.0015438	0.0164914	−0.0156368
PAPI1	0.0001590	0.0030812	0.0021719
PAPI2	0.0005620	0.0064373	0.0041842
PARO1	0.0004095	0.0052702	−0.0029053
PARO2	0.0006686	0.0061650	−0.0039032
PBC	0.0006693	0.0006209	0.0001041
PHCL	0.0364835	0.0079541	0.0000685
PLIM1	0.0006132	0.0060709	0.0046627
PLIM2	0.0008053	0.0066787	0.0045557
PM10	0.1477357	0.0031404	0.0009712
PM2.5	0.1477357	0.0031404	0.0009712
PMD	0.0103096	0.0006052	0.0000393
PNA	0.0194669	0.0027428	0.0006729
PNH4	0.0258893	0.0053421	0.0009581
PNO3	0.1205261	0.0122194	0.0085498
POLE1	0.0001298	0.0024552	−0.0003908
PPOA	0.0007059	0.0006252	0.0000256
PSO4	0.0233696	0.0083624	−0.0078290
SO2	0.0138640	0.0018535	0.0018026

Table 4.8: Errors between reference simulation and "optimized Gerber". $CVALK_1$ indicates the species ALK_1 in gaseous phase, $PALK_1$ the same species in aerosols.

formula for non submicronic particles. This leads to solve the following non-linear system with respect to the sedimentation velocity:

$$v_g = \sqrt{\frac{4g\,d_p\,C_c\,\rho_p}{3\,C_d v_g\,\rho_{air}}} \tag{4.8}$$

with g the gravity constant, d_p the particle diameter, ρ_p its density and ρ_{air} the air density. The Cunningham coefficient C_c is given by (4.24) and the drag coefficient C_d is a function of the particle Reynolds number and then of the gravitational velocity (expression is not detailed here).

The resolution of this algebraic equation is done with a Newton algorithm.

4.2.2 Below-cloud wet scavenging

In this section, the rain intensity p_0 i given in mm/h. Moreover, the aerosol radius (for a monodisperse distribution) is r_p, given in μm.

D_r (in meters) is the diameter of a rain droplet (eventually in a polydisperse distribution or as a representative diameter for a population which is assumed monodisperse). The aerosol diameter is d_p (also in meters).

Theorical model

We quote here the theorical modeling of the scavenging coefficient for the washout process (below-cloud scavenging), that corresponds to the scavenging of aerosols by falling raindrops.

A key point is the representation of the raindrops distribution and of the falling velocity.

Droplet distribution The raindrops distribution is usually described by a Gamma distribution with 4 parameters:

$$n_r(D_r) = \alpha_0\,D_r^{\alpha}\exp(-\beta\,D_r^{\gamma}) \tag{4.9}$$

The two classic cases correspond to the Marshall-Palmer ($\alpha = 0$; $\gamma = 1$) and to the Khrigian-Mazin ($\alpha = 2$, $\gamma = 1$) distribution.

The diameter ranges for the raindrops given by these parameterizations are function of the rain intensity in table 4.9.

We point out that in [Mircea et al., 2000], lognormal distributions are used, on the basis of measures.

Table 4.9: Typical ranges for raindrops diameter given by the Marshall-Palmer and Khrigian-Mazin distributions, from [Mircea and Stefan, 1998]. For a $[a/b - .]$ diameter range, a refers to the the value of the Marshall-Palmer distribution, b the value for Khrigian-Mazin.

Rain type	p_0 (mm/h)	D_r range (mm)
weak	[1-5]	[0/0.001-0.1]
moderate	[5-100]	[0/0.01-1]
intense	[100-500]	[0/0.1-10]

Representative diameter There exit numerous parameterizations for the *representative* diameter, in order to treat only one monodisperse population of raindrops:

1. In [Pruppacher and Klett, 1998] (page 34):

$$D_r = 0.976 \times 10^{-3} {p_0}^{0.21} \tag{4.10}$$

2. From a Marshall-Palmer distribution:

$$D_r = 0.243\, 10^{-3} {p_0}^{0.21} \tag{4.11}$$

3. In a similar way to the previous parameterization ([Andronache, 2004]):

$$D_r = 0.24364\, 10^{-3} {p_0}^{0.214} \tag{4.12}$$

4. In [Loosmore and Cederwall, 2004]:

$$D_r = 0.97\, 10^{-3} {p_0}^{0.158} \tag{4.13}$$

5. In [Mircea et al., 2000], parameterizations from measures taken in estern Meditarranea give:

$$D_r = [0.63 - 0.72]\, 10^{-3} p_0^{0.23} \tag{4.14}$$

   to compare with the first and the fourth equations.

6. At last, in [Underwood, 2001] (page 35), it is quoted that the original article of Slinn recommands:

$$D_r = 0.7\, 10^{-3} p_0^{0.25} \tag{4.15}$$

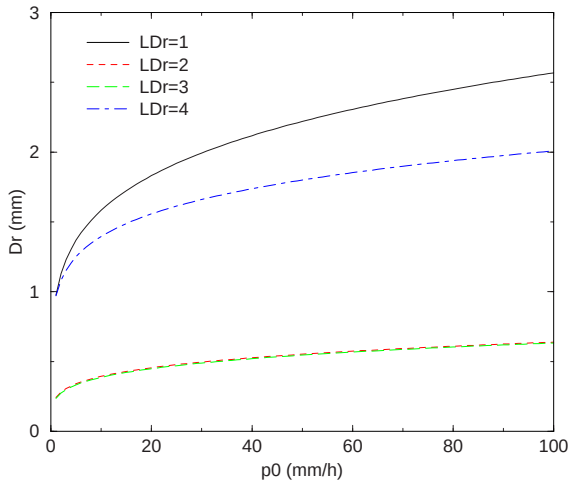

Figure 4.2: Evolution of the representative diameter with respect to the rain intensity, for some parameterizations. The order (LDr) is coherent with this of the references.

Globally, we have:

$$D_r = [0.2431 - 0.97]\, 10^{-3}\, D_r^{[0.158-0.25]} \tag{4.16}$$

The comparison of the fourth first parameterizations is given in the figure 4.2. We notice the high dispersion of the results: it is useally quoted that the Marshall-Palmer distribution overestimate the small droplets number, that leads to overestimate the collision efficiencies and then the scavenging.

Falling velocity Several parameterizations give an expression for the falling velocity U_{drop} (in $m.s^{-1}$) function of diameter:

1. Kessler's parameterization ([Andronache, 2003], page 143, and [Mircea and Stefan, 1998], table 2):
$$U_{drop} = 130\sqrt{D_r} \tag{4.17}$$

2. The parameterization cited in [Seinfeld, 1985] (page 632):
$$U_{drop} = 9.58\left[1 - \exp\left(-\left(\frac{D_r}{0.171 \times 10^{-2}}\right)^{1.147}\right)\right] \tag{4.18}$$

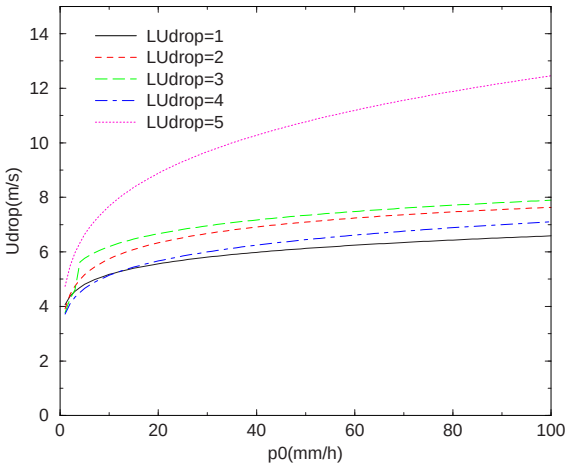

Figure 4.3: Evolution of the falling velocity with respect to the rain intensity, for several parameterizations for velocity. The representative diameter is computed with $LDr = 1$. The order ($LUdrop$) is consistent with this of the references.

3. The parameterization given in [Seinfeld and Pandis, 1998] or in [Mircea et al., 2000] that uses the droplet final velocity (to be computed by an algorithm because outside the domain of the Stokes formula).

4. The parameterization in [Andronache, 2004]:

$$U_{drop} = 3.778\,10^3\,D_r^{0.67} \tag{4.19}$$

5. At last, in [Loosmore and Cederwall, 2004]:

$$U_{drop} = 4.854\,D_r\,\exp(-195\,10^{-3}D_r) \tag{4.20}$$

D is in meter in all these formulas. Comparisons are given in figure 4.3 with the parameterization $LDr = 1$ for the representative diameter.

Expression for the scavenging coefficient

Monodisperse case The volume dragged by a raindrop with a diameter D_r is given by the following expression:

$$\frac{\pi}{4}\,{D_r}^2\,U_{drop}(D_r) \tag{4.21}$$

The collision volume or *effective volume*, that is to say the volume where the contact is efficient for one time unit, takes also into account the aerosol diameter d_p and its falling velocity u_{grav} (in $m.s^{-1}$):

$$\frac{\pi}{4}\left(D_r + d_p\right)^2 \left(U_{drop}(D_r) - u_{grav}(d_p)\right) \tag{4.22}$$

where the gravitational sedimentation velocity u_{grav} is given by the Stokes formula:

$$u_{grav} = \frac{{d_p}^2 \left(\rho_p - \rho_{air}\right) g\, C_c}{18\mu_{air}} \tag{4.23}$$

with ρ_p (in $kg.m^{-3}$) the particle volumic mass, μ_{air} the air dynamic viscosity (in $Pa.s$), g the gravity (in $m.s^{-2}$) and C_c the corrective Cunningham factor, meaning that slidings appear for small particles ($\simeq 1\mu m$). If we do not want to use tabulated values for C_c, the following expression could be used [Seinfeld and Pandis, 1998]:

$$C_c = 1 + \frac{2\,\lambda_{air}}{d_p}\left(1.257 + 0.4\,\exp\left(-0.55\frac{d_p}{\lambda_{air}}\right)\right) \tag{4.24}$$

with the free mean path for air λ_{air} (in m):

$$\lambda_{air} = \frac{2\,\mu_{air}}{P}\left(\frac{8}{\pi\, R_{air}\, T}\right)^{-1/2} \tag{4.25}$$

R_{air} is the ideal gas constant for air (in $J.K^{-1}.kg^{-1}$) and T is the temperature (in K).

This representation implies that every particle in the effective volume is captured and then neglect the effects of the air movement resulting from the fall of the raindrop which alters the particles trajectory. This effect is parametrised by a collision efficiency $E(D_r, d_p)$, defined as the fraction of particles with diameter d_p, in the collision volume of a droplet with diameter D_r, that are efficiency collected:

$$\frac{\pi}{4}\left(D_r + d_p\right)^2 \left(U_{drop}(D_r) - u_{grav}(d_p)\right) E(D_r, d_p) \tag{4.26}$$

Simplifications Two classical approximations allow to simplify the previous expression:

- $U_{drop}(D_r) \gg u_{grav}(d_p)$
- $(D_r + d_p)^2 \simeq D_r^2$

p_0 en mm/h		1	10	50
D_r en cm		0.0976	0.158	0.222
d_p en μm				
0.1	$U_{drop} =$	3.92	5.74	7.10
$(C_c = 2.85)$	$u_{grav} =$	8.4×10^{-7}	8.4×10^{-7}	8.4×10^{-7}
1	$U_{drop} =$	3.92	5.74	7.10
$(C_c = 1.164)$	$u_{grav} =$	3.4×10^{-5}	3.4×10^{-5}	3.4×10^{-5}
10	$U_{drop} =$	3.92	5.74	7.10
$(C_c = 1.016)$	$u_{grav} =$	3.0×10^{-3}	3.0×10^{-3}	3.0×10^{-3}

Table 4.10: Computation of representative diameters and falling velocities.

For $\rho_p = 1\, g/cm^3$, $g = 9.81\, m.s^{-2}$ and $\mu_{air} \simeq 1.72 \times 10^{-1}\, Pa.s$, we obtain for exemple the values in table 4.10 for D_r and U_{drop}, which allows to verify the approximations.

If N_r is the total droplet density (in m^{-3}), assumed monodisperse, we finally have:

$$\Lambda(d_p) = \frac{\pi}{4} {D_r}^2\, U_{drop}(D_r)\, E(D_r, d_p)\, N_r \tag{4.27}$$

By definition, the rain intensity p_0 may be written as:

$$p_0 = \int_0^\infty \frac{\pi}{6} D_r^3\, U_{drop}(D_r)\, n_r(D_r)\, dD_r$$

that is to say for the monodisperse case:

$$p_0 = \frac{\pi}{6} {D_r}^3\, U_{drop}(D_r)\, N_r \tag{4.28}$$

We finally have the classical expression:

$$\Lambda(d_p) = \frac{3}{2}\, \frac{E(D_r, d_p)\, p_0}{D_r} \tag{4.29}$$

where p_0 is in ISU (m/s).

Polydisperse case This frame may be applied to polydisperse populations of aerosol and droplets. Let us write respectively $n_p(d_p)$ and $n_r(D_r)$ (in $m^{-3}.m^{-1}$) the number distribution for aerosols and for raindrops.

The number of particles with a diameter in the range $[d_p, d_p + dd_p]$ collected in a time unit by raidrops is given by:

$$n_p(d_p)\, dd_p \int_0^\infty \frac{\pi}{4}(D_r + d_p)^2 \left(U_{drop}(D_r) - u_{grav}(d_p)\right) E(D_r, d_p)\, n_r(D_r)\, dD_r \tag{4.30}$$

On the basis of approximations, we directly obtain for the scavenging rate of the particles with diameter d_p, $\frac{dn_p(d_p)}{dt} = -\Lambda(d_p)\, n_p(d_p)$:

$$\Lambda(d_p) = \int_0^\infty \frac{\pi}{4} {D_r}^2\, U_{drop}(D_r)\, E(D_r, d_p)\, n_r(D_r)\, dD_r \tag{4.31}$$

Parameterization of the collision efficiency

A keypoint of the parameterization is the parameterization of the collision efficiency, defined as the ratio between the number of collisions between water droplets and particles, and the number of particles in the covered geometric volume.

E is equal to 1 if all particles are effectively captured but in practice $E \ll 1$. Measures shows that a collision results almost everytime in capture, collisions are then rare.

It is necessary to take into account different phenomena to explain the possible capture of a particle:

- *brownian diffusion* might place a particle on a droplet trajectory.

  The hypothesis concerning the equivalence collision/capture and the fact that brownian diffusion is more important for fine particles justifies that this process is in favour of the capture of small particles.

- Another phenomenon that privileges capture of bigger particles is *inertia*. It could provoke collision by preventing particles to follow streamlines around droplets. The last phenomenon is interception that results from the contact of a particle following a streamline around the droplet because of its size. The considerations about inertia and interception could not be strictly dissociated from considerations about particle density. Inertia actually concerns heavy particles and interception big ones.

Globally, these two processes explain that scavenging is important for small aerosols (typically diameter less than 0.01 μm) through brownian diffusion and for the big aerosols (typically diameter higher than 2 μm)

through inertia. Aerosols with intermediate diameters form what is usually referred as the *Greenfield Gap* or *scavenging gap*, in the range $[0.01; 2]\mu$m, and are weakly scavenged.

Note that experimentally, this scavenging default is less evident than predicted by theory (see below the neglected effets).

The expression proposed in [Seinfeld and Pandis, 1998] after a dimensional analysis and application of Buckingham's theorem gives E as a function of five adimensioned numbers:

- Reynolds number of raindrop

$$Re = \frac{D_r \, U_{drop}}{2\nu_{air}} \tag{4.32}$$

  where $\nu_{air} = \mu_{air}/\rho_{air}$ is the air kinematic viscosity (in m^2/s).

- Schmidt number of the captured particle:

$$Sc = \frac{\nu_{air}}{D_B} \tag{4.33}$$

  with D_B the brownian diffusivity coefficient of the particle (in $m^2.s^{-1}$):

$$D_B = \frac{k\,T}{3\,\pi\,\mu_{air}\,d_p} C_c \tag{4.34}$$

  where k is the Boltzmann's constant (in $J.K^{-1}$).

- Stokes number of the captured particle:

$$St = 2\tau \, \frac{U_{drop} - u_{grav}}{D_r} \tag{4.35}$$

  with τ a characteristic relaxation time taken equal to u_{grav}/g, that is to say:

$$\tau = \frac{(\rho_p - \rho_{air})\, d_p^2 \, C_c}{18\mu_{air}} \tag{4.36}$$

- the ratios between diameters (ϕ) and viscosities (ω):

$$\phi = \frac{d_p}{D_r} \ , \quad \omega = \frac{\mu_w}{\mu_{air}} \tag{4.37}$$

  with μ_w the viscosity of water.

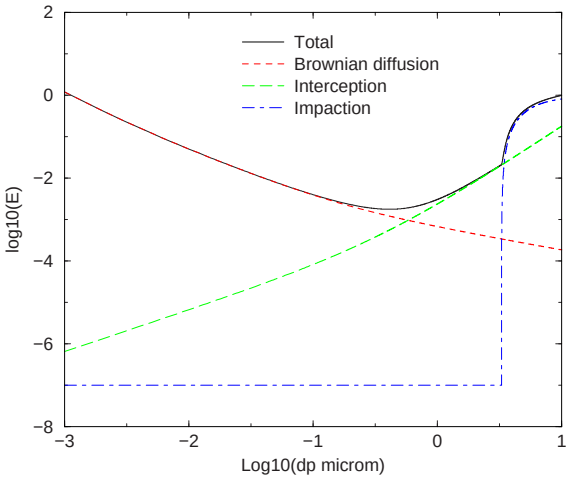

Figure 4.4: Contributions to the collision efficiency $E(D_r, d_p)$ for $D_r = 0.1$mm

The formula for E is then given by:

$$E = \frac{4}{Re\,Sc}\left(1 + 0.4\,Re^{1/2}\,Sc^{1/3} + 0.16\,Re^{1/2}\,Sc^{1/2}\right) + 4\,\phi\left(\omega^{-1} + [1 + 2\,Re^{1/2}]\,\phi\right) + \left(\frac{St - S^*}{St - S^* + 2/3}\right)^{3/2}\left(\frac{\rho_p}{\rho_w}\right)^{1/2} \tag{4.38}$$

with the critical Schmidt number $S^\star$:

$$S^* = \frac{1.2 + 1/12\,\ln(1 + Re)}{1 + \ln(1 + Re)} \tag{4.39}$$

The three terms respectively correspond to the terms of brownian diffusion, interception and impaction. The distribution $E(D_r, d_p)$ is given for a raindrop $D_r = 0.1$mm in figure 4.4.

The dependency of efficiency to the raindrop diameter is given in figure 4.5. The efficiency increases when diameter decreases. The amplitude of the differences has to be compared to the spread of representative diameters in figure 4.2.

Efficiency of scavenging a polydisperse aerosol population In [Mircea et al., 2000], the polydisperse nature of aerosols and rain distribution are taken into

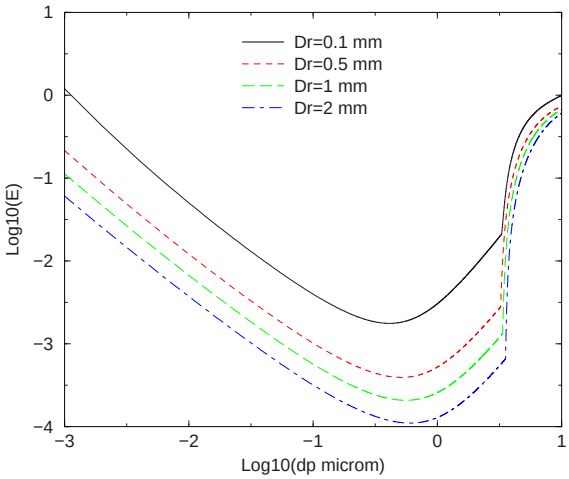

Figure 4.5: Collision efficiencies $E(D_r, d_p)$ for $D_r = 0.1$mm, 0.5mm, 1mm et 2mm.

account with lognormal distributions of aerosols. A parameterization is proposed for Λ :

$$\Lambda = a + b\, p_0 \tag{4.40}$$

(a, b) vary following the type of the chosen aerosol distribution (rural, urban, marine): $a \in [1.5810^{-2} - 1.98]$ and $b \in [2.1710^{-3} - 3.19\,10^{-1}]$ (maximal values correspond to the urban case, and minimal values to the marine case). It has to be noticed that:

1. The scavenging of a polydisperse aerosol population is greater of at least one order of magnitude than the scavenging of a monodisperse population;
2. the choice of the raindrop distribution is not very sensitive;
3. the scavenging in urban environment is greater of one order of magnitude than the scavenging in "remote" environment".

Notice that this affine parameterization is not classical (see below).

Justification of laws $\Lambda = A\, p_0^B$ In [Mircea and Stefan, 1998], a review of the different distribution laws for raindrops is given, with for instance Γ distributions or the Marshall-Palmer distribution. It is notably demonstrated that for a Γ distribution, if the collision efficiency is supposed to

be a constant, then the scavenging coefficient integrated over the whole distribution follows the law:

$$\Lambda \simeq A\, {p_0}^B \tag{4.41}$$

with B depending of the coefficients of the Γ law and the parameterization of the falling velocity (supposed to be parameterized as $U_{drop}(D_r) = u\, D_r^{\alpha}$).

All calculations done, discerning the three rain types already presented (table 4.9), the parameterisation becomes:

$$\Lambda \simeq \begin{cases} [0.753 - 0.875]\, E\, p_0^{[0.78-0.86]} \text{ for } \textit{violent} \text{ rain} \\ [1.91 - 1.95]\, E\, p_0^{[0.78-0.86]} \text{ for } \textit{moderate} \text{ rain} \\ [20.56 - 26.67]\, E\, p_0^{[0.78-0.86]} \text{ for } \textit{weak} \text{ rain} \end{cases} \tag{4.42}$$

with Λ in h^{-1} and E the collision efficiency supposed to be a constant. By taking a value of the order of $E \simeq 0.1$, we obtain for minimum value for violent rain $\Lambda \simeq 2\,10^{-5}\, p_0^{0.8}$ (in s^{-1}) and for maximum value for weak rain $\Lambda \simeq 7.4\,10^{-4}\, p_0^{0.8}$ (in s^{-1}).

A similar approach is carried on in [Andronache, 2003] with an adaptation of a model $\Lambda = A\, p_0^B$ on the basis of polydisperse models for raindrops (Marshall-Palmer) and the aerosol population. The results are given in tables 4.11 and 4.12.

It is easy to obtain similar results that justify that type of parameterization. Notice that with the variation range obtained for D_r in (4.16), we directly have with $\Lambda = 1.5\, E \times p_0/D_r$ and by taking into account the conversion factor $10^{-3}/3600$ for p_0:

$$\Lambda \simeq [0.43 - 1.71]\, 10^{-3} E\, p_0^{[0.75-0.842]} \tag{4.43}$$

For efficiencies $E \in [0.1 - 1]$, we obtain:

$$\Lambda \simeq [4.3\, 10^{-5} - 1.71\, 10^{-3}]\, p_0^{[0.75-0.842]} \tag{4.44}$$

4.2.3 Wet scavenging of aerosols: *in-cloud*

When they fall, raindrops aggregate cloud droplets, and suspended gas and aerosols. This is the wet scavenging phenomenon. Inside a cloud, pollutants (gas and particles) are almost absorbed by cloud droplets, so that wet scavenging is reduced to their aggregation by raindrops.

Table 4.11: Parameterizations obtained by adjustment on a theoretical polydisperse model for rain and aerosols [Andronache, 2003]. Case with a coarse fraction (more than 10 μm).

A	B	reference	Aerosol
$6.67\,10^{-5}$	0.7	[Andronache, 2003]	Urban
$1.28\,10^{-4}$	0.7	id.	Remote Continental
$1.39\,10^{-4}$	0.7	id.	Marine
$1.28\,10^{-4}$	0.7	id.	Rural
$1.89\,10^{-4}$	0.7	id.	Free Tropo.
$9.44\,10^{-5}$	0.7	id.	Polar
$2.44\,10^{-4}$	0.7	id.	Desert
$2.22\,10^{-4}$	0.7	id.	Marine
$8.33\,10^{-5}$	0.7	id.	Marine
$1.94\,10^{-4}$	0.7	id.	Sand
$1.00\,10^{-4}$	[0.67-0.76]	id.	Exp.data
$3.50\,10^{-4}$	0.78	id.	In-cloud

Table 4.12: Parameterizations obtained by adjustment on a theoretical polydisperse model for rain and aerosols [Andronache, 2003]. Case of a submicronic distribution.

A	B	reference	aerosol type
$2.33\,10^{-7}$	0.59	[Sparmacher et al., 1993]	Exp. ($d_p = 0.23$)
$3.14\,10^{-7}$	0.60	id.	Exp. ($d_p = 0.46$)
$2.56\,10^{-7}$	0.94	id.	Exp. ($d_p = 0.98$)
$1.72\,10^{-7}$	0.61	id.	Exp. ($d_p = 2.16$)
$6.90\,10^{-6}$	0.92	[Julya, 1999]	Exp. (radionuclides)
$[2.36\,10^{-7} - 1.4\,10^{-6}]$	[0.59-0.61]	[Andronache, 2003]	Marine
$[2.78\,10^{-8} - 3.89\,10^{-8}]$	0.59	id.	Marine
$2.36\,10^{-7}$	0.59	id.	Alpes

Giving a concentration of pollutant c, its evolution due to wet scavenging in clouds is governed by the equation:

$$\frac{\partial c}{\partial t}(x,y,z,t) = -\Lambda(x,y,z)c(x,y,z,t) \tag{4.45}$$

where Λ is the wet scavenging coefficient, expressed in seconds, and its expression depends on the collision process between cloud and rain droplets. For this reason it does not depend on the considered pollutant.

The integration of this equation between the initial (t_0) and final (t_1) times is done analytically:

$$c(x,y,z,t_1) = c(x,y,z,t_0)\exp[-\Lambda(x,y,z)(t_1 - t_0)] \tag{4.46}$$

Below we present the two parameterizations used in POLAIR3D : one is from the model CAMx ([ENVIRON, 2005]), and the other one from the Multiscale Air Quality (CMAQ) ([Roselle and Binkowski, 1999]).

1. Parameterization from CAMx:

   The volume covered by a falling raindrop per time unit is equal to:

   $$V = \frac{\pi}{4}(D_r + d_c)^2 U_{drop} \tag{4.47}$$

   where

   - D_r the raindrop diameter, in meters, is given by the empirical law ([Scott, 1978]) :

     $$D_r = 9.0 \times 10^{-4} p_0^{0.21} \tag{4.48}$$

     p_0 is the precipitation rate (in mm/hr).
   - d_c is the diameter of cloud droplets, in meters.
   - U_{drop} is the falling velocity of raindrops, in $m.s^{-1}$, given by the empirical law ([Scott, 1978]) :

     $$U_{drop} = 3100\ D_r \tag{4.49}$$

   The wet scavenging coefficient in clouds can be put under the form:

   $$\Lambda = E\frac{\pi}{4}(d_c + D_r)^2 U_{drop} N_r \tag{4.50}$$

   where

- N_r is the numerical concentration ($\#.m^{-3}$) of raindrops, that could be computed from the precipitation rate:

$$N_r = \frac{2.8 \times 10^{-7} p_0}{\pi (D_r)^3 U_{drop}/6} \tag{4.51}$$

  The number 2.8×10^{-7} takes into account the conversion of p_0 from mm/hr in m/s.
- E represents the probability that a cloud droplet on the trajectory of a raindrop is actually aggregated. The air fluxes created by the fall of the raindrop decrease this probability to 0.9.

We generally admit that the diameter of a cloud droplet can be neglected as compared to a raindrop diameter:

$$d_c \ll D_r \Longrightarrow \Lambda = \frac{\pi}{4} (D_r)^2 U_{drop} N_r \tag{4.52}$$

By replacing N_r by its expression (4.51) we obtain:

$$\Lambda = 4.2 \times 10^{-7} \frac{E\ p_0}{D_r} \tag{4.53}$$

With $E \simeq 0.9$ and D_r given by (4.48), one gets :

$$\Lambda = 4.2 \times 10^{-4} p_0^{0.79} \tag{4.54}$$

2. Parameterization from CMAQ:

   In this parameterization, the expression for the scavenging coefficient is:

$$\Lambda = -\frac{1 - e^{-\frac{\tau_{\text{cld}}}{\tau_{\text{washout}}}}}{\tau_{\text{cld}}} \tag{4.55}$$

   where

   - τ_{cld}, expressed in seconds, is equal to the 3D timestep of the dispersion model if the cloud size exceeds the mesh dimensions, and is equal to 1 hour otherwise,
   - τ_{washout} represents the time required for the volume of water to precipitate to the ground.

$$\tau_{\text{washout}} = \frac{W_T \Delta z_{\text{cld}}}{\rho_{\text{H}_2\text{O}} p_0} \tag{4.56}$$

     Δz_{cld} is the cloud depth, W_T is the liquid water content of the cloud (kg/m^3), and $\rho_{\text{H}_2\text{O}}$ the liquid water density.

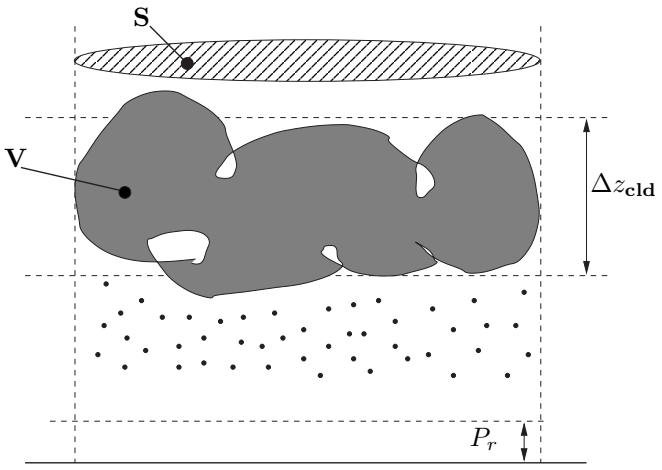

Figure 4.6: Washout.

Figure 4.6 illustrates the formula (4.56).

Let us justify equation (4.56). Giving a cloud volume V, the total mass of water contained in the cloud is equal to $W_T V$ (kg). That represents a water volume $W_T V/\rho_{\mathrm{H_2O}}$. The duration τ_{washout}, required for that volume to precipitate to the ground, depends on the precipitation rate p_0 $(m.s^{-1})$:

$$\frac{W_T V}{\rho_{\mathrm{H_2O}}} = \tau_{\mathrm{washout}} p_0 S \tag{4.57}$$

where S is the surface at ground covered by the cloud. Assume that the cloud volume is approximatively the product of this surface by the cloud depth, we get:

$$V \simeq S\Delta z_{\mathrm{cld}} \implies \frac{W_T \Delta z_{\mathrm{cld}}}{\rho_{\mathrm{H_2O}}} = \tau_{\mathrm{washout}} p_0 \tag{4.58}$$

4.2.4 Wet scavenging of a fog

In the case of a fog, diagnosed as a cloud whose first level is at ground, the wet scavenging is parametrised following [Fahey, 2003] with a scavenging coefficient given by:

$$\Lambda = \frac{0.014\, L^{1.67} + 0.009\, L^{1.08 d0}}{L * H_{fog}} \tag{4.59}$$

with L the average liquid water content and H_{fog} the height of the fog column.

4.2.5 Dry deposition

Dry deposition is applied as a boundary condition for diffusion:

$$K_z \nabla c \cdot \mathbf{n} = E - v_{dep} c \tag{4.60}$$

with K_z the vertical turbulent fluxes, E the surfacic emission and v_{dep} the deposition velocity. $\mathbf{n}$ is the unit vector upward oriented.

Here, we do not take into account the resuspension terms.

Theoretical model for dry deposition velocity

The dry deposition velocity is expressed for particles as a function of the dynamical and surface resistances:

$$v_d = v_g + \frac{1}{R_a + R_s} \tag{4.61}$$

Resistance parameterizations to the deposition for particles are inspired from those proposed by [Zhang et al., 2001].

Sedimentation velocity It expresses the conjugated effects of gravitational settling and friction on a particle in the non excited air. The parameterization of the sedimentation velocity used here is limited to the Stokes velocity.

Aerodynamic resistance The expression for aerodynamic resistance used for particles is similar to the one used for gases.

Surface resistance The surface resistance R_s takes into account several phenomena traducing the captation ability of the surface with respect to particles:

$$R_s = \frac{1}{3u_*(E_B + E_{IM} + E_{INT})R_1} \tag{4.62}$$

with:

- u_*, the friction velocity (in $m.s^{-1}$).

- E_B represents the part of contact particle/surface induced by the brownian diffusion. The tendency of this phenomenon is to equalize the particle concentrations between reference height and surface.

$$E_B = \frac{\nu_{air}}{D_B}^{-\gamma} \tag{4.63}$$

with γ a parameter of the model [Zhang et al., 2001].

- E_{IM} is the impact coefficient and traduces the deposition directly due to the particles inertia:

$$E_{IM} = \left(\frac{St}{\alpha + St}\right)^2 \tag{4.64}$$

with α a parameter of the model [Zhang et al., 2001] and St the Stokes number defined in function of the terrain type:

$$St = \begin{cases} u_{grav}\frac{u_*}{g\,A}_2 & \text{for "rough" surfaces} \\ u_{grav}\frac{{u_*}^2}{g\,\nu_{air}} & \text{for "smooth" surfaces} \end{cases} \tag{4.65}$$

A is a parameter of the model called "characteristic radius of receptors" (in m).

- E_{INT} is the interception coefficient of the particles by the surface:

$$E_{INT} = \frac{1}{2}\left(\frac{d_p}{A}\right)^2 \tag{4.66}$$

.

- R_1 is the corrector coefficient for the rebound and describes the possible rebound of a particle on the surface:

$$R_1 = \exp\left(-\sqrt{St}\right) \tag{4.67}$$

with St the Stokes number defined above.

4.2.6 Wet scavenging for gases

For the gaseous phase, the wet below-cloud scavenging is parametrised by $L_{wet}(c_i) = -\Lambda_i\, c_i$ with c_i the concentration of the chemical species i. The coefficient Λ_i is detailed in [Sportisse and Du Bois, 2002].

A specific point related to multiphase modeling corresponds to the estimation of the raindrop pH for the computation of Henry law's coefficients.

During the below-cloud scavenging, equilibrium concentrations of soluble gaseous species can be significantly affected by the ions dissociation during the dissolution in water. To take this ionisation process into account, effective Henry coefficients are computed giving the raindrops pH for the following species: SO_2, NH_3, HNO_3, HNO_2, HCl.

pH is computed in the aqueous module. If this one is not called, pH is taken constant and equal to $4,16$.

The dissociation of SO_2 in water gives

$$SO_2 + H_2O \overset{K_1}{\rightleftharpoons} H^+ + HSO_3^-$$

$$HSO_3^- \overset{K_2}{\rightleftharpoons} H^+ + SO_3^{2-}$$

with K_i the equilibrium constants.

The Henry's effective coefficient for SO_2 is

$$H^*_{SO_2} = H_{SO_2}\left(1 + \frac{K_1}{[H^+]} + \frac{K_1 K_2}{[H^+]^2}\right) \tag{4.68}$$

The absorption of NH_3 in water gives:

$$NH_3 + H_2O \overset{K_3}{\rightleftharpoons} NH_4^+ + OH^-$$

The Henry's effective coefficient for NH_3 is

$$H^*_{NH_3} = H_{NH_3}\left[H^+\right]\frac{K_3}{K_w} \tag{4.69}$$

After dissolution,

$$HNO_3 \overset{K_4}{\rightleftharpoons} NO_3^- + H^+$$

The Henry's effective coefficient for HNO_3 is

$$H^*_{HNO_3} = H_{HNO_3}\left(1 + \frac{K_4}{[H^+]}\right) \tag{4.70}$$

After dissolution,

$$HNO_2 \overset{K_5}{\rightleftharpoons} NO_2^- + H^+$$

The Henry's effective coefficient for HNO_2 is

$$H^*_{HNO_2} = H_{HNO_2}\left(1 + \frac{K_5}{[H^+]}\right) \tag{4.71}$$

After dissolution,

$$HCl \overset{K_6}{\rightleftharpoons} Cl^- + H^+$$

The Henry's effective coefficient for HCl is

$$H^*_{HCl} = H_{HCl}\left(1 + \frac{K_6}{[H^+]}\right) \tag{4.72}$$

The values of equilibrium constants K_1 to K_6 and their variations with temperature are detailed in [Pruppacher and Klett, 1998] (page 749).

4.2.7 Emissions

Anthropogenic emissions

The data for emission of primary aerosols are usually given in total masses. For example, the EMEP european emission inventory provides yearly quantities for PM2.5 and PM10 (particles with diameter respectively less than 2.5 μm and 10 μm) or PM coarse (particles with diameter between 2.5 and 10 μm).

As our model needs a more precise information as input, these brute data have to be temporally, chemically and granulometrically speciated. In the EMEP report [Simpson et al., 2003], a parameterization for chemical and granulometric speciation is given for PM2.5 and PM coarse.

- The PM coarse fraction is attributed to mineral dust.
- The PM2.5 fraction is first chemically speciated in three species: mineral dust (MD), primary organics aerosols (POA) and black carbon (BC) by source sector or SNAP code (see table 4.13). Then each species is distributed over two modes, the Aitken and the accumulation modes (see table 4.14).

Finally, it remains to redistribute the quantities over the size discretisation of the aerosol model. For the size-resolved model SIREAM, approximation is made that each bin belongs to one mode, then the emissions are equally reparted over each bin of the mode. Sensitivity tests show that redistribution of emissions along the size distribution has not a great influence as compared to other parameters.

Source sector	POA	BC	MD
S1: Power generation	33	33	33
S2: Non-industrial combustion	50	20	30
S3: Industrial combustion	33	33	33
S4: Production processes	0	20	80
S5: Extraction and distribution of fossil fuel	40	50	10
S6: Solvent and other product use	40	20	40
S7: Road transport	40	20	40
S8: Other mobile sources and machinery	40	20	40
S9: Waste treatment and disposal	10	60	30
S10: Agriculture	70	0	30

Table 4.13: Chemical speciation of primary PM emissions (in %).

Mode	POA	BC	MD
Aitken: between 0.02 μm and 0.1 μm	15	15	0
Accumulation: between 0.1 μm and 2.5 μm	85	85	100

Table 4.14: Granulometric speciation of primary PM emissions (in %).

Sea-salt

Sea-salt aerosols are believed to be generated mostly by the evaporation of sea spray produced by bursting bubbles during whitecap formations due to surface wind.

Rate of sea-salt generation Two mechanisms are considered: indirect generation by bubbles and direct generation by spumes. Following the Monahan parameterization ([Monahan et al., 1986] and [Gong and L.A., 1997]), these two mechanisms may be modelled by the density functions dF_0/dr (indirect generation) and dF_1/dr (direct generation) respectively

$$\frac{dF_0}{dr} = 1.373\, U_{10}^{3.41}\, r^{-3}\, \left(1 + 0.057\, r^{1.05}\right) 10^{1.19\, e^{-B^2}} \tag{4.73}$$

$$\frac{dF_1}{dr} = \begin{cases} 0 & r < 10\ \mu m \\ 8.60\ 10^{-6}\ e^{2.08\, U_{10}\, r^{-2}} & 10\ \mu m \leq r \leq 75\ \mu m \\ 4.83\ 10^{-2}\ e^{2.08\, U_{10}\, r^{-4}} & 75\ \mu m \leq r \leq 100\ \mu m \\ 8.60\ 10^{6}\ e^{2.08\, U_{10}\, r^{-8}} & r \geq 100 \mu m \end{cases} \tag{4.74}$$

where r is the wet droplet radius and U_{10} is the wind velocity at 10m level and $B = (0.38 - \log r)/0.65$.

The total density function

$$\frac{dF}{dr} = \frac{dF_0}{dr} + \frac{dF_1}{dr} \tag{4.75}$$

corresponds to the rate of sea-salt droplet generation per unit area of sea surface, per increment of wet droplet radius (in particles $m^{-2}\ s^{-1}\mu m^{-1}$).

According to [Monahan et al., 1986] and [Gong and L.A., 1997], the parameterization of dF_0/dr is valid only for radius in the range $0.8 - 10\mu m$. Because, according to [Gong and L.A., 1997], dF_1/dr generates too much big sea-salt particles at high wind speeds compared to observations, it is not taken into account here and only dF_0/dr is considered. For radius smaller than $0.8\mu m$, the parameterization of [Martensson et al., 2003] may be used, as done in [Foltescu et al., 2005], or a modified version of the Monahan parameterization ([Gong, 2003]). For radius larger than $10\mu m$, the parameterization of [Smith and Harrison, 1998], which models both direct and indirect generation, may be used.

Generalisation The rate dF/dr_{80}, given by the Monahan parameterization, corresponds to a wet radius r_{80} at 80% humidity. The parameterization needs to be generalised to relative humidities ranging between 0 and 100%, or to be expressed in terms of dry radius.

[Zhang et al., 2005] provides a generalisation of the Monahan parameterization to RH ranging between 45% and 99% based on the laboratory measurements of sea-salt particles by [Tang et al., 1997]. However, [Lewis and Schwartz, 2006] shows that the generalisation of Zhang may not be valid for seawater of salinity other than 35.

According to [Lewis and Schwartz, 2006], the wet radius r_{80} at 80% humidity is related to the dry radius r_d within about 1% as follows

$$r_{80} \approx 2\ r_d. \tag{4.76}$$

This relation can be checked using the empirical formula of [Gerber, 1985b]

$$r_{80} = \left(\frac{C_1\ r_d^{C_2}}{C_3\ r_d^{C_4} - \log 0.80} + r_d^3 \right)^{1/3} \tag{4.77}$$

where r_d and r_{80} are in centimeters, and for sea-salt aerosols $C_1 = 0.7674$, $C_2 = 3.079$, $C_3 = 2.573\ 10^{-11}\,[1 + 0.004\,(298 - T)]$, where T is the temperature in Kelvins, and $C_4 = -1.424$. As shown in figure 4.7, the ratio r_{80}/r_d varies between 1.97 and 2.1 in the size range of interest.

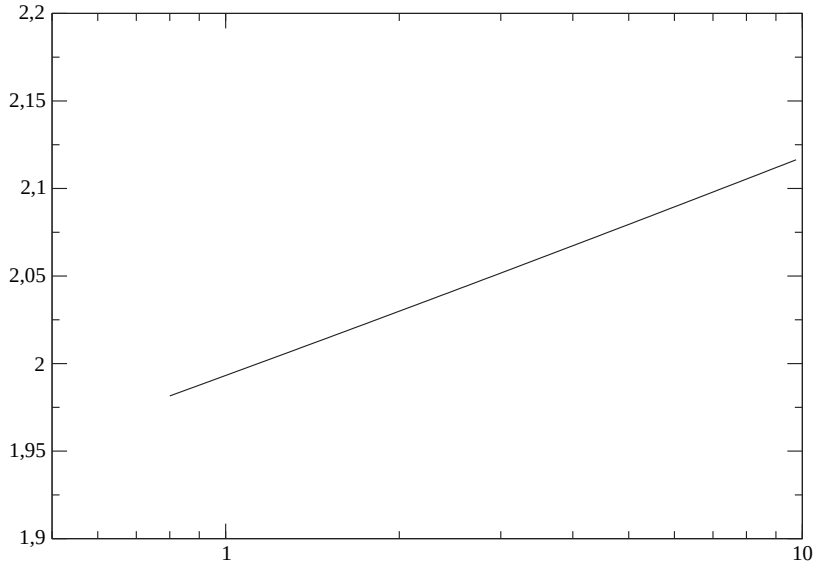

Figure 4.7: Ratio of the wet diameter at 80% relative humidity over the dry diameter (r_{80}/r_d) for dry diameters between 0.01μm and 10μm (the wet diameter is computed using the Gerber formula).

By approximating $r_{80} \approx 2\ r_d$, the rate of sea-salt generation, dF/dr_d, may be deduced from the rate dF/dr_{80}, given by the Monahan parameterization for a wet radius r_{80}, by

$$\frac{dF}{dr_d} = C_{80}\frac{dF}{dr_{80}} \tag{4.78}$$

with $C_{80} = 2$.

The dry rate of sea-salt generation for mass dF_M/dr_d may be obtained from the rate of sea-salt generation for number dF/dr_d

$$\frac{dF_M}{dr_d} = \frac{dF}{dr_d}\frac{4\pi}{3}\rho_p\ r^3 \tag{4.79}$$

where the density of dry sea salt is taken equal to $2.165 gcm^{-3}$ following [Lewis and Schwartz, 2006] and [Seinfeld and Pandis, 1998].

Integration In Polair3D, because we work with the dry rather than the wet aerosol distribution, the bounds of the different bins of the emitted distribution are dry radius. Let us denote $r_{d,i}$ and $r_{d,i+1}$ the bound radius of the bin i of the dry aerosol distribution.

The emitted mass of sea salt E_{ss} between $r_{d,i}$ and $r_{d,i+1}$ is computed by integrating equation (4.79)

$$E_{ss} = \int_{r_{d,i}}^{r_{d,i+1}} \frac{dF_M}{dr} dr \quad = \quad \frac{4\pi}{3} \rho_P \int_{r_{d,i}}^{r_{d,i+1}} r_d^3 \frac{dF}{dr_d} dr_d \tag{4.80}$$

To integrate (4.80), the integral is written as function of $dr_{80} = C_{80} dr_d$

$$E_{ss} \quad = \quad \frac{4\pi \ \rho_P}{3 \ C_{80}^3} \int_{r_{80,i}}^{r_{80,i+1}} r_{80}^3 \ \frac{dF}{dr_{80}} dr_{80} \tag{4.81}$$

where $r_{80,i} = C_{80} \ r_{d,i}$ and $r_{80,i+1} = C_{80} \ r_{d,i+1}$.

The numerical integration between $r_{80,i}$ and $r_{80,i+1}$ is done using the Simpson's rule. The interval $[r_{80,i}, \ r_{80,i+1}]$ is first refined with $2N+1$ points a_j $(j = 0, \ ..., 2N)$ such that

$$a_j = r_{80,i} + (r_{80,i+1} - r_{80,i}) \ \frac{j}{2N}.$$

The integral of equation (4.81) is then computed as

$$\begin{aligned} \int_{r_{80,i}}^{r_{80,i+1}} r_{80}^3 \frac{dF}{dr_{80}} dr \quad = \quad & \frac{h}{3} \left(a_0^3 \ \frac{dF}{dr_{80}}(a_0) + 4 \ a_1^3 \ \frac{dF}{dr_{80}}(a_1) + 2 \ a_2^3 \ \frac{dF}{dr_{80}}(a_2) + \right. \\ & 4 \ a_3^3 \ \frac{dF}{dr_{80}}(a_3) + 2 \ a_4^3 \ \frac{dF}{dr_{80}}(a_4) + \ ... + \\ & \left. 4 \ a_{2N-1}^3 \ \frac{dF}{dr_{80}}(a_{2N-1}) + a_{2N}^3 \ \frac{dF}{dr_{80}}(a_{2N}) \right) \end{aligned} \tag{4.82}$$

Finally, the dry mass of emitted sodium, chloride and sulfate by sea-salt are computed as

$$\begin{aligned} E_{Na} \quad &= \quad E_{ss} \ x_{Na} \\ E_{CL} \quad &= \quad E_{ss} \ x_{Cl} \\ E_{SO_4} \quad &= \quad E_{ss} \ x_{SO_4} \end{aligned} \tag{4.83}$$

where x_{Na}, x_{Cl} and x_{SO_4} are the mass fraction of sodium, chloride and sulfate in sea-salt, as given by [Zhang et al., 2005] and page 444 of [Seinfeld and Pandis, 1998] ($x_{Na} = 30.61\%$, $x_{Cl} = 55.14\%$ and $x_{SO4} = 7.68\%$).

Conclusion and future works

This report has presented the development of two aerosol models, SIREAM and MAM. Both models are based on state-of-the-science parameterizations and numerical algorithms. One novelty is that both models gather the same parameterizations through the AtmoData library and only differ by the discretization of aerosol distributions (sire-resolved approach versus modal approach).

Many specific points have also been investigated:

- For parameterizations:
  - parameterization and reduction of aqueous-phase chemistry;
  - limitation in H^+ c/e flux;
  - parameterization of the aerosol wet diameter with optimized coefficients of a Gerber's formula;
  - parameterization of sea-salt emissions with effects of relative humidity;
  - benchmark of scavenging parameterizations;
  - below-cloud scavenging of gas-phase species with pH effects;
  - ...
- For numerics:
  - numerical algorithms for aqueous-phase chemistry;
  - modal merging and splitting for modal models;
  - use of a fourth mode for modal models;
  - hybrid algorithms for condensation/evaporation;
  - new closure algorithms for lagrangian methods of c/e (redistribution onto a fixed grid and interpolation);
  - numerical time integration methods;
  - ...

These models have been hosted by the 3D Chemistry-Transport Model Polair3D. Model-to-data comparisons have been performed at regional and continental scales ([Fahey et al., 2005, Hayami and al, 2006, Sartelet et al., 2006]).

A comprehensive sensitivity analysis with respect to many uncertain parameters and numerical algorithms has also been performed ([Sartelet and al, 2006, Sartelet and Hayami, 2005, Tombette et al., 2005]).

The models are developed under a Gnu/GPL licence and are downloadable from the website `http://www.enpc.fr/cerea/polyphemus`.

There are still many points to investigate.

The modeling of SVOC is a weakness of both models. An update of the SOA module is planned.

Dry deposition does not take into account codeposition effects for NH_3 and SO_2. A new parameterization for dry deposition has to be developed.

Following previous works led with the POLYPHEMUS system, studies devoted to data assimilation of aerosols are also planned in near future.

Bibliography

[Andronache, 2003] Andronache, C. (2003). Estimated variability of below-cloud aerosol removal by rainfall for observed aerosol size distribution. *Atmos. Chem. Phys.*, 3:131–143.

[Andronache, 2004] Andronache, C. (2004). Diffusion and electric charge contributions to below-cloud wet removal of atmospheric ultre-fine aerosol particles. *Aerosol Sc. and Tech.*, 35:1467–1482.

[Binkowski and Roselle, 2003] Binkowski, F. and Roselle, S. (2003). Models-3 Community Multiscale Air Quality (CMAQ) model aerosol component. 1. Model description. *J. Geophys. Res.*, 108(D6-4183):doi:10.1029/2001JD001409.

[Capaldo et al., 2000] Capaldo, K., Pilinis, C., and Pandis, S. (2000). A computationally efficient hybrid approach for dynamic gas/aerosol transfer in air quality models. *Atmos. Env.*, 34:3617–3627.

[Dahneke, 1983] Dahneke, B. (1983). *Theory of Dispersed Multiphase Flow.* Academic press, New York.

[Debry, 2004] Debry, E. (2004). *Modelling and simulation of an atmospheric aerosol distribution.* PhD thesis, ENPC, CEREA.

[Debry and Sportisse, 2005] Debry, E. and Sportisse, B. (2005). Reduction of the condensation/evaporation dynamics for atmospheric aerosols: theoretical and numerical investigation of hybrid methods. *J. Aerosol Sci.* Accepted for publication.

[Djouad et al., 2003a] Djouad, R., Audiffren, N., and Sportisse, B. (2003a). Sensitivity analysis using automatic differentiation applied to a multiphase chemical mechanism. *Atmos. Env.*, 37(22):3029:3038.

[Djouad et al., 2002] Djouad, R., Sportisse, B., and Audiffren, N. (2002). Numerical simulation of aqueous-phase atmospheric models : use of a non-autonomous Rosenbrock method. *Atmos. Env.*, 36:873–879.

[Djouad et al., 2003b] Djouad, R., Sportisse, B., and Audiffren, N. (2003b). Reduction of multiphase atmospheric chemistry. *Journal of Atmospheric Chemistry*, 46:131–157.

[ENVIRON, 2005] ENVIRON (2005). User's Guide CAMx - Version 4.20. Technical report, ENVIRON International Corporation.

[Fahey, 2003] Fahey, K. (2003). *Cloud and fog processing of aerosols: modeling the evolution of atmospheric species in the aqueous phase.* PhD thesis, Carnegie Mellon University.

[Fahey et al., 2005] Fahey, K., Debry, E., Foudhil, H., and Sportisse, B. (2005). Formulation, development and preliminary validation of the SIze REsolved Aerosol Model, SIREAM. In *Proceedings GLOREAM 2004*.

[Fahey and Pandis, 2001] Fahey, K. and Pandis, S. (2001). The role of variable droplet size-resolution in aqueous phase atmospheric chemistry modeling. In Sportisse, B., editor, *Proceedings APMS 2001*, Geosciences. Springer.

[Fernàndez-Dìaz et al., 2000] Fernàndez-Dìaz, J., Gonzàlez-Pola Muñiz, C., Rodrìguez Braña, M., Arganza Garcìa, B., and Garcìa Nieto, P. (2000). A modified semi-implicit method to obtain the evolution of an aerosol by coagulation. *Atmos. Env.*, 34:4301–4314.

[Foltescu et al., 2005] Foltescu, V. L., S.C., P., and C., B. (2005). Sea salt generation, dispersion and removal on the regional scale. *Atmos. Env.*, 39:2123–2133.

[Fuchs, 1964] Fuchs, N. (1964). *Mechanics of Aerosols.* Pergamon,N.Y.

[Gaydos et al., 2003] Gaydos, T., Koo, B., Pandis, S., and Chock, D. (2003). Development and application of an efficient moving sectional approach for the solution of the atmospheric aerosol condensation/evaporation equations. *Atmos. Env.*, 37(23):3303–3316.

[Gerber, 1985a] Gerber, H. (1985a). Relative-humidity parameterization of the navy aerosol model (NAM). Technical Report 8956, National Research Laboratory, Washington, D.C.

[Gerber, 1985b] Gerber, H. (1985b). Relative-humidity parameterization of the navy aerosol model (nam). Technical Report 8956, Natl. Res. Lab. Washington D.C.

[Gong, 2003] Gong, S. (2003). A parameterization of sea-salt aerosol source function for sub- and super-micron particles. *Global Biochemical Cycles*, 17:1097.

[Gong and L.A., 1997] Gong, S. and L.A., B. (1997). Modeling sea-salt aerosols in the atmosphere. 1. model development. *J. Geophys. Res.*, 102:3805–3818.

[Griffin et al., 2002a] Griffin, R., Dabdub, D., Kleeman, M., Fraser, M., Cass, G., and Seinfeld, J. (2002a). Secondary organic aerosol 3. urban/regional scale model of size- and composition-resolved aerosols. *J. Geophys. Res.*, 107(D17).

[Griffin et al., 2002b] Griffin, R., Dabdub, D., and Seinfeld, J. (2002b). Secondary organic aerosol 1. Atmospheric chemical mechanism for production of molecular constituents. *J. Geophys. Res.*, 107(D17).

[H. Byrd and Zhu, 1995] H. Byrd, P. Lu, J. N. and Zhu, C. (1995). limited memory algorithm for bound constrained optimization. *SIAM J. Sci. Comp.*, 16(5):1190–1208.

[Hayami and al, 2006] Hayami, H. and al (2006). MICS-Asia Phase II study: Aerosols, comparison to data. *Atmos. Env.* Submitted.

[Jacob, 2000] Jacob, D. (2000). Heterogeneous chemistry and tropospheric ozone. *Atmos. Env.*, 34:2131–2159.

[Jacobson, 2002] Jacobson, M. (2002). Analysis of aerosol interactions with numerical techniques for solving coagulation, nucleation, condensation, dissolution, and reversible chemistry among multiple size distributions. *J. Geophys. Res.*, 107(D19).

[Jacobson et al., 1996] Jacobson, M., Tabazadeh, A., and Turco, R. (1996). Simulating equilibrium within aerosols and nonequilibrium between gases and aerosols. *J. Geophys. Res.*, 101(D4):9079–9091. American Geophysical Union.

[Julya, 1999] Julya, K. (1999). Relationship between the scavenging coefficient for pollutants in precipitation and the radar reflectivity factor. Part I: derivation. *J. Applied Meteor.*, pages 1421–1434.

[Koo and Pandis, 2003] Koo, B. and Pandis, S. (2003). Evaluation of the equilibrium, dynamic, and hybrid aerosol modeling approaches. *Aerosol Sc. and Tech.*, 37:53–64.

[Kulmala et al., 1998] Kulmala, M., laaksonen, A., and Pirjola, L. (1998). Parameterizations for sulfuric acid/water nucleation rates. *J. Geophys. Res.*, 103(D7):8301–8307.

[Landgrebe and Pratsinis, 1990] Landgrebe, J. and Pratsinis, S. (1990). A discrete-sectional model for particulate production by gas-phase chemical reaction and aerosol coagulation in the free-molecular regime. *J. Colloid Interf. Sci.*, 139:63–86.

[Lewis and Schwartz, 2006] Lewis, E. and Schwartz, S. (2006). Comment on "size distribution of sea-salt emissions as a function of relative humidity". *Atmos. Env.*, 40:588–590.

[Loosmore and Cederwall, 2004] Loosmore, G. and Cederwall, R. (2004). Precipitation scavenging of atmospheric aerosols for emergency response applications: testing an updated model with new real-time data. *Atmos. Env.*, 38:993:1003.

[Mallet and Sportisse, 2005] Mallet, V. and Sportisse, B. (2005). Data processing and parameterizations in atmospheric chemistry and physics: the AtmoData library. *Submitted to Env.Model.Software*.

[Martensson et al., 2003] Martensson, E., Nilsson, E., de Leeuw, G., and L.H., C. (2003). Laboratory simulations and parameterization of the primary marine aerosol production. *J. Geophys. Res.*, 108:doi:10.1029/2002JD002263.

[Meng et al., 1998] Meng, Z., Dabdub, D., and Seinfeld, J. (1998). Size-resolved and chemically resolved model of atmospheric aerosol dynamics. *J. Geophys. Res.*, 103:3419–3435.

[Meng and Seinfeld, 1996] Meng, Z. and Seinfeld, J. (1996). Time scales to achieve atmospheric gas-aerosol equilibrium for volatile species. *Atmos. Env.*, 30(16):2889–2900.

[Mircea and Stefan, 1998] Mircea, M. and Stefan, S. (1998). A theoretical study of the microphysical parameterization of the scavenging coefficient as a function of precipitation type and rate. *Atmos. Env.*, 32(17):2931:2938.

[Mircea et al., 2000] Mircea, M., Stefan, S., and Fuzzi, S. (2000). Precipitation scavenging coefficient: influence of measured aerosol and raindrop size distribution. *Atmos. Env.*, 34:5169:5174.

[Monahan et al., 1986] Monahan, E., D.E., S., and K.L., D. (1986). A model of marine aerosol generation via whitecaps and wave disruption. In *Oceanic whitecaps*, pages 167–174. D. Reidel.

[Napari et al., 2002] Napari, I., Noppel, M., Vehkamäki, H., and Kulmala, M. (2002). Parametrization of ternary nucleation rates for H2SO4-NH3-H2O vapors. *J. Geophys. Res.*, 107(D19).

[Nenes et al., 1998] Nenes, A., Pandis, S., and Pilinis, C. (1998). ISORROPIA : A new thermodynamic equilibrium model for multicomponent inorganic aerosols. *Aquatic geochemistry*, 4:123–152.

[Pandis et al., 1993] Pandis, S., Wexler, A., and Seinfeld, J. (1993). Secondary organic aerosol formation and transport -II. Predicting the ambient secondary organic aerosol size distribution. *Atmos. Env.*, 27A(15):2403–2416.

[Pilinis et al., 2000] Pilinis, C., Capaldo, K., Nenes, A., and Pandis, S. (2000). MADM - a new multi-component Aerosol Dynamic Model. *Aerosol Sc. and Tech.*, 32:482–502.

[Pilinis and Seinfeld, 1988] Pilinis, C. and Seinfeld, J. (1988). Development and evaluation of an eulerian photochemical gas-aerosol model. *Atmos. Env.*, 22:1985:2001.

[Pirjola et al., 1999] Pirjola, L., Kulmala, M., Wilck, M., Bischoff, A., Stratmann, F., and Otto, E. (1999). Formation of sulfuric acid aerosols and cloud condensation nuclei: an expression for significant nucleation and model comparison. *J. Aerosol Sci.*, 30:1079–1094.

[Pirjola et al., 2003] Pirjola, L., Tsyro, S., Tarrason, L., and M., K. (2003). A monodisperse aerosol dynamics module, a promising candidate for use in long-range transport models: Box model tests. *J. Geophys. Res.*, 108(D94258):doi:1029/2002JD002867.

[Pruppacher and Klett, 1998] Pruppacher, H. and Klett, J. (1998). *Microphysics of Clouds and Precipitation*. Kluwer Academic Publishers.

[Pun et al., 2002] Pun, B., Griffin, R., Seigneur, C., and Seinfeld, J. (2002). Secondary organic aerosol 2. Thermodynamic model for gas/particle partitioning of molecular constituents. *J. Geophys. Res.*, 107(D17).

[Putaud et al., 2003] Putaud, J., Dingenen, R., Baltensperger, U., Brüggemann, E., Charron, A., Facchini, M., Decesari, S., Fuzzi, S., Gehrig, R., Hansson, H., Harrison, R., Jones, A., Laj, P., Lorbeer, G., Maenhaut, W., Mihalopoulos, N., Müller, K., Palmgren, F., Querol, X., Rodriguez, S., Schneider, J., Spindler, G., Brink, H., Tunved, P., Torseth, K., Weingartner, E., Wiedensohler, A., Wahlin, P., and Raes, F. (2003). A european aerosol phenomenology. Technical report, Joint Research Centre, Institute for Environment and Sustainability.

[Roselle and Binkowski, 1999] Roselle, S. and Binkowski, F. (1999). Cloud dynamics and chemistry. Technical report, U.S. Environmental Protection Agency. chapter 11.

[Rosenbrock, 1963] Rosenbrock, H. (1963). Some general implicit processes for the numerical solution of differential equations. *Computer j.*, 5:329–330.

[Sartelet, 2004] Sartelet, K. (2004). Modal aerosol model MAM – technical description. Technical Report 22, CEREA.

[Sartelet and al, 2006] Sartelet, K. and al (2006). MICS-Asia Phase II: sensitivity to the aerosol module. *Atmos. Env.* Submitted.

[Sartelet et al., 2006] Sartelet, K., Debry, E., Fahey, K., Tombette, M., and Sportisse, B. (2006). Simulation of aerosols and related species over Europe with the POLYPHEMUS system. Part I: model-to-data comparison for year 2001. *J. Geophys. Res.* In submission.

[Sartelet and Hayami, 2005] Sartelet, K. N. and Hayami, H. (2005). MICS-Asia: sensitivity to the aerosol module using the CTM Polair3D. In *Proceedings of the 46th annual meeting of Japan Society for Atmospheric Environmnent*, page 588.

[Sartelet et al., 2005] Sartelet, K. N., Hayami, H., Albriet, B., and Sportisse, B. (2005). Development and preliminary validation of a modal aerosol model for tropospheric chemistry: MAM. *Aerosol Sc. and Tech.*, 40(2):118–127.

[Schell, 2000] Schell, B. (2000). *Die Behandlung sekundärer organischer Aerosole in einem komplexen Chemie-Transport-Modell.* PhD thesis, Univ. Köln.

[Schell et al., 2001] Schell, B., Ackermann, I., Hass, H., Binkowski, F., and Ebel, A. (2001). Modeling the formation of secondary organic aerosol within a comprehensive air quality model system. *J. Geophys. Res.*, 106:28275.

[Scott, 1978] Scott, B. (1978). Parameterization of sulfate removal by precipitation. *J. Applied Meteor.*, 17:1375–1389.

[Seinfeld, 1985] Seinfeld, J. (1985). *Atmospheric Physics and Chemistry of Air Pollution.* Wiley.

[Seinfeld and Pandis, 1998] Seinfeld, J. and Pandis, S. (1998). *Atmospheric Chemistry and Physics.* Wiley-interscience.

[Simpson et al., 2003] Simpson, D., Fagerli, H., Jonson, J. E., Tsyro, S., Wind, P., and Tuovinen, J.-P. (2003). Transboundary acidification, euthrophication and ground level ozone in Europe. Part I: Unified EMEP model description. Technical report, EMEP.

[Smith and Harrison, 1998] Smith, M. and Harrison, N. (1998). The sea spray generation function. *J. Aerosol Sci.*, 29 Suppl.1:S189–S190.

[Sparmacher et al., 1993] Sparmacher, H., Fülber, K., and Bonka, H. (1993). Below-cloud scavenging of aerosol particles: particle-bound radionuclides. Experimental. *Atmos. Env.*, 27A(4):605–618.

[Sportisse and Djouad, 2003] Sportisse, B. and Djouad, R. (2003). Mathematical investigation of mass transfer for atmospheric pollutants into a fixed droplet with aqueous chemistry. *J. Geophys. Res.*, 108(D2):4073.

[Sportisse and Du Bois, 2002] Sportisse, B. and Du Bois, L. (2002). Numerical and theoretical investigation of a simplified model for the parameterization of below-cloud scavenging by falling raindrops. *Atmos. Env.*, 36:5719–5727.

[Stockwell et al., 1997] Stockwell, W., Kirchner, F., Kuhn, M., and Seefeld, S. (1997). A new mechanism for regional atmospheric chemistry modeling. *J. Geophys. Res.*, 95(D10):16343:16367.

[Strader et al., 1998] Strader, R., Gurciullo, C., Pandis, S., Kumar, N., and Lurmann, F. (1998). Development of gas-phase chemistry, secondary organic aerosol and aqueous-phase chemistry modules for pm modeling. Technical report, STI.

[Tang et al., 1997] Tang, I., Tridico, A., and Fung, K. (1997). Thermodynamic and optical properties of sea salt aerosols. *J. Geophys. Res.*, 102:23269–23275.

[Tombette et al., 2005] Tombette, M., Fahey, K., Sartelet, K., and Sportisse, B. (2005). Aerosol modelling at regional scale: a sensitivity study with the Polyphemus platform. In *Proceedings of GLOREAM 2005*. Also as Report CEREA 2005-50.

[Underwood, 2001] Underwood, B. (2001). Review of deposition velocity and washout coefficient. Technical report, AEA Technology, Harwell.

[Vehkamäki et al., 2002] Vehkamäki, H., Kulmala, M., Napari, I., K.E.J., L., Timmreck, C., Noppel, M., and Laaksonen, A. (2002). An improved parameterization for sulfuric acid-water nucleation rates for tropospheric and stratospheric conditions. *J. Geophys. Res.*, 107(D22):4622.

[Wexler et al., 1994] Wexler, A., Lurmann, W., and Seinfeld, J. (1994). Modelling urban and regional aerosols - model development. *Atmos. Env.*, 28:531–546.

[Wexler and Seinfeld, 1990] Wexler, A. and Seinfeld, J. (1990). The distribution of ammonium salts among a size and composition dispersed aerosol. *Atmos. Env.*, 24A(5):1231–1246.

[Whitby and McMurry, 1997] Whitby, E. and McMurry, P. (1997). Modal aerosol dynamics modeling. *Aerosol Sc. and Tech.*, 27:673–688.

[Whitby et al., 2002] Whitby, E., Stratmann, F., and Wilck, M. (2002). Merging and remapping modes in a modal aerosol dynamics models: a "dynamic mode manager". *J. Aerosol Sci.*, 33:623–645.

[Zhang et al., 2001] Zhang, L., Gong, S., Padro, J., and Barrie, L. (2001). A size-segregated particle dry deposition scheme for an atmospheric aerosol module. *Atmos. Env.*, pages 549–560.

[Zhang et al., 2005] Zhang, M. K., E.M., K., A.S., W., P.V., B., and G.S., T. (2005). Size distribution of sea-salt emissions as a function of relative humidity. *Atmos. Env.*, 39:3373–3379.

Appendix A

Update of the AtmoData library

The following functions related to aerosol modeling have been added to the AtmoData library ([Mallet and Sportisse, 2005]).

1. COMPUTE_DYNAMIC_VISCOSITY

   This function computes the dynamic air viscosity with the Sutherland law.

   Inputs:

   T : temperature [K].

   Outputs:

   μ_{air}: dynamic air viscosity ([kg/m/s]).

2. COMPUTE_CC

   This function computes the correction Cunningham factor for a particle of diameter d_p.

   Reference: Equation (4.24).

   Inputs:

   $(d_p)_{wet}$: wet aerosol diameter ([m]).
   λ_{air}: air free mean path ([m]).

   Outputs:

   Cunningham factor ([]).

3. COMPUTE_VSTOKES

   This subroutine computes the Stokes settling velocity for a particle.

   Reference: Equation (4.23).

   Inputs:

   $(d_p)_{wet}$: wet aerosol diameter ([μm]).
   ρ_p: aerosol density ([kg.m^{-3}])
   Cunningham factor ([]).
   μ_{air}: dynamic air viscosity ([kg/m/s]).

   Outputs:

   v_{Stokes}: Stokes settling velocity ([m/s]).

4. COMPUTE_CD

   This function computes the drag coefficent as a function of the particle Reynolds number.

   Inputs:

   Re_p : particle Reynolds Number.

   Outputs:

   CD : drag coefficient ([]).

5. COMPUTE_AIR_FREE_MEAN_PATH

   This function computes the free mean path for air molecules on the basis of thermodynamic variables. It also returns dynamic viscosity.

   Reference: Equation (4.25).

   Inputs:

   T : temperature [K]
   P : pressure ([Pa]).

   Outputs:

   λ_{air}: air free mean path ([μm]).
   μ_{air}: dynamic air viscosity ([kg/m/s]).

6. COMPUTE_GRAVITATIONAL_SETTLING

   This routine computes the gravitational settling velocity. It also computes the mean air free path.

   Reference: Equation (4.8).

Inputs:

I_Stokes: a flag equal to 0 if the Stokes velocity is computed, 1 otherwise.
T : temperature ([K]).
P : pressure ([Pa]).
ρ_p: aerosol density ([kg.m^{-3}]).
$(d_p)_{wet}$: wet aerosol diameter ([m]).

Outputs:

v_g: gravitational settling velocity ([m/s]).
λ_{air}: air free mean path ([m]).

7. COMPUTE_BIDISPERSE_COAGULATION_KERNEL

This subroutine computes coagulation kernels for bidispersed aerosols.

Reference: section 1.2.1.

Inputs:

T : temperature [K]
λ_{air}: air free mean path ([μm]).
d_{p_1}: diameter of the first coagulating particle ([μm]).
d_{p_2}: diameter of the second coagulating particle ([μm]).
m_{p_1}: mass of the first coagulating particle ([μg]).
m_{p_2}: mass of the second coagulating particle ([μg]).

Outputs:

K_{12} : coagulation kernel ([m^3.s^{-1}]).

8. COMPUTE_COLLISION_INTEGRAL

This routine computes the collision integral for gas-phase diffusion, based on Lennard-Jones potential. It is a dimensionless function of temperature and is tabulated in (Hirschelder, 1954).

Inputs:

k_bT/ϵ_{12}: with k_b the Boltzmann constant, T the temperature, and ϵ_{12} the Lennard-Jones molecular interaction parameter.

Outputs:

Ω: collision integral.

9. COMPUTE_CONDENSATION_COEFFFICIENT

This subroutine computes the condensation/evaporation kernel for one given semivolatile species. There are three regimes according to the Knudsen number.

Reference: Equation (1.15).

Inputs:

D_g: gas phase diffusion coefficient ([$m^2.s^{-1}$]).
$\bar{c}$: quadratic mean velocity ([$m.s^{-1}$]).
α: gas-phase accomodation coefficient ([]).
$(d_p)_{wet}$: wet aerosol diameter ([μm]).

Outputs:

Condensation/evaporation kernel coefficient ([$m^3.s^{-1}$]).

10. COMPUTE_GAS_DIFFUSIVITY

This subroutine computes the gas-phase diffusion coefficients for a set of species.

Inputs:

N : number of gases.
P : pressure ([Pa]).
T : temperature ([K]).
$\{\sigma_i\}_{i=1,N}$: aerosol fixed surface tension ([$N.m^{-1}$]).
$\{\sigma_i\}_{i=1,N}$: collision factor.
$\{M_i\}_{i=1,N}$: molar mass ([$\mu g.mol^{-1}$]).

Outputs:

$\{D_g^i\}_{i=1,N}$: gas-phase diffusivity ([$m^2.s^{-1}$]).

11. COMPUTE_GERBER

This routine computes the wet aerosol diameter as a function of the kind of aerosols, its dry diameter, temperature and humidity according to a Gerber's formula with optimized parameters (fitted to ISORROPIA computations).

Reference: Equation (4.1).

Inputs:

RH: relative humidity ([%]).
T: temperature ([K]).
$(d_p)_{dry}$: dry aerosol diameter ([μm]).

Outputs:

$(d_p)_{wet}$: wet aerosol diameter ([μm]).

12. COMPUTE_KELVIN_COEFFICIENT

This subroutine computes the correction factor due to Kelvin effect for a set of N given species. The factor is limited.

Reference: Equation (1.17).

Inputs:

N: number of species.
$\{M_i\}_{i=1,N}$: molar mass ([μg.mol^{-1}]).
$(d_p)_{wet}$: wet aerosol diameter ([μm]).
$\{\sigma_i\}_{i=1,N}$: aerosol fixed surface tension ([N.m^{-1}]).
T: temperature ([K]).
ρ_p: aerosol density ([μg.m^{-3}]).

Outputs:

η: Kelvin coefficient ([]).

13. COMPUTE_QUADRATIC_MEAN_VELOCITY

This subroutine computes the quadratic mean molecular velocity for a set of N volatile species.

Reference: Equation (1.11).

Inputs:

N: number of species.
T: temperature ([K]).
$\{M_i\}_{i=1,N}$: molar mass ([μg.mol^{-1}]).

Outputs:

$\{\bar{c}_i\}_{i=1,N}$: quadratic mean velocity ([m.s^{-1}]).

14. COMPUTE_RELATIVE_HUMIDITY

This routine computes the relative humidity.

Inputs:

T: temperature ([K]).
P : pressure ([Pa]).
q_s : specific humidity ($(m_{water}/(m_{water} + m_{dryair})$).

Outputs:

RH: relative humidity ([0-1]).

15. COMPUTE_SOA_SATURATION_CONCENTRATION

This subroutine computes the saturation concentration for a set of SVOCs at a given temperature. The reference temperature is 298 K.

Reference: Equations (1.43) and (1.40).

Inputs:

N: number of species.
$\{p_i^{sat}(298\,K)\}_{i=1,N}$: saturation vapor pressure at 298 K ([Pa]).
$\{(\Delta H_{vap})_i\}_{i=1,N}$: enthalpy of vaporisation ([J.mol^{-1}]).
$\{M_i\}_{i=1,N}$: molar mass ([μg.mol^{-1}]).
T: temperature ([K]).

Outputs:

$\{q_i^{sat}\}_{i=1,N}$: saturation concentration at T ([μg.m^{-3}]).

16. COMPUTE_BINARY_NUCLEATION_KERNEL

This subroutine computes the binary nucleation rate H_2SO_4-H_2O on the basis of the parameterization [Vehkamäki et al., 2002].

Reference: section 1.2.3.

Inputs:

RH : relative humidity ([0-1]).
T : temperature ([K]).
$[H_2SO_4]$: gas H_2SO_4 concentration ([molec.cm^{-3}]).

Outputs:

J_0 : nucleation rate ([part.cm^{-3}.s^{-1}]).
n_{nucl} : number of molecules in the critical cluster size ([]).
$x^\star$: molar fraction of H_2SO_4 in the nucleated aerosol ([]).
$(d_p)_{nucl}$: nucleation diameter ([nm]).

17. COMPUTE_TERNARY_NUCLEATION

This subroutine computes a ternary nucleation rate on the basis of the parameterization proposed in [Napari et al., 2002] for the H_2SO_4-NH_3-H_2O system.

Reference: section 1.2.3.

Inputs:

RH : relative humidity ([0-1]).
T : temperature ([K]).
[H_2SO_4]: gas H_2SO_4 concentration ([molec.cm^{-3}]).
[NH_3]: gas NH_3 concentration ([ppt]).

Outputs:

J_0 : nucleation rate ([part.cm^{-3}.s^{-1}]).
$n_{H_2SO_4}$: number of H_2SO_4 molecules in the critical cluster size ([]).
n_{NH_3} : number of NH_3 molecules in the critical cluster size ([]).
$(d_p)_{nucl}$: nucleation diameter ([nm]).